Response of atmospheric pCO_2 to a strong AMOC weakening under climate change

Amber Adore Boot[1], Anna S. von der Heydt[2], and Henk A. Dijkstra[3]

[1]Institute for Marine and Atmospheric Research Utrecht
[2]Institute for Marine and Atmospheric research Utrecht, Utrecht University
[3]Institute for Marine and Atmospheric research Utrecht

September 30, 2023

Abstract

The Earth System is warming due to anthropogenic greenhouse gas emissions which increases the risk of passing a tipping point in the Earth System, such as a collapse of the Atlantic Meridional Overturning Circulation (AMOC). An AMOC weakening can have large climate impacts which influences the marine and terrestrial carbon cycle and hence atmospheric pCO2. However, the sign and mechanism of this response are subject to uncertainty. Here, we use a state-of-the-art Earth System Model, the Community Earth System Model v2 (CESM2), to study the atmospheric pCO2 response to an AMOC weakening under low (SSP1-2.6) and high (SSP5-8.5) emission scenarios. A freshwater flux anomaly in the North Atlantic strongly weakens the AMOC, and we simulate a weak positive pCO2 response of 0.45 and 1.3 ppm increase per AMOC decrease in Sv for SSP1-2.6 and SSP5-8.5, respectively. For SSP1-2.6 this response is driven by both the oceanic and terrestrial carbon cycles, whereas in SSP5-8.5 it is solely the ocean that drives the response. However, the spatial patterns of both the climate and carbon cycle response are similar in both emission scenarios over the course of the simulation period (2015-2100), showing that the response pattern is not dependent on cumulative CO2 emissions up to 2100. Though the global atmospheric pCO2 response might be small, locally large changes in both the carbon cycle and the climate system occur due to the AMOC weakening, which can have large detrimental effects on ecosystems and society.

Response of atmospheric pCO_2 to a strong AMOC weakening under climate change

A. A. Boot[1], A. S. von der Heydt[1,2], and H. A. Dijkstra[1,2]

[1]Institute for Marine and Atmospheric research Utrecht, Department of Physics,Utrecht University, Utrecht, the Netherlands
[2]Center for Complex Systems Studies, Utrecht University, Utrecht, the Netherlands

Key Points:

- First results on the carbon cycle response to AMOC weakening in a CMIP6 Earth System Model are presented.
- Strong weakening of the AMOC does not result in a large response of atmospheric pCO_2 under climate change.
- The spatial patterns of the carbon cycle response to an AMOC weakening are not dependent on cumulative CO_2 emissions.

Corresponding author: Amber Boot, `a.a.boot@uu.nl`

Abstract

The Earth System is warming due to anthropogenic greenhouse gas emissions which increases the risk of passing a tipping point in the Earth System, such as a collapse of the Atlantic Meridional Overturning Circulation (AMOC). An AMOC weakening can have large climate impacts which influences the marine and terrestrial carbon cycle and hence atmospheric pCO_2. However, the sign and mechanism of this response are subject to uncertainty. Here, we use a state-of-the-art Earth System Model, the Community Earth System Model v2 (CESM2), to study the atmospheric pCO_2 response to an AMOC weakening under low (SSP1-2.6) and high (SSP5-8.5) emission scenarios. A freshwater flux anomaly in the North Atlantic strongly weakens the AMOC, and we simulate a weak positive pCO_2 response of 0.45 and 1.3 ppm increase per AMOC decrease in Sv for SSP1-2.6 and SSP5-8.5, respectively. For SSP1-2.6 this response is driven by both the oceanic and terrestrial carbon cycles, whereas in SSP5-8.5 it is solely the ocean that drives the response. However, the spatial patterns of both the climate and carbon cycle response are similar in both emission scenarios over the course of the simulation period (2015-2100), showing that the response pattern is not dependent on cumulative CO_2 emissions up to 2100. Though the global atmospheric pCO_2 response might be small, locally large changes in both the carbon cycle and the climate system occur due to the AMOC weakening, which can have large detrimental effects on ecosystems and society.

Plain Language Summary

The Atlantic Meridional Overturning Circulation (AMOC) modulates global climate by transporting heat from the Southern to the Northern Hemisphere. The AMOC is considered to be a tipping element with a possible future collapse under climate change. An AMOC weakening can have large climate impacts which influences the marine and terrestrial carbon cycle and hence the atmospheric pCO_2. Here, we use a state-of-the-art Earth System Model to study the atmospheric pCO_2 response to an AMOC weakening under low and high emission scenarios. We use simulations where we artificially weaken the AMOC, which results in a weak positive response of 0.45 and 1.3 ppm pCO_2 increase per decrease in Sv for low and high emissions, respectively. For low emissions this response is driven by both the oceanic and terrestrial carbon cycle processes, whereas in the high emission scenario it is solely the ocean that drives the response. Spatial patterns, both the climate and carbon cycle response, are similar in both emission scenarios over the course of the simulation period (2015-2100). The global atmospheric pCO_2 response is small, but locally large changes in both the carbon cycle and the climate system can occur due to the AMOC weakening.

1 Introduction

Anthropogenic emissions of greenhouse gases cause the Earth System to change and warm up. As temperatures increase, we are at risk of crossing tipping points with possibly large detrimental effects on our climate, biodiversity and human communities (Lenton et al., 2008; McKay et al., 2022). One of these tipping points can occur in the Atlantic Meridional Overturning Circulation (AMOC) (Lenton et al., 2008). Currently, the AMOC is in a so-called on-state where it transports heat from the Southern Hemisphere to the Northern Hemisphere and thereby modulates global and especially European climate (Buckley & Marshall, 2016). In models, the AMOC can be strongly weakened and in this so-called collapsed state (or off-state), the northward heat transport is disrupted with large global climatic effects (Orihuela-Pinto et al., 2022).

Proxy-based evidence suggest that AMOC collapses have occurred frequently during the Pleistocene where they are a main source of millennial variability (e.g. the Dansgaard-Oeschger cycles; Rahmstorf, 2002; Lynch-Stieglitz, 2017). The disrupted heat transport causes warming of surface air temperature (SAT) and sea surface temperature (SST) in the Southern Hemisphere, while the Northern Hemisphere cools (also called the 'bipolar seesaw'; Vellinga & Wood, 2002; Caesar et al., 2018), with local SAT changes up to 10°C (Cuffey & Clow, 1997; Rahmstorf, 2002). In models, the bipolar seesaw results in an increased northern hemispheric sea-ice extent and changes in atmospheric dynamics (Vellinga & Wood, 2002; Orihuela-Pinto et al., 2022). The changes in atmospheric dynamics are, for example, seen in wind fields with strengthened trade winds and strengthened Pacific Walker Circulation (Orihuela-Pinto et al., 2022), and a southward shift of the Intertropical Convergence Zone (ITCZ) (Zhang & Delworth, 2005; Jackson et al., 2015). The tipping threshold for the AMOC is estimated to be around 4 °C of warming relative to pre-industrial climate (McKay et al., 2022).

In addition to the climate system, also the carbon cycle is affected by an AMOC collapse. In the ocean, the change in ocean circulation affects the advection of important tracers such as Dissolved Inorganic Carbon (DIC) and nutrients (Zickfeld et al., 2008). An AMOC collapse can also change upwelling rates and surface stratification, processes that are important for driving Net Primary Production (NPP) and carbon sequestration in the deep ocean. Terrestrial primary productivity is affected by the changing temperature and precipitation patterns. Locally, this can lead to both a reduction or an increased uptake of CO_2 (e.g. Köhler et al., 2005). Several studies have looked into a potential feedback between AMOC dynamics and atmospheric pCO_2, which is controlled by the exchange of the atmosphere with the ocean and land carbon stocks. These studies (e.g. Marchal et al., 1998; Köhler et al., 2005; Schmittner & Galbraith, 2008), mostly focused on Pleistocene and pre-industrial conditions, show a wide range of possible responses. There is no clear consensus on the responses of the terrestrial and ocean carbon stock to an AMOC weakening, or to the net effect on atmospheric pCO_2, which can be attributed to different climatic boundary conditions, timescales assessed, and model detail used (Gottschalk et al., 2019). In CMIP6 models, the AMOC gradually weakens up to 2100 and, independent of the used emission scenario (Weijer et al., 2020), no AMOC tipping is found. However, these models are thought to be biased towards a too stable AMOC (e.g. Cheng et al., 2018; Weijer et al., 2019), and a recent observation based study has indicated that the AMOC may tip between 2025 and 2095 (Ditlevsen & Ditlevsen, 2023).

The carbon cycle is also affected by climate change. In the ocean, the effect on the solubility pump is relatively straight forward: increased warming, and increased CO_2 concentrations, reduce ocean pH and the solubility of CO_2, which reduces the uptake capacity of the ocean (Sarmiento et al., 1998). The biological pump in Coupled Model Intercomparison Project 6 (CMIP6; Eyring et al., 2016) models is much more uncertain though (Henson et al., 2022; Wilson et al., 2022), especially given that the spread in NPP and Export Production (EP) has increased from CMIP5 to CMIP6 (Kwiatkowski et al., 2020; Tagliabue et al., 2021). The terrestrial biosphere is affected for example through increased primary production related to CO_2 fertilization (Zhu et al., 2022), but also increased respiration due to permafrost melt (Burke et al., 2020).

Studies looking at the combined effect of strong AMOC weakening and anthropogenic climate change on the future carbon cycle are limited. A projected AMOC weakening affects both the solubility and the biological carbon pumps (Liu et al., 2023), and generally leads to reduced uptake of (anthropogenic) carbon in the ocean (Obata, 2007; Zickfeld et al., 2008; Liu et al., 2023), which can be partially compensated for by the terrestrial biosphere (Zickfeld et al., 2008). However, the net effect has been found to be small due to competing effects (Swingedouw et al., 2007; Zickfeld et al., 2008). Though global effects might be weak, local effects can be quite strong. For example, a weakening of the AMOC can also result in a local reduction in primary productivity (Whitt & Jansen, 2020), changes in the plankton stock (Schmittner, 2005) and plankton composition (Boot et al., 2023a), which all can lead to reduced CO_2 uptake of the ocean (e.g. Yamamoto et al., 2018; Boot et al., 2023a). These local changes related to an AMOC weakening are strongest in the Atlantic Ocean (Katavouta & Williams, 2021).

The novel aspect of this paper is that we consider the effect of AMOC weakening on the carbon cycle under climate change in a state-of-the-art global climate model, the Community Earth System Model v2 (CESM2; Danabasoglu et al., 2020), as explained in section 2. We use a strong freshwater forcing in the North Atlantic to artificially weaken the AMOC and consider two different emission scenarios, Shared Socioeconomic Pathways (SSPs), with low (SSP1-2.6) and high (SSP5-8.5) emissions (O'Neill et al., 2020). In the results of section 3 and the subsequent analysis, we focus on the mechanisms how a forced AMOC weakening affects atmospheric pCO_2 under climate change.

2 Method

In the CESM2 (Danabasoglu et al., 2020), the atmosphere is represented by the CAM6 model, the land by the CLM5 model (Lawrence et al., 2019), sea ice by the CICE model, ocean circulation by POP2 (Smith et al., 2010), and ocean biogeochemistry by MARBL (Long et al., 2021). The ocean models POP2 and MARBL are both run on a displaced Greenland pole grid at a nominal horizontal resolution of 1°, with 60 non-equidistant vertical levels. The ocean biogeochemical module MARBL is based on a NPZD-model, where four nutrients (N, P, Fe, and Si) together with light co-limit the production of three phytoplankton groups (diatoms, diazotrophs and small phytoplankton) which are grazed upon by one zooplankton group. The terrestrial carbon cycle is represented with CLM5. This module represents several surface processes such as biogeochemistry, ecology, human influences, biogeophysics and the hydrological cycle. As we use the default CESM2 version, there is no dynamic vegetation. For a complete overview of the CESM2 model and submodules we refer the reader to Danabasoglu et al. (2020) (CESM2), Long et al. (2021) (MARBL), and Lawrence et al. (2019) (CLM5).

We performed emission forced CESM2 simulations with two different emission scenarios, the low emission scenario SSP1-2.6 (126) and the high emission scenario SSP5-8.5 (585). For each emission scenario, a control (CTL) and a hosing (HOS) simulation were carried out. The CTL simulations were only forced with the greenhouse gas emissions, while the HOS simulations were forced with greenhouse gas emissions and an additional, artificial freshwater flux in the North Atlantic. This freshwater forcing is located in the North Atlantic Ocean over the latitudes 50°N - 70°N (Fig. S1), and is kept constant at a rate of 0.5 Sv over the entire simulation period. We will refer to the simulations by their simulation type (CTL or HOS) and the respective emission scenario (126 or 585), e.g. as CTL-126 and HOS-585. All simulations are run from year 2015 to year 2100 and are initialized by values of the NCAR CMIP6 emission driven historical simulation (Danabasoglu, 2019). The used model output is based on monthly means, and line plots are smoothed with a 5 year running mean. When looking at the difference between the HOS and CTL simulations, we subtract the CTL simulations from the HOS simulations.

3 Results

3.1 Climate reponse

In CTL-126, an increase in atmospheric CO_2 concentration from 400 ppm to 467 ppm in the 2050s is found, after which the concentration decreases to 432 ppm in 2100 (Fig. 1c). This is accompanied by an increase in global mean surface temperature (GMST) of 1 °C (Fig. 1b), and an AMOC decrease from 17 Sv in 2015 to 9 Sv in 2100 (Fig. 1a). The weakening of the AMOC results in a cooling of the North Atlantic Ocean, while the rest of the Earth warms with largest temperature increases found near the poles (Fig. 2a, b) as a response to the increase in greenhouse gas concentrations. In the water cy-

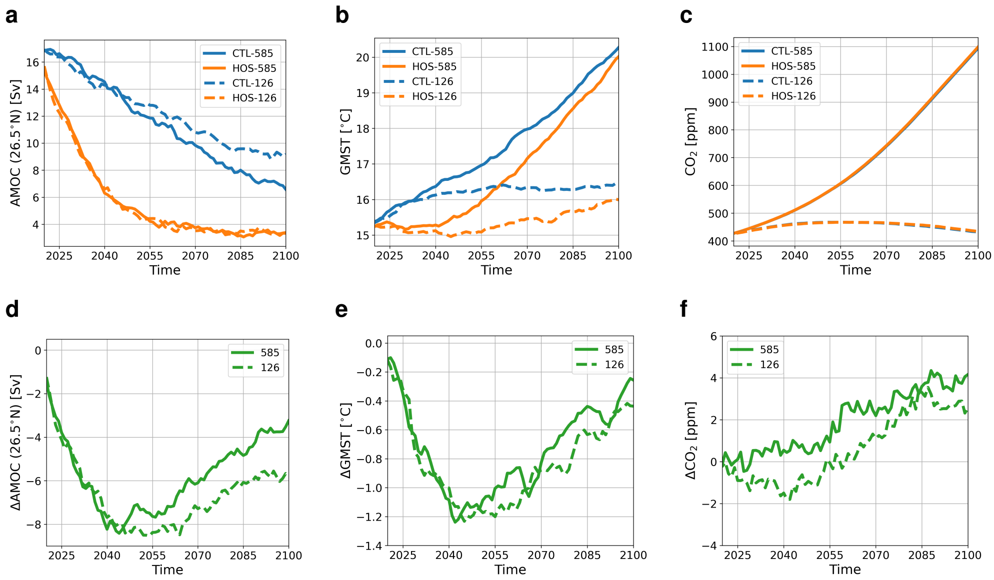

Figure 1. (a) AMOC strength at 26.5°N in Sv. (b) GMST in °C. (c) Atmospheric CO_2 concentration in ppm. In (a-c) blue lines represent the control (CTL) simulations, and orange lines the HOS simulations. (d-f) as in (a-c) but for the difference between the HOS simulations and the control simulations. In all subplots dashed lines represent SSP1-2.6 (126) and solid lines SSP5-8.5 (585).

cle we see a southward shift of the Pacific InterTropical Convergence Zone (ITCZ) of a few degrees (Fig. S2a, b). Furthermore, wind fields in the Northern Hemisphere show a small weakening, whereas in the Southern Hemisphere the winds intensify (Fig. S3a, b).

In CTL-585, the emissions increase the atmospheric CO_2 concentration from 400 ppm to 1094 ppm in 2100 (Fig. 1c) which results in a GMST warming of 5 °C (Fig. 1b). The AMOC weakens from 17 Sv to 7 Sv (Fig. 1a), which leads to a region without warming in the North Atlantic, whereas we see strong warming everywhere else (Fig. 2d, e). There is a strong southward shift of the ITCZ in the Pacific and a moderate shift in the Atlantic Ocean (Fig. S2d, e). The changes in the wind field show similar patterns as CTL-126 but with a larger amplitude (Fig. S3d, e).

The net effect of the AMOC weakening (i.e. HOS minus CTL) is shown in Fig. 1def. In the year 2100, atmospheric CO_2 concentrations are 2.6 ppm and 4.2 ppm higher in HOS-126 and HOS-585 compared to their respective CTL simulations. In both HOS simulations the AMOC quickly weakens from 17 Sv in 2015 to 6 Sv in 2045 after which the AMOC weakening starts to level off until the AMOC is weaker than 4 Sv in 2100 (Fig. 1d). Due to the AMOC weakening we observe a relative cooling of (locally) more than 3 °C in the Northern Hemisphere and warming in the Southern Hemisphere (Fig. 2c, f) (i.e. the bipolar seesaw). The cooling in the Northern Hemisphere results into an increase in sea-ice cover of the Arctic Ocean (Fig. S4), which for HOS-126 persists throughout the entire simulation period. The AMOC weakening also results into a stronger southward shift of the ITCZ in both the Pacific and Atlantic Ocean (Fig. S2c, f), and winds are relatively intensified in the Northern Hemisphere and weakened in the Southern Hemisphere (Fig. S3c, f), with a stronger response in SSP5-8.5.

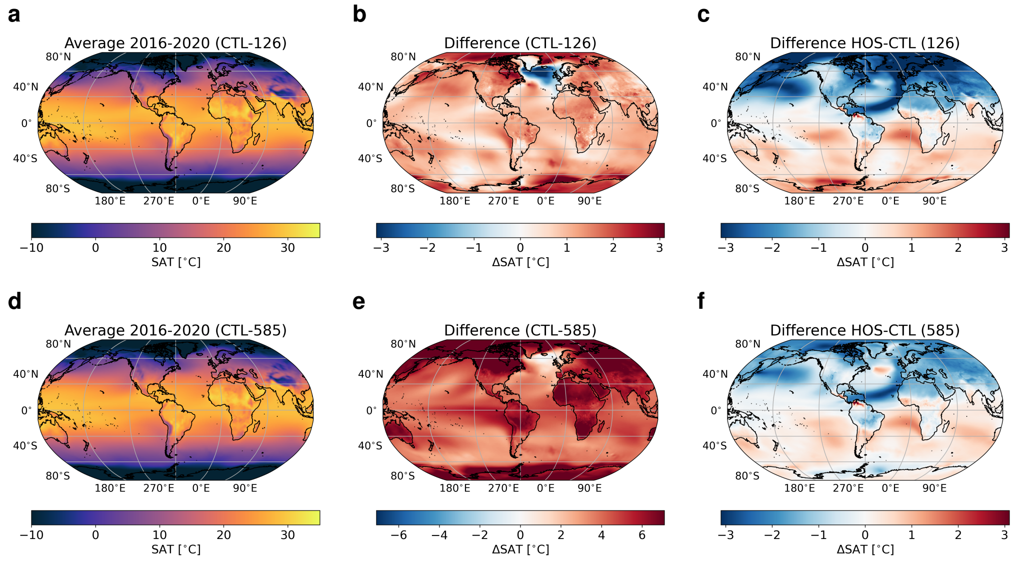

Figure 2. Results for Surface Air Temperature (SAT) in °C. The top row (a-c) is for SSP1-2.6, and the bottom row (d-f) for SSP5-8.5. The left column (a, d) represents the average over 2016-2020 in the control simulations. The middle row (b, e) represents the difference between the average of 2096-2100 and 2016-2020 for the control simulations. The right row (c, f) represents the difference between the HOS and CTL simulations averaged over 2096-2100. Note the different scaling between b and e.

3.2 Marine carbon cycle response

In CTL-126 we see that, integrated over the entire simulation period, there are regions in the ocean with net carbon uptake, and net carbon outgassing (Fig. 3a). The Southern Ocean between 45°S and 60°S, and the equatorial Pacific Ocean, are regions of carbon release from the ocean to the atmosphere. The region of strongest outgassing in the Pacific is located in the upwelling regions on the eastern side of the basin. Carbon uptake generally occurs in the rest of the ocean with the strongest uptake located in the Sea of Japan and the high latitude North Atlantic Ocean. Looking at the development over time (Fig. 4a, b) we see a negative trend over almost the entire ocean, meaning regions which take up carbon in the beginning of the simulation have lower uptake at the end, and regions which emit carbon in 2015 emit more carbon at the end of the simulation. Some regions, e.g. in the Southern Ocean, shift from a carbon uptake region to a region of outgassing.

In CTL-585, also integrated over the simulation period, only the eastern equatorial Pacific shows strong outgassing (Fig. 3d). In the other equatorial basins, there are also some small patches that show net outgassing, but the rest of the ocean shows net carbon uptake. Except for the high latitude North Atlantic Ocean and some small other regions, we see a positive trend (Fig. 4d, e), meaning that regions that take up carbon in the beginning, take up more carbon at the end of the simulation, and regions which show outgassing in the beginning show either reduced outgassing or go from being a region of outgassing to a region of CO_2 uptake. A remarkable region is the high latitude North Atlantic Ocean where the flux from the atmosphere into the ocean strongly decreases while atmospheric pCO_2 almost triples. Integrated over time, the spatial pattern of regions that see increased or decreased exchange with the atmosphere is very sim-

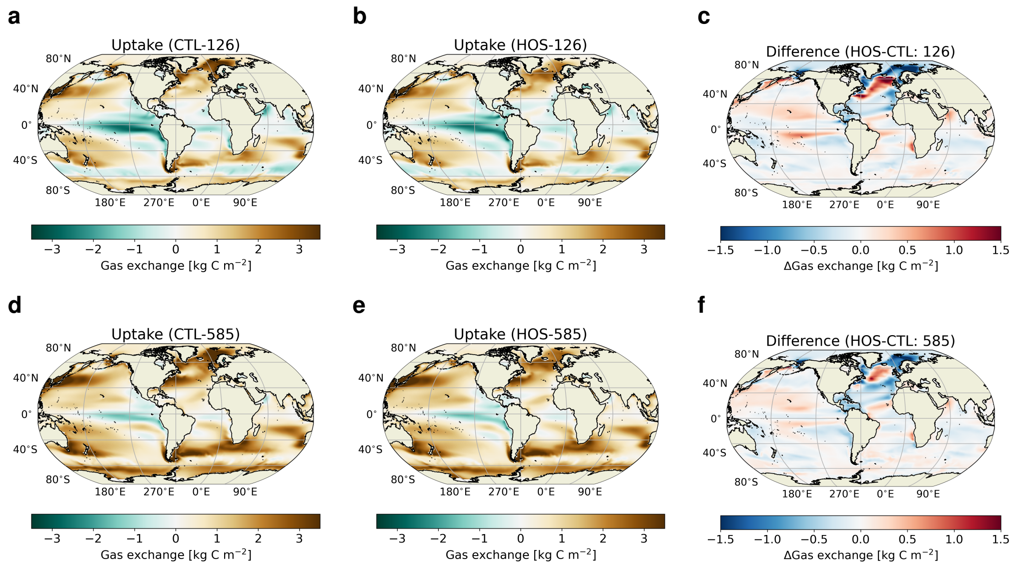

Figure 3. Results for the oceanic CO_2 uptake integrated over the entire simulation period in kg C m^{-2}. The top row (a-c) represents SSP1-2.6 and the bottom row (d-f) represents SSP5-8.5. The left column (a, d) represents the uptake in the control simulations, the middle column (b, e) the uptake in the HOS simulations, and the right column (c, f) the difference between the HOS and CTL simulations. In a, b, d, and e positive values (brown colors) represent net uptake, and negative values (blue colors) represent net outgassing.

ilar for SSP1-2.6 as for SSP5-8.5 (Fig. 3c, f). In total, the ocean takes up 7.4 PgC less due to the AMOC weakening in SSP1-2.6 and 15.6 PgC less in SSP5-8.5 (Fig. 5a, d).

Even though the climate system changes a lot due to the AMOC weakening, the CO_2 uptake of the ocean does not change a lot because of compensating effects. To obtain a better understanding of the mechanisms behind the reduced uptake, we have divided the ocean into 5 basins: the Arctic (north of 66°N), the Southern (south of 35°S), the Atlantic, Pacific and Indian Ocean (Fig. 5b, e). In the response (i.e. HOS-CTL), for both emission scenarios, all basins show the same sign, i.e. more uptake or less uptake due to the AMOC weakening.

In both emission scenarios the Arctic Ocean shows a decreased uptake (-6.0 PgC in SSP1-2.6 and -4.4 PgC in SSP5-8.5), which can be explained by looking at the sea-ice cover (Fig. S4). The cooling in the Northern Hemisphere following the AMOC weakening in the HOS simulations, increases the sea-ice cover. The increase in sea-ice cover has two effects on the uptake of CO_2: (1) it reduces the ocean area available for exchange with the atmosphere; and (2) it increases light limitation and thereby reduces net primary production (NPP; Fig. S6) and the carbon export to the subsurface ocean. In SSP5-8.5 most of the sea ice still disappears due to the strong warming, but in SSP1-2.6 most of the sea ice persists throughout the simulation period, which explains why the Arctic Ocean in SSP1-2.6 responds stronger compared to SSP5-8.5. We also find this effect in the sea-ice covered regions in the North Atlantic (e.g. the Labrador Sea).

The Pacific Ocean takes up more carbon in the HOS than in the CTL simulations (+4.9 PgC in SSP1-2.6 and +1.7 PgC in SSP5-8.5). To analyze what is happening in the Pacific, we considered three different regions: (1) the North Pacific (20°N-66°N), the Equatorial Pacific (20°N-10°S), and the South Pacific (10°S-35°S). In the North Pacific,

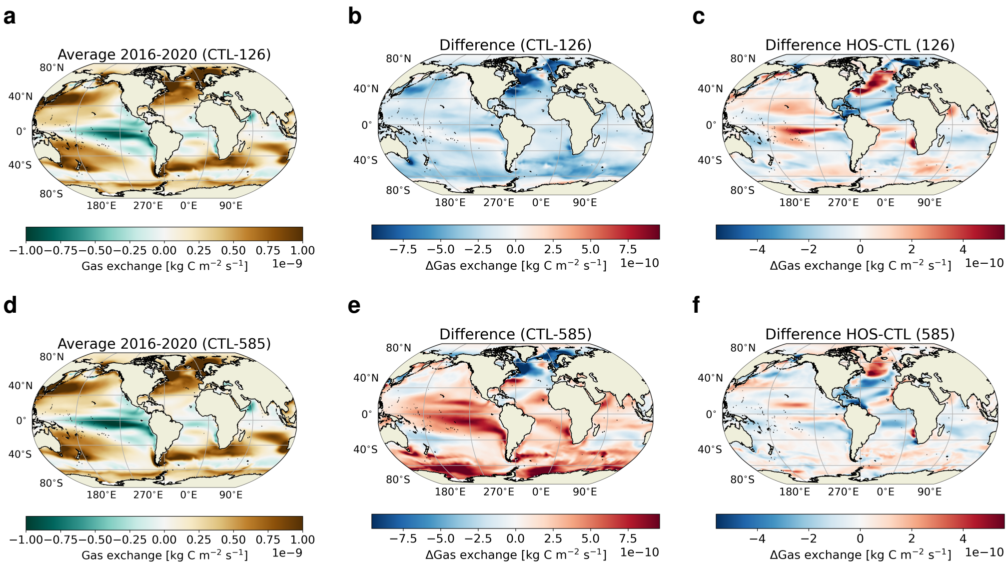

Figure 4. Results for oceanic CO_2 uptake in kg C m^{-2} s^{-1}. Panels represent the same as in Fig. 2. Positive values (brown colors) in a and d represent uptake by the ocean and negative values (blue colors) represent outgassing.

the relative cooling of the surface ocean (Fig. S7) results in an increase of solubility of CO_2 driving increased uptake (Fig. 3e, f). A similar, but opposite, response is seen in the South Pacific. Here the surface ocean becomes relatively warmer inhibiting the uptake of CO_2. The equatorial Pacific is characterized by a band with reduced uptake and one with increased uptake. This can be related to the stronger southward shift of the ITCZ in the Pacific in HOS compared to the CTL (Fig. S2). Due to this shift, the dilutive fluxes related to net precipitation shift southward, causing relative increases of salinity in the northern section due to reduced precipitation, and relative decreases due to increased precipitation in the southern section (Fig. S8). This, in turn, also affects the stratification in these regions with a weakening in the north and a strengthening in the south (Fig. S9). These changes affect the solubility of CO_2 in the equatorial regions causing decreased uptake in the northern section and increased uptake in the southern section.

We find the largest difference in carbon uptake (-2.0 PgC in SSP1-2.6 and -9.3 PgC in SSP5-8.5) in the Atlantic. The regions with sea ice show similar behavior as the Arctic Ocean with decreased uptake related to a larger sea-ice cover in the HOS simulations. In the ice-free subpolar region, an increase in uptake is observed which is associated to decreases in sea surface salinity (SSS; Fig. S8) due to the applied freshwater forcing in this region which promotes the uptake of CO_2. In the subtropical region we generally see a decrease in uptake. To explain this we consider several variables, i.e. SST (Fig. S7), SSS (Fig. S8), DIC (Fig. S12), Alk (Fig. S13) and NPP (Fig. S6), which all show a relative decrease in this region. The net effect of the changes in these variables is a reduction in pH (Fig. S16) and reduced uptake capacity of the ocean. In the Canary Upwelling System and along the North Equatorial Current we do see an increase in NPP (Fig. S6), due to increased nutrient concentrations (Fig. S11) related to increased upwelling of nutrients (Fig. S10 and S15). In the region of the North Equatorial Current this leads to increased uptake of the ocean, and only in SSP5-8.5 also in the Canary Upwelling System. Outside the North Atlantic, large responses are seen in the equatorial region and the Benguela Upwelling System which are characterized by reduced upwelling (Fig. S10),

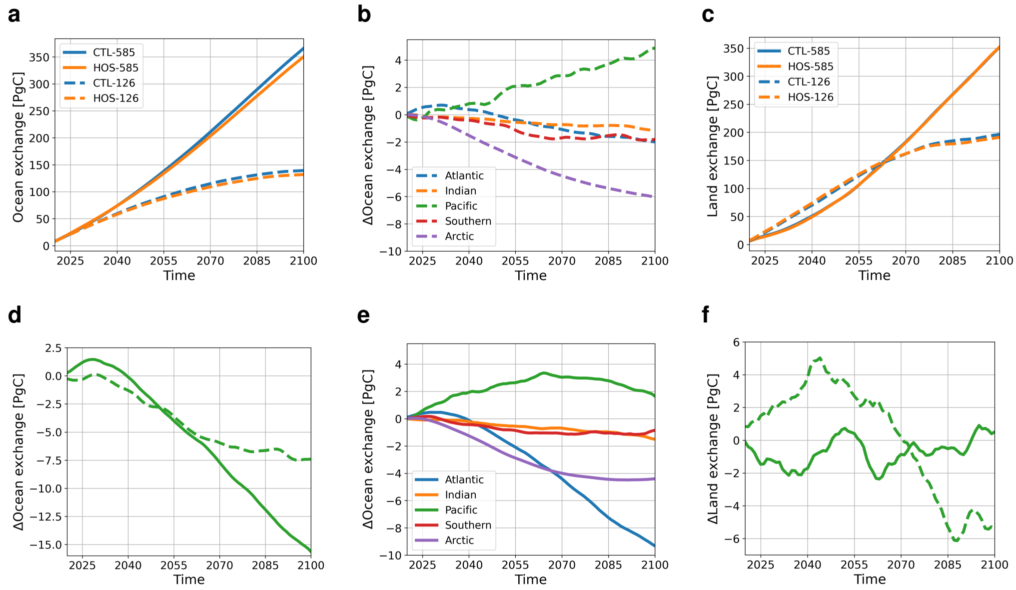

Figure 5. (a) Cumulative uptake of CO_2 in the ocean from 2016 onward in PgC. (b) Difference in the cumulative oceanic CO_2 uptake between the HOS and CTL simulations in SSP1-2.6 for different ocean basins. (c) As (a) but for the land. (d) The difference in the cumulative oceanic CO_2 uptake between the HOS and CTL simulations. (e) As in (b) but for SSP5-8.5. (f) As in (d) but for the land. In a and c blue lines represent the control simulations, and the orange lines the HOS simulations. In all subplots dashed lines represent SSP1-2.6 and solid lines SSP5-8.5. Negative values in b, d-f represent reduced uptake in the HOS simulations compared to the CTL simulations.

promoting additional uptake of CO_2 in the ocean. In the Atlantic Ocean, we find that DIC (Fig. 6) and nutrient (Fig. 7) concentrations decrease in the surface ocean due to the weakening of the AMOC and increase in the deep ocean. The reduction in DIC clearly shows the reduced uptake capacity of the ocean, and the reduction in PO_4 also explains the decrease in NPP (Fig. S6) observed in the Atlantic basin.

The Indian Ocean has a relatively weak response and is very similar for both emission scenarios with a small decrease in uptake (-1.2 PgC in SSP1-2.6 and -1.5 PgC in SSP5-8.5). This is related to the relatively warmer SSTs in the HOS simulations (Fig. S7). The Southern Ocean also has a small decrease in uptake, with a larger decrease in SSP1-2.6 (-1.8 PgC compared to -0.9 PgC in SSP5-8.5). This larger decrease can be explained by the fact that the sea-ice cover is larger in SSP1-2.6 compared to SSP5-8.5 (Fig. S5).

3.3 Terrestrial carbon cycle response

In CTL-126, the terrestrial biosphere, integrated over the entire simulation period, shows a net uptake of CO_2 in most regions (Fig. 8a). The Net Biosphere Production (NBP) maxima are located on the equator for the tropical rainforests, the boreal forests in the high latitude Northern Hemisphere, and the eastern United States and China. The few locations that show net emission of CO_2 are very local and present in the high latitude Northern Hemisphere, the Tibetan Plateau, South East Asia and South America. If we look at the development over time (Fig. 9a, b) we see that the tropical rainforests have

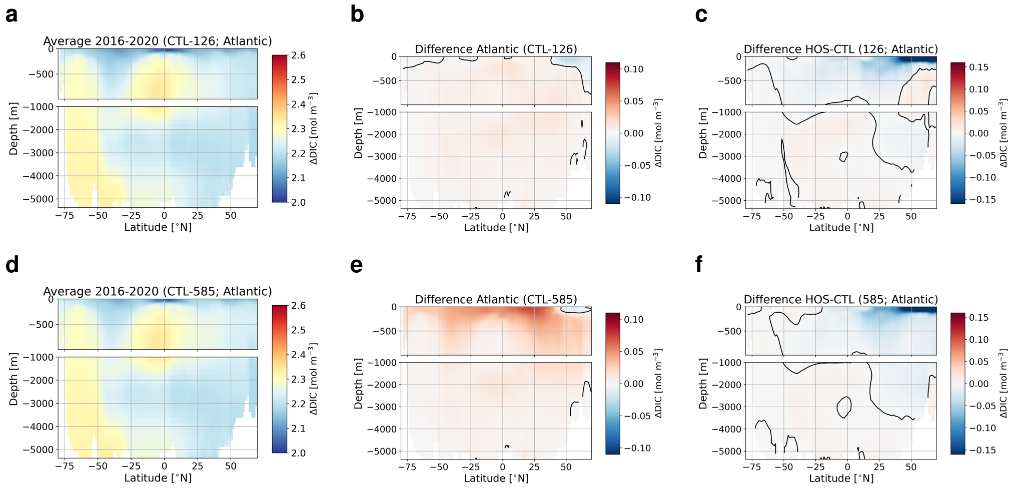

Figure 6. Results for zonally averaged DIC concentrations in the Atlantic basin in mol m^{-3}. Panels represent the same as in Fig. 2. Black contour lines in b, c, e and f represent the 0 mol m^{-3} contour. Note the different scaling of the surface ocean (top 1000 m) compared to the deep ocean.

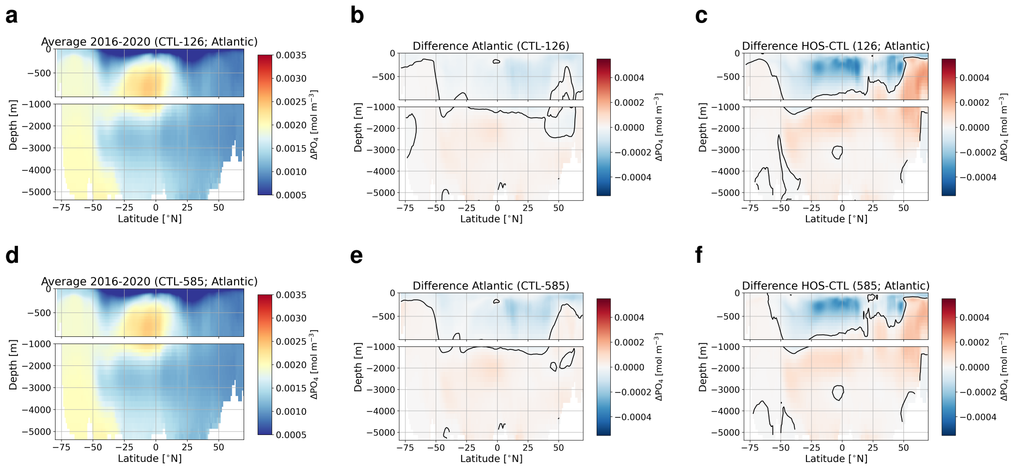

Figure 7. Results for zonally averaged PO_4 concentrations in the Atlantic basin in mol m^{-3}. Panels represent the same as in Fig. 2. Black contour lines in b, c, e and f represent the 0 mol m^{-3} contour. Note the different scaling of the surface ocean (top 1000 m) compared to the deep ocean.

a lower NBP at the end of the simulation. There are some regions that have a higher NBP in 2100, e.g. the boreal forests in Scandinavia.

The response in CTL-585 is very similar to CTL-126 with respect to the spatial pattern, except in central Africa (Fig. 8d). However, the amplitude of the response is much larger due to the CO_2 fertilization effect. Especially the tropical rainforests, but also the boreal forests, show more carbon uptake compared to CTL-126. The same is also true for regions that emit carbon, i.e., the region in the high latitude Northern Hemisphere that emits carbon is larger, and the amount of carbon emitted is also higher. The main difference with respect to CTL-126 is a region in the Congo basin which emits CO_2 in CTL-585 whereas in CTL-126 it is a region of relatively strong uptake, which is possibly related to increased wildfire activity in this region in SSP5-8.5 (Fig. S17). When we look at the development over time (Fig. 9d, e) we find a completely different pattern in CTL-585 compared with CTL-126. The tropical rainforests show an increase in NBP related to the CO_2 fertilization effect whereas northern Siberia shows a decrease related to increased respiration due to permafrost melt (Fig. S19 and S20).

Integrated globally the terrestrial biosphere takes up 5.3 PgC less in SSP1-2.6 and 0.5 PgC more in SSP5-8.5 (Fig. 5) in the HOS simulations compared to the CTL simulations. However, looking at spatial patterns of the cumulative uptake, we see a very similar response to the AMOC weakening (HOS-CTL) for both emission scenarios (Fig. 8c, f). In both emission scenarios we find that the increased southward shift in the ITCZ in the HOS simulations lead to decreased NBP in central America, and increased NBP in Southern America. A similar shift can be seen in Africa, but with a smaller latitudinal shift and amplitude. The shift and amplitude are slightly stronger in SSP1-2.6. The boreal forests become relatively lower in NBP in the HOS simulations with a larger amplitude in SSP1-2.6. This is because in SSP1-2.6, the forests have lower Gross Primary Production (GPP; Fig. S18) over the course of the century which can be related to the relative cooling in the Northern Hemisphere seen in the HOS simulations (Fig. S8). This relative cooling is stronger in SSP1-2.6, related to the increased sea-ice cover and therefore higher albedo in the Arctic. Another effect of the Northern Hemispheric cooling is an increase in NBP in the permafrost regions in Siberia and North America in the HOS simulations. The cooling reduces permafrost melt (Fig. S19) and therefore reduces soil respiration (Fig. S20), with a larger amplitude in Siberia for SSP5-8.5.

3.4 Total response

In total we see an increase of atmospheric CO_2 concentration of 2.6 and 4.2 ppm in 2100 in SSP1-2.6 and SSP5-8.5 due to the AMOC weakening (HOS-CTL). In SSP1-2.6 this response is caused partly due to reduced uptake of the ocean and partly due to reduced uptake of the land. In SSP5-8.5 it is completely driven by the ocean as the globally integrated uptake over the land is approximately the same in CTL-585 as in HOS-585. Eventually the AMOC strength in 2100 has decreased by 5.8 and 3.2 Sv in the HOS simulations compared to the CTL simulations. Under the assumption of linearity, this results in a positive feedback strength of 0.44 ppm Sv^{-1} and 1.3 ppm Sv^{-1} for SSP1-2.6 and SSP5-8.5 respectively. This can be considered a positive feedback since increased CO_2 concentrations in future climates are generally associated with a weakening of the AMOC (e.g. Weijer et al., 2020). This AMOC-pCO_2 feedback is small on the global scale, due to competing effects but locally large changes in carbon uptake can occur.

Fig. 10 gives an overview of the most important climate changes and how the marine and terrestrial respond to these changes. In Fig. 10c, d the difference between SSP1-2.6 and 5-8.5 is highlighted. In the terrestrial biosphere the prime effect of the AMOC weakening is the southward shift of the GPP maxima in the tropical rainforests (Fig. S18). Though this could potentially have beneficial effects for the southern regions, it could have detrimental effects for the northern regions (e.g. the Sahel region) and could for example increase the latitudinal extent of the Sahara desert. This shift, caused by a shift in precipitation (Fig. S2), also has effects for the probability of wildfires (Fig. S17), which can increase in regions with reduced precipitation. We cannot conclude whether the AMOC

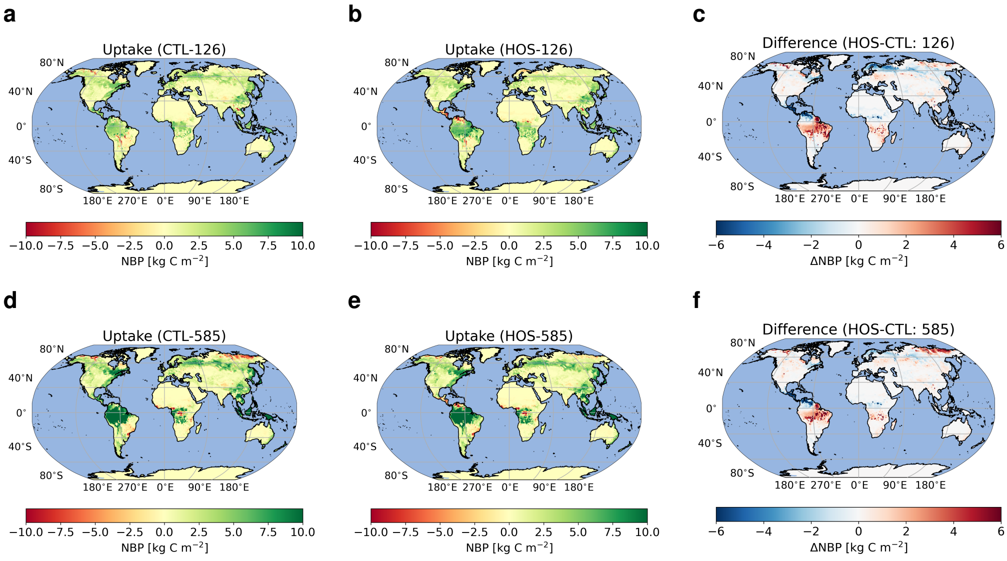

Figure 8. Results for the CO_2 exchange with the land integrated over the entire simulation period in kg C m^{-2}. The top row (a-c) represents SSP1-2.6 and the bottom row (d-f) represents SSP5-8.5. The left column (a, d) represents the uptake in the control simulations, the middle column (b, e) the uptake in the HOS simulations, and the right column (c, f) the difference between the HOS and CTL simulations. In a, b, d, and e green colors represent net CO_2 uptake by the land, and red colors represent net emissions into the atmosphere.

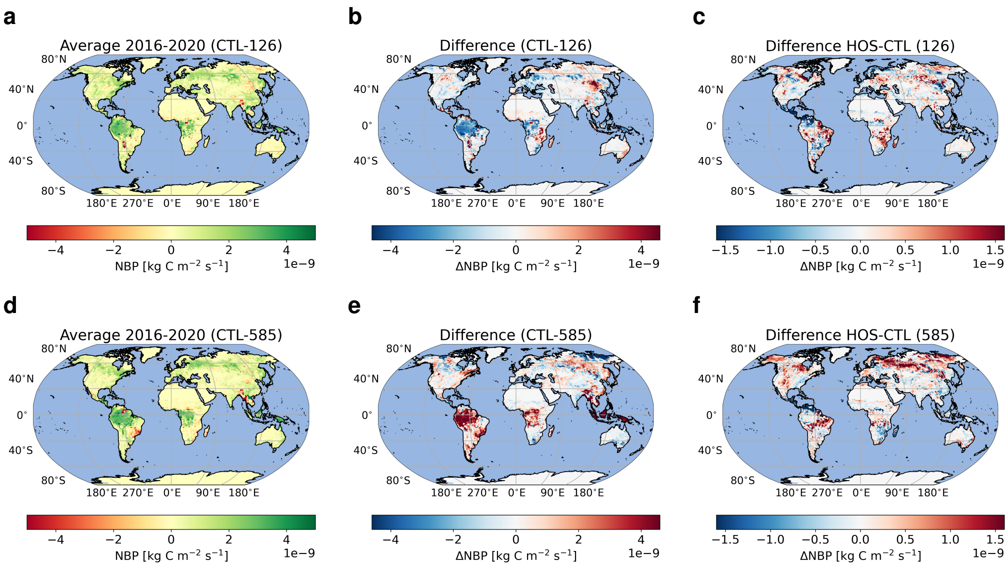

Figure 9. Results for Net Biosphere Production (NBP) in kg C m^{-2} s^{-1}. Panels represent the same as in Fig. 2. Green colors represent uptake of CO_2 into the land and red colors represent emission of CO_2 to the atmosphere.

weakening would result into a collapse of the Amazonian rainforests or an increase in the Sahara desert since the model is used without a dynamic vegetation model. In the ocean, a decrease in NPP (Fig. S6) and surface nutrient concentrations (Fig. S11) occurs. The changes in NPP can have effects on the entire food web and thereby have a negative impact on ecosystems and ecosystem functions. If the trend of the surface ocean becoming more depleted of nutrients (Fig. 7) continues, this might drive a large decline in NPP for the coming centuries. Another important effect of the AMOC weakening is increased ocean acidification (i.e. a decrease in pH; Fig. S16). Lower pH values increase the stress on calcifying organisms and reduces the uptake capacity of the ocean, which might increase the AMOC-pCO_2 feedback strength on longer timescales.

In many climate and carbon cycle variables we see a similar response in spatial pattern, but sometimes with a slightly different amplitude (Fig. 10c, d). In the terrestrial biosphere, the main differences are seen in the boreal forests in Scandinavia and Russia (box 1 in Fig. 10), and in the Siberian permafrost regions (box 2). The difference in the boreal forests can be explained by looking at the temperature differences between the HOS and CTL simulations. In SSP1-2.6, the northern hemisphere cools more, which causes increased GPP reduction in the boreal forests. For the permafrost region we find a stronger response in SSP5-8.5, because in SSP1-2.6 there is not much permafrost melt in the CTL simulation; therefore the additional cooling in the HOS simulation does not have a large effect on the permafrost melt. In the ocean, we find the largest changes in the subpolar North Atlantic and the Arctic sea-ice regions (boxes 7 and 8 in Fig. 10). In the subpolar region there is a relatively stronger decrease in SSS and SST (Fig. S7 and S8) in SSP1-2.6 compared to 5-8.5 leading to a larger increase in solubility of CO_2 and therefore more uptake. Because of the increased cooling, and lower background temperatures in SSP1-2.6, sea-ice cover does not diminish over the simulation whereas in SSP5-8.5 we see in both simulations a strong reduction in sea-ice cover (Fig. S4). This is the reason why we see a stronger reduction in the Arctic in SSP1-2.6.

4 Summary and discussion

In this study, we have investigated the carbon cycle response to a weakening of the Atlantic Meridional Overturning Circulation (AMOC) under climate change scenarios. We did this by forcing a state-of-the-art Earth System Model, the Community Earth System Model v2 (CESM2), on a nominal 1° resolution with emissions from two different SSP scenarios (SSP1-2.6 and SSP5-8.5) and an additional freshwater flux in the North Atlantic to artificially decrease the AMOC. To our knowledge, this is the first study that utilizes a model of this high complexity with a horizontal resolution of 1° to study the effects of an AMOC weakening on the carbon cycle. We find a positive feedback in both emission scenarios of 0.44 ppm Sv^{-1} and 1.3 ppm Sv^{-1} for SSP1-2.6 and SSP5-8.5, respectively. The response in SSP1-2.6 is driven by both the land and ocean carbon reservoirs, whereas in SSP5-8.5 it is driven solely by the ocean. The response is small, being the effect of many compensating effects over both the land and the ocean. Looking at regional response patterns, both emission scenarios show similar behavior in many climate and carbon cycle variables. In absolute numbers, the response is stronger in SSP5-8.5, but when the high CO_2 concentrations are taken into account, the relative response is actually weaker in SSP5-8.5 compared to SSP1-2.6.

Our simulations show the climate response to an AMOC weakening, such as a southward shift of the ITCZ and the bipolar seesaw, similar to many previous studies (Obata, 2007; Zickfeld et al., 2008; Orihuela-Pinto et al., 2022). The AMOC weakening in our simulations follows a very similar trajectory as in Orihuela-Pinto et al. (2022), which used an older version of CESM (i.e. v1.2) under pre-industrial boundary conditions. In our study, the AMOC weakening results in a small increase in atmospheric CO_2 concentrations. This small effect, especially on the multi-decadal to centennial timescales assessed here, was also found in more idealized models (e.g. Zickfeld et al., 2008; Nielsen et al., 2019; Gottschalk et al., 2019), but as described in Gottschalk et al. (2019) the relative response of the ocean and land reservoirs are dependent on climatic boundary conditions and the used model. Here, we have used a member of the newest generation of Earth System Models with a relatively high spatial resolution (i.e. nominal 1°× 1° ocean grid). When considering studies with induced AMOC weakening we find, integrated over the entire ocean, a similar response as in Zickfeld et al. (2008), and spatially as in Obata (2007), though local differences remain which can be attributed to the use of a higher resolution, and a more complex model in our study. It is also possible to collapse the AMOC without an additional freshwater forcing. In Nielsen et al. (2019) they used such an alternative method under Pleistocene conditions, which resulted in a much slower response in the ocean compared to our simulations. The response of the terrestrial biosphere, especially the changes related to the southward shift of the ITCZ, is also similar to that of previous studies using static vegetation (e.g. Obata, 2007; Nielsen et al., 2019). In Köhler et al. (2005) a dynamic vegetation model is used, and they show that an AMOC collapse affects vegetation type. This leads to reduced carbon storage in the high latitudes and increased carbon storage in the Northern Hemisphere midlatitudes. This dynamic behavior is not captured in our simulations and unfortunately, it is not possible to assess what the effect of dynamic vegetation would be based on Köhler et al. (2005) since they consider Pleistocene conditions.

The result that the pattern of the carbon cycle response to an AMOC weakening is independent of the cumulative CO_2 emissions on multi-decadal to centennial timescales has been shown before. In Zickfeld et al. (2008), for example, the marine carbon cycle remains independent on the used emission scenario for the first 200 years of their simulation, and for the terrestrial carbon cycle this is 150 years. After this period the different emissions start to diverge, though the qualitative behavior remains similar. In our simulations, globally integrated variables show little change as a response to the AMOC weakening. However, on regional scales the effects of an AMOC weakening can be large, e.g. SATs can decrease or increase by more than 3 °C locally (Fig. 2) and some regions become much drier and other see a large increase in precipitation (Fig. S2). These changing climate conditions, on top of already greenhouse gas driven climate change, require climate adaptation which might be difficult to achieve in such a short time frame (i.e. decades). The climate changes associated to an AMOC weakening also cause changes in the carbon cycle. Such changes can increase, for example, desertification and reduce (but also increase) crop yields. This may lead locally to increased food stress, potentially leading to more frequent and more severe famines. The changes in the ocean can lead to more frequent marine heatwaves in the Southern Hemisphere due to the warming, and reduced (global) NPP due to changing nutrient distributions, which might impact food web dynamics and ecosystem function. However, due to the cooling effect of the bipolar seesaw we would can also expect a (relative) reduction in marine heatwaves in the Northern Hemisphere. These effects show that an AMOC collapse can have local effects that have a beneficiary impact or a detrimental impact on the terrestrial and marine biospheres.

Interestingly, the relative effects on multi-decadal timescales are independent to the (cumulative) greenhouse gas emissions. This means that the uncertainty around the effects of a possible AMOC collapse or weakening is not related to past emissions. However, in a future climate without AMOC weakening, emissions do have an influence on when the AMOC might collapse. Furthermore, the small positive feedback found in this study might make the AMOC more likely to tip earlier. Even though on these timescales the relative effects are not dependent on the greenhouse gas emissions, this might be different on intermediate (multi-centennial to millennial) timescales. Because the ocean circulation is associated with timescales on the intermediate timescales, we can expect the most important effects to occur in this time frame. We find, for example, that the surface ocean is becoming more depleted of nutrients (Fig. 7), which might depress NPP for centuries.

Other long term effects that might be relevant are tipping cascades (e.g. Dekker et al., 2018), meaning that a collapse of the AMOC could set off an other tipping element in the Earth System. In our simulations, we find decreasing temperatures in the Northern Hemisphere due to the AMOC weakening, which reduces the probability of tipping for example melting of the Greenland Ice Sheet, Arctic sea ice, and Northern Hemispheric permafrost. However, due to the bipolar seesaw, the Southern Hemisphere becomes warmer, which might increase the probability of tipping the Antarctic Ice Sheets. Another tipping point connected to the AMOC is the die off of the Amazonian rainforest. Because we do not use a dynamic vegetation model in this study, we cannot investigate whether the AMOC weakening in our simulations would lead to such a die off.

By using a low and a high emission scenario we have tried to cover uncertainties regarding future emissions. However, we have only used one Earth System Model, which means that the results presented here could be model dependent. Especially ocean productivity shows large spread in the CMIP6 ensemble, which can influence the uptake capacity of the ocean. Another bias in Earth System Models is a too stable AMOC, meaning we need a large freshwater flux in the North Atlantic Ocean to weaken the AMOC. This flux is generally too high to represent for example Greenland Ice Sheet melt, but necessary to achieve a weakened AMOC. This large freshwater flux also leads to freshening of the surface ocean in the subpolar gyre which influences the carbonate chemistry and carbon uptake capacity unrealistically. We have not taken this effect into account explicitly, but it could potentially result in reduced uptake capacity of the ocean, and therefore more CO_2 in the atmosphere, increasing the feedback strength.

Finally, we have shown in a relatively high resolution, state-of-the-art Earth System Model, that the spatial pattern of the carbon cycle response to an AMOC weakening is not dependent on cumulative CO_2 emissions. As a follow up study it would be interesting to see what happens on multi-centennial and longer timescales, and what the pCO_2 response would be under an AMOC recovery. Though not analyzed thoroughly, NPP in the ocean shows large decreases due to the AMOC weakening. This could effect food web dynamics in the ocean with possible (detrimental) changes in fishery yields, food securities and income. These ecosystem and socio-economic effects are worth investigating, to see how a change in the climate system cascades through ecosystems to socio-economic systems.

Appendix A Open Science

Yearly output for the most important variables, data necessary to replicate the figures, and the scripts used for creating the figures can be downloaded from `https://doi.org/10.5281/zenodo.8376701` (Boot et al., 2023b).

Acknowledgments

This study has been supported by the Netherlands Earth System Science Centre (NESSC), which is financially supported by the Ministry of Education, Culture and Science (OCW; grant no. 024.002.001). The authors want to thank Michael Kliphuis (IMAU, Utrecht University) for performing the CESM2 simulations, which were performed at at SURFsara in Amsterdam on the Dutch Supercomputer Snellius within NWO-SURF project 17239.

References

Behrenfeld, M. J., O'Malley, R. T., Siegel, D. A., McClain, C. R., Sarmiento, J. L., Feldman, G. C., . . . Boss, E. S. (2006). Climate-driven trends in contemporary ocean productivity. *Nature*, *444* (7120), 752–755. Retrieved from `https://doi.org/10.1038/nature05317` doi: 10.1038/nature05317

Boot, A., von der Heydt, A. S., & Dijkstra, H. A. (2022). Effect of the Atlantic Meridional Overturning Circulation on atmospheric pCO$_{2}$ variations. *Earth System Dynamics*, *13*(3), 1041–1058. Retrieved from `https://esd.copernicus.org/articles/13/1041/2022/` doi: 10.5194/esd-13-1041-2022

Boot, A., von der Heydt, A. S., & Dijkstra, H. A. (2023a). Effect of Plankton Composition Shifts in the North Atlantic on Atmospheric pCO2. *Geophysical Research Letters*, *50*(2), e2022GL100230. Retrieved from `https://agupubs.onlinelibrary.wiley.com/doi/abs/10.1029/2022GL100230` doi: https://doi.org/10.1029/2022GL100230

Boot, A., von der Heydt, A. S., & Dijkstra, H. A. (2023b, September). *GBC_2023: v1.1_25_09_23 (v1.1).* [dataset]. Zenodo. doi: 10.5281/zenodo.8376701

Buckley, M. W., & Marshall, J. (2016, mar). Observations, inferences, and mechanisms of the Atlantic Meridional Overturning Circulation: A review. *Reviews of Geophysics*, *54*(1), 5–63. Retrieved from `https://doi.org/10.1002/2015RG000493` doi: https://doi.org/10.1002/2015RG000493

Burke, E. J., Zhang, Y., & Krinner, G. (2020). Evaluating permafrost physics in the Coupled Model Intercomparison Project 6 (CMIP6) models and their sensitivity to climate change. *The Cryosphere*, *14*(9), 3155–3174. Retrieved from `https://tc.copernicus.org/articles/14/3155/2020/` doi: 10.5194/tc-14-3155-2020

Caesar, L., Rahmstorf, S., Robinson, A., Feulner, G., & Saba, V. (2018). Observed fingerprint of a weakening Atlantic Ocean overturning circulation. *Nature*, *556*(7700), 191–196. Retrieved from `https://doi.org/10.1038/s41586-018-0006-5` doi: 10.1038/s41586-018-0006-5

Cheng, W., Weijer, W., Kim, W. M., Danabasoglu, G., Yeager, S. G., Gent, P. R., ... Zhang, J. (2018). Can the Salt-Advection Feedback Be Detected in Internal Variability of the Atlantic Meridional Overturning Circulation? *Journal of Climate*, *31*(16), 6649–6667. Retrieved from `https://journals.ametsoc.org/view/journals/clim/31/16/jcli-d-17-0825.1.xml` doi: https://doi.org/10.1175/JCLI-D-17-0825.1

Cuffey, K. M., & Clow, G. D. (1997, nov). Temperature, accumulation, and ice sheet elevation in central Greenland through the last deglacial transition. *Journal of Geophysical Research: Oceans*, *102*(C12), 26383–26396. Retrieved from `https://doi.org/10.1029/96JC03981` doi: https://doi.org/10.1029/96JC03981

Danabasoglu, G. (2019). *NCAR CESM2 model output prepared for CMIP6 CMIP esm-hist.* Earth System Grid Federation. Retrieved from `https://doi.org/10.22033/ESGF/CMIP6.7575` doi: 10.22033/ESGF/CMIP6.7575

Danabasoglu, G., Lamarque, J.-F., Bacmeister, J., Bailey, D. A., DuVivier, A. K., Edwards, J., ... Strand, W. G. (2020). The Community Earth System Model Version 2 (CESM2). *Journal of Advances in Modeling Earth Systems*, *12*(2), e2019MS001916. Retrieved from `https://doi.org/10.1029/2019MS001916` doi: https://doi.org/10.1029/2019MS001916

Dekker, M. M., von der Heydt, A. S., & Dijkstra, H. A. (2018). Cascading transitions in the climate system. *Earth System Dynamics*, *9*(4), 1243–1260. Retrieved from `https://esd.copernicus.org/articles/9/1243/2018/` doi: 10.5194/esd-9-1243-2018

Ditlevsen, P., & Ditlevsen, S. (2023). Warning of a forthcoming collapse of the Atlantic meridional overturning circulation. *Nature Communications*, *14*(1), 4254.

Eyring, V., Bony, S., Meehl, G. A., Senior, C. A., Stevens, B., Stouffer, R. J., & Taylor, K. E. (2016, may). Overview of the Coupled Model Intercomparison Project Phase 6 (CMIP6) experimental design and organization. *Geosci. Model Dev.*, *9*(5), 1937–1958. Retrieved from `https://gmd.copernicus.org/`

articles/9/1937/2016/https://gmd.copernicus.org/articles/9/1937/2016/gmd-9-1937-2016.pdf doi: 10.5194/gmd-9-1937-2016

Gottschalk, J., Battaglia, G., Fischer, H., Frölicher, T. L., Jaccard, S. L., Jeltsch-Thömmes, A., … Stocker, T. F. (2019). Mechanisms of millennial-scale atmospheric CO2 change in numerical model simulations. *Quaternary Science Reviews*, *220*, 30–74. Retrieved from http://www.sciencedirect.com/science/article/pii/S0277379118310473 doi: https://doi.org/10.1016/j.quascirev.2019.05.013

Henson, S. A., Laufkötter, C., Leung, S., Giering, S. L. C., Palevsky, H. I., & Cavan, E. L. (2022). Uncertain response of ocean biological carbon export in a changing world. *Nature Geoscience*, *15*(4), 248–254. Retrieved from https://doi.org/10.1038/s41561-022-00927-0 doi: 10.1038/s41561-022-00927-0

Jackson, L. C., Kahana, R., Graham, T., Ringer, M. A., Woollings, T., Mecking, J. V., & Wood, R. A. (2015). Global and European climate impacts of a slowdown of the AMOC in a high resolution GCM. *Climate Dynamics*, *45*(11), 3299–3316. Retrieved from https://doi.org/10.1007/s00382-015-2540-2 doi: 10.1007/s00382-015-2540-2

Katavouta, A., & Williams, R. G. (2021). Ocean carbon cycle feedbacks in CMIP6 models: contributions from different basins. *Biogeosciences*, *18*(10), 3189–3218. Retrieved from https://bg.copernicus.org/articles/18/3189/2021/ doi: 10.5194/bg-18-3189-2021

Köhler, P., Joos, F., Gerber, S., & Knutti, R. (2005). Simulated changes in vegetation distribution, land carbon storage, and atmospheric CO2 in response to a collapse of the North Atlantic thermohaline circulation. *Climate Dynamics*, *25*(7), 689. Retrieved from https://doi.org/10.1007/s00382-005-0058-8 doi: 10.1007/s00382-005-0058-8

Kwiatkowski, L., Torres, O., Bopp, L., Aumont, O., Chamberlain, M., Christian, J. R., … Ziehn, T. (2020). Twenty-first century ocean warming, acidification, deoxygenation, and upper-ocean nutrient and primary production decline from CMIP6 model projections. *Biogeosciences*, *17*(13), 3439–3470. Retrieved from https://bg.copernicus.org/articles/17/3439/2020/ doi: 10.5194/bg-17-3439-2020

Lawrence, D. M., Fisher, R. A., Koven, C. D., Oleson, K. W., Swenson, S. C., Bonan, G., … Zeng, X. (2019, dec). The Community Land Model Version 5: Description of New Features, Benchmarking, and Impact of Forcing Uncertainty. *Journal of Advances in Modeling Earth Systems*, *11*(12), 4245–4287. Retrieved from https://doi.org/10.1029/2018MS001583 doi: https://doi.org/10.1029/2018MS001583

Lenton, T. M., Held, H., Kriegler, E., Hall, J. W., Lucht, W., Rahmstorf, S., & Schellnhuber, H. J. (2008). Tipping elements in the Earth's climate system. *Proceedings of the National Academy of Sciences*, *105*(6), 1786–1793. Retrieved from https://www.pnas.org/doi/abs/10.1073/pnas.0705414105 doi: 10.1073/pnas.0705414105

Liu, Y., Moore, J. K., Primeau, F., & Wang, W. L. (2023). Reduced CO2 uptake and growing nutrient sequestration from slowing overturning circulation. *Nature Climate Change*, *13*(1), 83–90. Retrieved from https://doi.org/10.1038/s41558-022-01555-7 doi: 10.1038/s41558-022-01555-7

Long, M. C., Moore, J. K., Lindsay, K., Levy, M., Doney, S. C., Luo, J. Y., … Sylvester, Z. T. (2021). Simulations With the Marine Biogeochemistry Library (MARBL). *Journal of Advances in Modeling Earth Systems*, *13*(12), e2021MS002647. Retrieved from https://doi.org/10.1029/2021MS002647 doi: https://doi.org/10.1029/2021MS002647

Lynch-Stieglitz, J. (2017). The Atlantic Meridional Overturning Circulation and Abrupt Climate Change. *Annual Review of Marine Science*, *9*(1), 83–104. Retrieved from https://doi.org/10.1146/annurev-marine-010816-060415 doi: 10.1146/annurev-marine-010816-060415

Marchal, O., Stocker, T. F., & Joos, F. (1998, jun). Impact of oceanic reorganizations on the ocean carbon cycle and atmospheric carbon dioxide content. *Paleoceanography*, *13*(3), 225–244. Retrieved from https://doi.org/10.1029/98PA00726 doi: https://doi.org/10.1029/98PA00726

McKay, D. I. A., Staal, A., Abrams, J. F., Winkelmann, R., Sakschewski, B., Loriani, S., … Lenton, T. M. (2022). Exceeding 1.5°C global warming could trigger multiple climate tipping points. *Science*, *377*(6611), eabn7950. Retrieved from https://www.science.org/doi/abs/10.1126/science.abn7950 doi: 10.1126/science.abn7950

Nielsen, S. B., Jochum, M., Pedro, J. B., Eden, C., & Nuterman, R. (2019, apr). Two-Timescale Carbon Cycle Response to an AMOC Collapse. *Paleoceanography and Paleoclimatology*, *34*(4), 511–523. Retrieved from https://doi.org/10.1029/2018PA003481 doi: https://doi.org/10.1029/2018PA003481

Nohara, D., Yoshida, Y., Misumi, K., & Ohba, M. (2013, mar). Dependency of climate change and carbon cycle on CO2 emission pathways. *Environmental Research Letters*, *8*(1), 14047. Retrieved from https://dx.doi.org/10.1088/1748-9326/8/1/014047 doi: 10.1088/1748-9326/8/1/014047

Obata, A. (2007, dec). Climate Carbon Cycle Model Response to Freshwater Discharge into the North Atlantic. *Journal of Climate - J CLIMATE*, *20*, 5962–5976. doi: 10.1175/2007JCLI1808.1

O'Neill, B. C., Carter, T. R., Ebi, K., Harrison, P. A., Kemp-Benedict, E., Kok, K., … Pichs-Madruga, R. (2020). Achievements and needs for the climate change scenario framework. *Nature Climate Change*, *10*(12), 1074–1084. Retrieved from https://doi.org/10.1038/s41558-020-00952-0 doi: 10.1038/s41558-020-00952-0

Orihuela-Pinto, B., England, M. H., & Taschetto, A. S. (2022). Interbasin and interhemispheric impacts of a collapsed Atlantic Overturning Circulation. *Nature Climate Change*, *12*(6), 558–565. Retrieved from https://doi.org/10.1038/s41558-022-01380-y doi: 10.1038/s41558-022-01380-y

Rahmstorf, S. (2002). Ocean circulation and climate during the past 120,000 years. *Nature*, *419*(6903), 207–214. Retrieved from https://doi.org/10.1038/nature01090 doi: 10.1038/nature01090

Sarmiento, J. L., Hughes, T. M. C., Stouffer, R. J., & Manabe, S. (1998). Simulated response of the ocean carbon cycle to anthropogenic climate warming. *Nature*, *393*(6682), 245–249. Retrieved from https://doi.org/10.1038/30455 doi: 10.1038/30455

Schmittner, A. (2005). Decline of the marine ecosystem caused by a reduction in the Atlantic overturning circulation. *Nature*, *434*(7033), 628–633. Retrieved from https://doi.org/10.1038/nature03476 doi: 10.1038/nature03476

Schmittner, A., & Galbraith, E. D. (2008). Glacial greenhouse-gas fluctuations controlled by ocean circulation changes. *Nature*, *456*(7220), 373–376. Retrieved from https://doi.org/10.1038/nature07531 doi: 10.1038/nature07531

Smith, R., Jones, P. W., Briegleb, P. A., Bryan, O., Danabasoglu, G., Dennis, M. L., … Yeager, S. G. (2010). The Parallel Ocean Program (POP) reference manual: Ocean component of the Community Climate System Model (CCSM)..

Swingedouw, D., Bopp, L., Matras, A., & Braconnot, P. (2007, dec). Effect of land-ice melting and associated changes in the AMOC result in little overall impact on oceanic CO2 uptake. *Geophysical Research Letters*, *34*(23). Retrieved from https://doi.org/10.1029/2007GL031990 doi: https://doi.org/10.1029/2007GL031990

Tagliabue, A., Kwiatkowski, L., Bopp, L., Butenschön, M., Cheung, W., Lengaigne, M., & Vialard, J. (2021). Persistent Uncertainties in Ocean Net Primary Production Climate Change Projections at Regional Scales Raise Challenges for Assessing Impacts on Ecosystem Services. *Frontiers in Climate*, *3*. Retrieved from https://www.frontiersin.org/articles/10.3389/fclim.2021.738224 doi: 10.3389/fclim.2021.738224

Vellinga, M., & Wood, R. A. (2002). Global Climatic Impacts of a Collapse of the Atlantic Thermohaline Circulation. *Climatic Change*, *54*(3), 251–267. Retrieved from https://doi.org/10.1023/A:1016168827653 doi: 10.1023/A:1016168827653

Weijer, W., Cheng, W., Drijfhout, S. S., Fedorov, A. V., Hu, A., Jackson, L. C., ... Zhang, J. (2019, aug). Stability of the Atlantic Meridional Overturning Circulation: A Review and Synthesis. *Journal of Geophysical Research: Oceans*, *124*(8), 5336–5375. Retrieved from https://doi.org/10.1029/2019JC015083 doi: https://doi.org/10.1029/2019JC015083

Weijer, W., Cheng, W., Garuba, O. A., Hu, A., & Nadiga, B. T. (2020, jun). CMIP6 Models Predict Significant 21st Century Decline of the Atlantic Meridional Overturning Circulation. *Geophysical Research Letters*, *47*(12), e2019GL086075. Retrieved from https://doi.org/10.1029/2019GL086075 doi: https://doi.org/10.1029/2019GL086075

Whitt, D. B., & Jansen, M. F. (2020, jul). Slower nutrient stream suppresses Subarctic Atlantic Ocean biological productivity in global warming. *Proceedings of the National Academy of Sciences*, *117*(27), 15504–15510. Retrieved from https://doi.org/10.1073/pnas.2000851117 doi: 10.1073/pnas.2000851117

Wilson, J. D., Andrews, O., Katavouta, A., de Melo Viríssimo, F., Death, R. M., Adloff, M., ... Ying, R. (2022). The biological carbon pump in CMIP6 models: 21st century trends and uncertainties. *Proceedings of the National Academy of Sciences*, *119*(29), e2204369119. Retrieved from https://www.pnas.org/doi/abs/10.1073/pnas.2204369119 doi: 10.1073/pnas.2204369119

Yamamoto, A., Abe-Ouchi, A., & Yamanaka, Y. (2018). Long-term response of oceanic carbon uptake to global warming via physical and biological pumps. *Biogeosciences*, *15*(13), 4163–4180. Retrieved from https://bg.copernicus.org/articles/15/4163/2018/ doi: 10.5194/bg-15-4163-2018

Zhang, R., & Delworth, T. L. (2005). Simulated Tropical Response to a Substantial Weakening of the Atlantic Thermohaline Circulation. *Journal of Climate*, *18*(12), 1853–1860. Retrieved from https://journals.ametsoc.org/view/journals/clim/18/12/jcli3460.1.xml doi: https://doi.org/10.1175/JCLI3460.1

Zhu, J., Zeng, X., Gao, X., & Zhang, H. (2022). Response of Terrestrial Net Primary Production to Quadrupled CO2 Forcing: A Comparison between the CAS-ESM2 and CMIP6 Models. *Biology*, *11*(12). Retrieved from https://doi.org/10.3390/biology11121693 doi: https://doi.org/10.3390/biology11121693

Zickfeld, K., Eby, M., & Weaver, A. J. (2008, sep). Carbon-cycle feedbacks of changes in the Atlantic meridional overturning circulation under future atmospheric CO2. *Global Biogeochemical Cycles*, *22*(3). Retrieved from https://doi.org/10.1029/2007GB003118 doi: https://doi.org/10.1029/2007GB003118

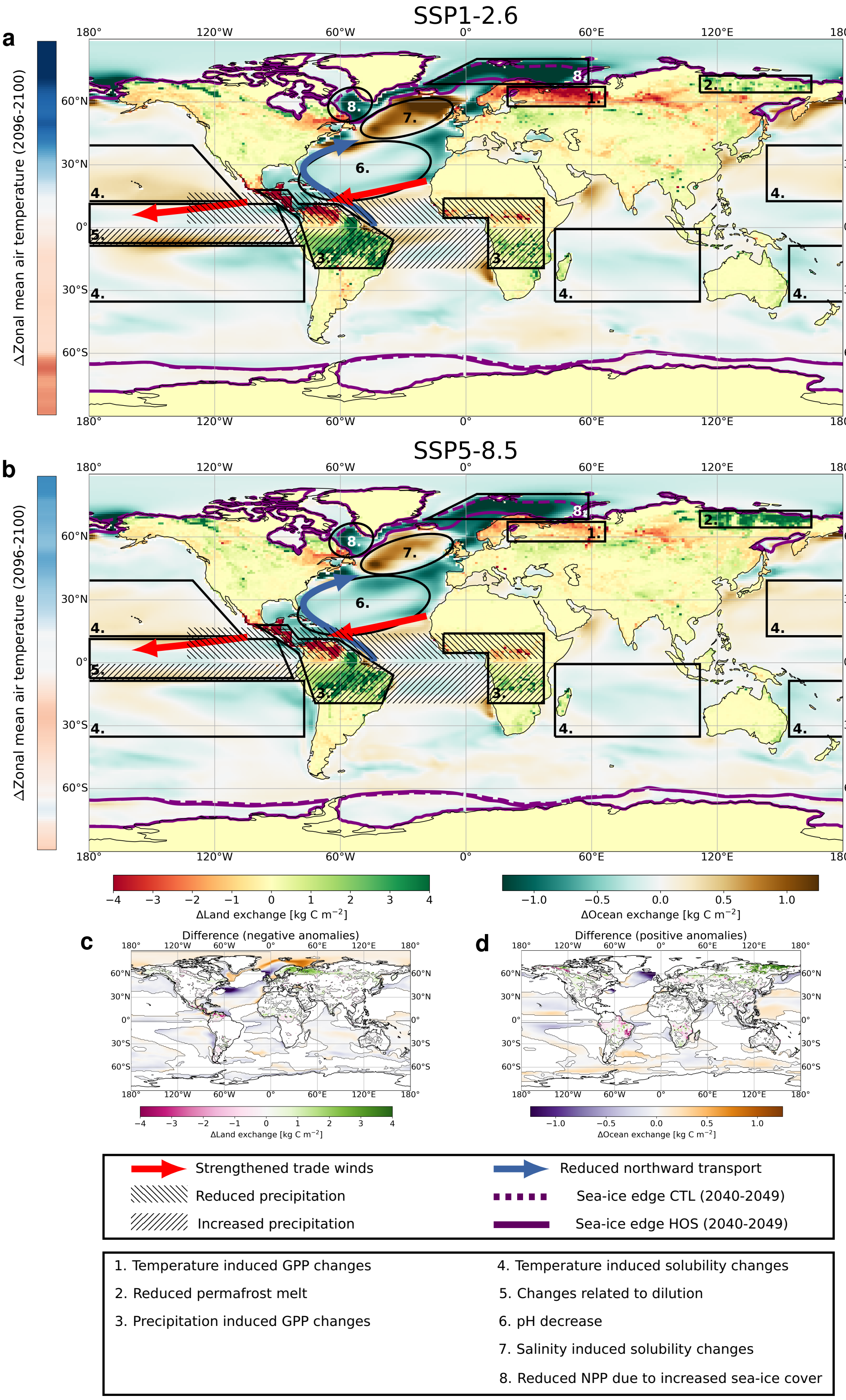

Figure 10. Summarizing figure with dominant mechanisms included for SSP1-2.6 (a) and SSP5-8.5 (b). (a) and (b) represent results from HOS minus the CTL simulations. The sea-ice edge is taken as where the ice fraction is 0.25 and denoted by the purple lines, where dashed lines represent the CTL simulations and solid lines the HOS simulations. The bar at the left shows the difference in zonal mean surface air temperature averaged over 2096-2100 between HOS and CTL. The scaling of this bar is between -2.5°C (dark blue) and 2.5°C (dark red). (c) The difference between SSP5-8.5 (b) and SSP1-2.6 (a) in the regions where (b) is negative. Negative values represent a higher negative anomaly in SSP5-8.5 compared to SSP1-2.6. (d) as in (c) but for positive anomalies. Positive values represent a higher positive anomaly in SSP5-8.5 compared to SSP1-2.6. The color bars in (c) and (d) apply to both subfigures.

Response of atmospheric pCO_2 to a strong AMOC weakening under climate change

A. A. Boot[1], A. S. von der Heydt[1,2], and H. A. Dijkstra[1,2]

[1]Institute for Marine and Atmospheric research Utrecht, Department of Physics,Utrecht University, Utrecht, the Netherlands
[2]Center for Complex Systems Studies, Utrecht University, Utrecht, the Netherlands

Key Points:

- First results on the carbon cycle response to AMOC weakening in a CMIP6 Earth System Model are presented.
- Strong weakening of the AMOC does not result in a large response of atmospheric pCO_2 under climate change.
- The spatial patterns of the carbon cycle response to an AMOC weakening are not dependent on cumulative CO_2 emissions.

Corresponding author: Amber Boot, `a.a.boot@uu.nl`

Abstract

The Earth System is warming due to anthropogenic greenhouse gas emissions which increases the risk of passing a tipping point in the Earth System, such as a collapse of the Atlantic Meridional Overturning Circulation (AMOC). An AMOC weakening can have large climate impacts which influences the marine and terrestrial carbon cycle and hence atmospheric pCO_2. However, the sign and mechanism of this response are subject to uncertainty. Here, we use a state-of-the-art Earth System Model, the Community Earth System Model v2 (CESM2), to study the atmospheric pCO_2 response to an AMOC weakening under low (SSP1-2.6) and high (SSP5-8.5) emission scenarios. A freshwater flux anomaly in the North Atlantic strongly weakens the AMOC, and we simulate a weak positive pCO_2 response of 0.45 and 1.3 ppm increase per AMOC decrease in Sv for SSP1-2.6 and SSP5-8.5, respectively. For SSP1-2.6 this response is driven by both the oceanic and terrestrial carbon cycles, whereas in SSP5-8.5 it is solely the ocean that drives the response. However, the spatial patterns of both the climate and carbon cycle response are similar in both emission scenarios over the course of the simulation period (2015-2100), showing that the response pattern is not dependent on cumulative CO_2 emissions up to 2100. Though the global atmospheric pCO_2 response might be small, locally large changes in both the carbon cycle and the climate system occur due to the AMOC weakening, which can have large detrimental effects on ecosystems and society.

Plain Language Summary

The Atlantic Meridional Overturning Circulation (AMOC) modulates global climate by transporting heat from the Southern to the Northern Hemisphere. The AMOC is considered to be a tipping element with a possible future collapse under climate change. An AMOC weakening can have large climate impacts which influences the marine and terrestrial carbon cycle and hence the atmospheric pCO_2. Here, we use a state-of-the-art Earth System Model to study the atmospheric pCO_2 response to an AMOC weakening under low and high emission scenarios. We use simulations where we artificially weaken the AMOC, which results in a weak positive response of 0.45 and 1.3 ppm pCO_2 increase per decrease in Sv for low and high emissions, respectively. For low emissions this response is driven by both the oceanic and terrestrial carbon cycle processes, whereas in the high emission scenario it is solely the ocean that drives the response. Spatial patterns, both the climate and carbon cycle response, are similar in both emission scenarios over the course of the simulation period (2015-2100). The global atmospheric pCO_2 response is small, but locally large changes in both the carbon cycle and the climate system can occur due to the AMOC weakening.

1 Introduction

Anthropogenic emissions of greenhouse gases cause the Earth System to change and warm up. As temperatures increase, we are at risk of crossing tipping points with possibly large detrimental effects on our climate, biodiversity and human communities (Lenton et al., 2008; McKay et al., 2022). One of these tipping points can occur in the Atlantic Meridional Overturning Circulation (AMOC) (Lenton et al., 2008). Currently, the AMOC is in a so-called on-state where it transports heat from the Southern Hemisphere to the Northern Hemisphere and thereby modulates global and especially European climate (Buckley & Marshall, 2016). In models, the AMOC can be strongly weakened and in this so-called collapsed state (or off-state), the northward heat transport is disrupted with large global climatic effects (Orihuela-Pinto et al., 2022).

Proxy-based evidence suggest that AMOC collapses have occurred frequently during the Pleistocene where they are a main source of millennial variability (e.g. the Dansgaard-Oeschger cycles; Rahmstorf, 2002; Lynch-Stieglitz, 2017). The disrupted heat transport causes warming of surface air temperature (SAT) and sea surface temperature (SST) in the Southern Hemisphere, while the Northern Hemisphere cools (also called the 'bipolar seesaw'; Vellinga & Wood, 2002; Caesar et al., 2018), with local SAT changes up to 10°C (Cuffey & Clow, 1997; Rahmstorf, 2002). In models, the bipolar seesaw results in an increased northern hemispheric sea-ice extent and changes in atmospheric dynamics (Vellinga & Wood, 2002; Orihuela-Pinto et al., 2022). The changes in atmospheric dynamics are, for example, seen in wind fields with strengthened trade winds and strengthened Pacific Walker Circulation (Orihuela-Pinto et al., 2022), and a southward shift of the Intertropical Convergence Zone (ITCZ) (Zhang & Delworth, 2005; Jackson et al., 2015). The tipping threshold for the AMOC is estimated to be around 4 °C of warming relative to pre-industrial climate (McKay et al., 2022).

In addition to the climate system, also the carbon cycle is affected by an AMOC collapse. In the ocean, the change in ocean circulation affects the advection of important tracers such as Dissolved Inorganic Carbon (DIC) and nutrients (Zickfeld et al., 2008). An AMOC collapse can also change upwelling rates and surface stratification, processes that are important for driving Net Primary Production (NPP) and carbon sequestration in the deep ocean. Terrestrial primary productivity is affected by the changing temperature and precipitation patterns. Locally, this can lead to both a reduction or an increased uptake of CO_2 (e.g. Köhler et al., 2005). Several studies have looked into a potential feedback between AMOC dynamics and atmospheric pCO_2, which is controlled by the exchange of the atmosphere with the ocean and land carbon stocks. These studies (e.g. Marchal et al., 1998; Köhler et al., 2005; Schmittner & Galbraith, 2008), mostly focused on Pleistocene and pre-industrial conditions, show a wide range of possible responses. There is no clear consensus on the responses of the terrestrial and ocean carbon stock to an AMOC weakening, or to the net effect on atmospheric pCO_2, which can be attributed to different climatic boundary conditions, timescales assessed, and model detail used (Gottschalk et al., 2019). In CMIP6 models, the AMOC gradually weakens up to 2100 and, independent of the used emission scenario (Weijer et al., 2020), no AMOC tipping is found. However, these models are thought to be biased towards a too stable AMOC (e.g. Cheng et al., 2018; Weijer et al., 2019), and a recent observation based study has indicated that the AMOC may tip between 2025 and 2095 (Ditlevsen & Ditlevsen, 2023).

The carbon cycle is also affected by climate change. In the ocean, the effect on the solubility pump is relatively straight forward: increased warming, and increased CO_2 concentrations, reduce ocean pH and the solubility of CO_2, which reduces the uptake capacity of the ocean (Sarmiento et al., 1998). The biological pump in Coupled Model Intercomparison Project 6 (CMIP6; Eyring et al., 2016) models is much more uncertain though (Henson et al., 2022; Wilson et al., 2022), especially given that the spread in NPP and Export Production (EP) has increased from CMIP5 to CMIP6 (Kwiatkowski et al., 2020; Tagliabue et al., 2021). The terrestrial biosphere is affected for example through increased primary production related to CO_2 fertilization (Zhu et al., 2022), but also increased respiration due to permafrost melt (Burke et al., 2020).

Studies looking at the combined effect of strong AMOC weakening and anthropogenic climate change on the future carbon cycle are limited. A projected AMOC weakening affects both the solubility and the biological carbon pumps (Liu et al., 2023), and generally leads to reduced uptake of (anthropogenic) carbon in the ocean (Obata, 2007; Zickfeld et al., 2008; Liu et al., 2023), which can be partially compensated for by the terrestrial biosphere (Zickfeld et al., 2008). However, the net effect has been found to be small due to competing effects (Swingedouw et al., 2007; Zickfeld et al., 2008). Though global effects might be weak, local effects can be quite strong. For example, a weakening of the AMOC can also result in a local reduction in primary productivity (Whitt & Jansen, 2020), changes in the plankton stock (Schmittner, 2005) and plankton composition (Boot et al., 2023a), which all can lead to reduced CO_2 uptake of the ocean (e.g. Yamamoto et al., 2018; Boot et al., 2023a). These local changes related to an AMOC weakening are strongest in the Atlantic Ocean (Katavouta & Williams, 2021).

The novel aspect of this paper is that we consider the effect of AMOC weakening on the carbon cycle under climate change in a state-of-the-art global climate model, the Community Earth System Model v2 (CESM2; Danabasoglu et al., 2020), as explained in section 2. We use a strong freshwater forcing in the North Atlantic to artificially weaken the AMOC and consider two different emission scenarios, Shared Socioeconomic Pathways (SSPs), with low (SSP1-2.6) and high (SSP5-8.5) emissions (O'Neill et al., 2020). In the results of section 3 and the subsequent analysis, we focus on the mechanisms how a forced AMOC weakening affects atmospheric pCO_2 under climate change.

2 Method

In the CESM2 (Danabasoglu et al., 2020), the atmosphere is represented by the CAM6 model, the land by the CLM5 model (Lawrence et al., 2019), sea ice by the CICE model, ocean circulation by POP2 (Smith et al., 2010), and ocean biogeochemistry by MARBL (Long et al., 2021). The ocean models POP2 and MARBL are both run on a displaced Greenland pole grid at a nominal horizontal resolution of 1°, with 60 non-equidistant vertical levels. The ocean biogeochemical module MARBL is based on a NPZD-model, where four nutrients (N, P, Fe, and Si) together with light co-limit the production of three phytoplankton groups (diatoms, diazotrophs and small phytoplankton) which are grazed upon by one zooplankton group. The terrestrial carbon cycle is represented with CLM5. This module represents several surface processes such as biogeochemistry, ecology, human influences, biogeophysics and the hydrological cycle. As we use the default CESM2 version, there is no dynamic vegetation. For a complete overview of the CESM2 model and submodules we refer the reader to Danabasoglu et al. (2020) (CESM2), Long et al. (2021) (MARBL), and Lawrence et al. (2019) (CLM5).

We performed emission forced CESM2 simulations with two different emission scenarios, the low emission scenario SSP1-2.6 (126) and the high emission scenario SSP5-8.5 (585). For each emission scenario, a control (CTL) and a hosing (HOS) simulation were carried out. The CTL simulations were only forced with the greenhouse gas emissions, while the HOS simulations were forced with greenhouse gas emissions and an additional, artificial freshwater flux in the North Atlantic. This freshwater forcing is located in the North Atlantic Ocean over the latitudes 50°N - 70°N (Fig. S1), and is kept constant at a rate of 0.5 Sv over the entire simulation period. We will refer to the simulations by their simulation type (CTL or HOS) and the respective emission scenario (126 or 585), e.g. as CTL-126 and HOS-585. All simulations are run from year 2015 to year 2100 and are initialized by values of the NCAR CMIP6 emission driven historical simulation (Danabasoglu, 2019). The used model output is based on monthly means, and line plots are smoothed with a 5 year running mean. When looking at the difference between the HOS and CTL simulations, we subtract the CTL simulations from the HOS simulations.

3 Results

3.1 Climate reponse

In CTL-126, an increase in atmospheric CO_2 concentration from 400 ppm to 467 ppm in the 2050s is found, after which the concentration decreases to 432 ppm in 2100 (Fig. 1c). This is accompanied by an increase in global mean surface temperature (GMST) of 1 °C (Fig. 1b), and an AMOC decrease from 17 Sv in 2015 to 9 Sv in 2100 (Fig. 1a). The weakening of the AMOC results in a cooling of the North Atlantic Ocean, while the rest of the Earth warms with largest temperature increases found near the poles (Fig. 2a, b) as a response to the increase in greenhouse gas concentrations. In the water cy-

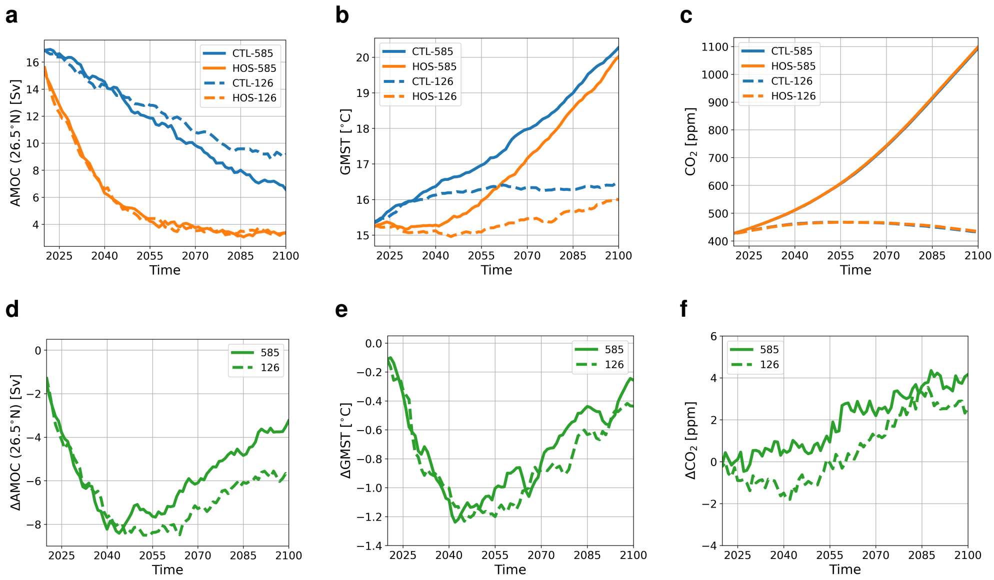

Figure 1. (a) AMOC strength at 26.5°N in Sv. (b) GMST in °C. (c) Atmospheric CO_2 concentration in ppm. In (a-c) blue lines represent the control (CTL) simulations, and orange lines the HOS simulations. (d-f) as in (a-c) but for the difference between the HOS simulations and the control simulations. In all subplots dashed lines represent SSP1-2.6 (126) and solid lines SSP5-8.5 (585).

cle we see a southward shift of the Pacific InterTropical Convergence Zone (ITCZ) of a few degrees (Fig. S2a, b). Furthermore, wind fields in the Northern Hemisphere show a small weakening, whereas in the Southern Hemisphere the winds intensify (Fig. S3a, b).

In CTL-585, the emissions increase the atmospheric CO_2 concentration from 400 ppm to 1094 ppm in 2100 (Fig. 1c) which results in a GMST warming of 5 °C (Fig. 1b). The AMOC weakens from 17 Sv to 7 Sv (Fig. 1a), which leads to a region without warming in the North Atlantic, whereas we see strong warming everywhere else (Fig. 2d, e). There is a strong southward shift of the ITCZ in the Pacific and a moderate shift in the Atlantic Ocean (Fig. S2d, e). The changes in the wind field show similar patterns as CTL-126 but with a larger amplitude (Fig. S3d, e).

The net effect of the AMOC weakening (i.e. HOS minus CTL) is shown in Fig. 1def. In the year 2100, atmospheric CO_2 concentrations are 2.6 ppm and 4.2 ppm higher in HOS-126 and HOS-585 compared to their respective CTL simulations. In both HOS simulations the AMOC quickly weakens from 17 Sv in 2015 to 6 Sv in 2045 after which the AMOC weakening starts to level off until the AMOC is weaker than 4 Sv in 2100 (Fig. 1d). Due to the AMOC weakening we observe a relative cooling of (locally) more than 3 °C in the Northern Hemisphere and warming in the Southern Hemisphere (Fig. 2c, f) (i.e. the bipolar seesaw). The cooling in the Northern Hemisphere results into an increase in sea-ice cover of the Arctic Ocean (Fig. S4), which for HOS-126 persists throughout the entire simulation period. The AMOC weakening also results into a stronger southward shift of the ITCZ in both the Pacific and Atlantic Ocean (Fig. S2c, f), and winds are relatively intensified in the Northern Hemisphere and weakened in the Southern Hemisphere (Fig. S3c, f), with a stronger response in SSP5-8.5.

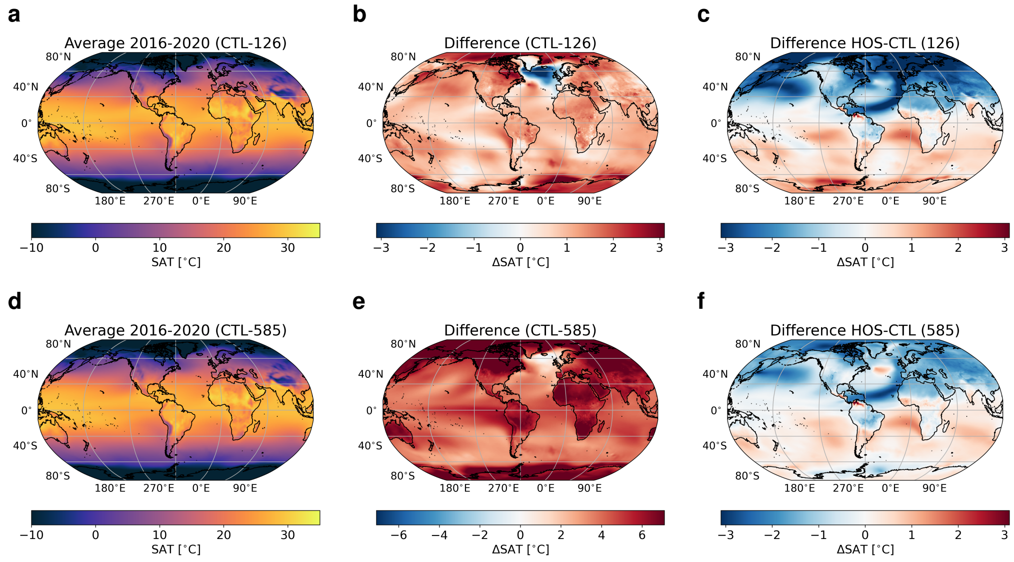

Figure 2. Results for Surface Air Temperature (SAT) in °C. The top row (a-c) is for SSP1-2.6, and the bottom row (d-f) for SSP5-8.5. The left column (a, d) represents the average over 2016-2020 in the control simulations. The middle row (b, e) represents the difference between the average of 2096-2100 and 2016-2020 for the control simulations. The right row (c, f) represents the difference between the HOS and CTL simulations averaged over 2096-2100. Note the different scaling between b and e.

3.2 Marine carbon cycle response

In CTL-126 we see that, integrated over the entire simulation period, there are regions in the ocean with net carbon uptake, and net carbon outgassing (Fig. 3a). The Southern Ocean between 45°S and 60°S, and the equatorial Pacific Ocean, are regions of carbon release from the ocean to the atmosphere. The region of strongest outgassing in the Pacific is located in the upwelling regions on the eastern side of the basin. Carbon uptake generally occurs in the rest of the ocean with the strongest uptake located in the Sea of Japan and the high latitude North Atlantic Ocean. Looking at the development over time (Fig. 4a, b) we see a negative trend over almost the entire ocean, meaning regions which take up carbon in the beginning of the simulation have lower uptake at the end, and regions which emit carbon in 2015 emit more carbon at the end of the simulation. Some regions, e.g. in the Southern Ocean, shift from a carbon uptake region to a region of outgassing.

In CTL-585, also integrated over the simulation period, only the eastern equatorial Pacific shows strong outgassing (Fig. 3d). In the other equatorial basins, there are also some small patches that show net outgassing, but the rest of the ocean shows net carbon uptake. Except for the high latitude North Atlantic Ocean and some small other regions, we see a positive trend (Fig. 4d, e), meaning that regions that take up carbon in the beginning, take up more carbon at the end of the simulation, and regions which show outgassing in the beginning show either reduced outgassing or go from being a region of outgassing to a region of CO_2 uptake. A remarkable region is the high latitude North Atlantic Ocean where the flux from the atmosphere into the ocean strongly decreases while atmospheric pCO_2 almost triples. Integrated over time, the spatial pattern of regions that see increased or decreased exchange with the atmosphere is very sim-

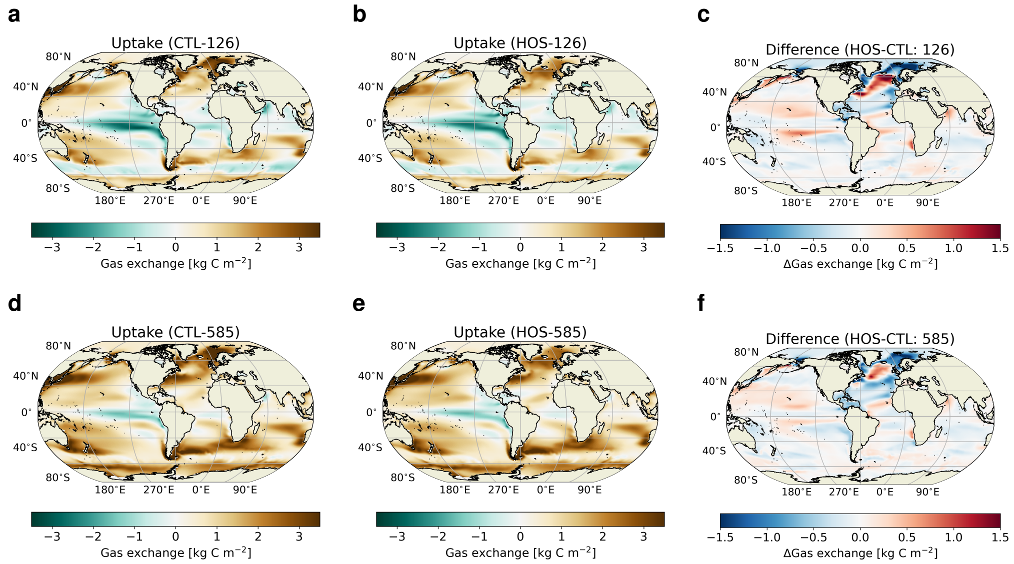

Figure 3. Results for the oceanic CO_2 uptake integrated over the entire simulation period in kg C m^{-2}. The top row (a-c) represents SSP1-2.6 and the bottom row (d-f) represents SSP5-8.5. The left column (a, d) represents the uptake in the control simulations, the middle column (b, e) the uptake in the HOS simulations, and the right column (c, f) the difference between the HOS and CTL simulations. In a, b, d, and e positive values (brown colors) represent net uptake, and negative values (blue colors) represent net outgassing.

ilar for SSP1-2.6 as for SSP5-8.5 (Fig. 3c, f). In total, the ocean takes up 7.4 PgC less due to the AMOC weakening in SSP1-2.6 and 15.6 PgC less in SSP5-8.5 (Fig. 5a, d).

Even though the climate system changes a lot due to the AMOC weakening, the CO_2 uptake of the ocean does not change a lot because of compensating effects. To obtain a better understanding of the mechanisms behind the reduced uptake, we have divided the ocean into 5 basins: the Arctic (north of 66°N), the Southern (south of 35°S), the Atlantic, Pacific and Indian Ocean (Fig. 5b, e). In the response (i.e. HOS-CTL), for both emission scenarios, all basins show the same sign, i.e. more uptake or less uptake due to the AMOC weakening.

In both emission scenarios the Arctic Ocean shows a decreased uptake (-6.0 PgC in SSP1-2.6 and -4.4 PgC in SSP5-8.5), which can be explained by looking at the sea-ice cover (Fig. S4). The cooling in the Northern Hemisphere following the AMOC weakening in the HOS simulations, increases the sea-ice cover. The increase in sea-ice cover has two effects on the uptake of CO_2: (1) it reduces the ocean area available for exchange with the atmosphere; and (2) it increases light limitation and thereby reduces net primary production (NPP; Fig. S6) and the carbon export to the subsurface ocean. In SSP5-8.5 most of the sea ice still disappears due to the strong warming, but in SSP1-2.6 most of the sea ice persists throughout the simulation period, which explains why the Arctic Ocean in SSP1-2.6 responds stronger compared to SSP5-8.5. We also find this effect in the sea-ice covered regions in the North Atlantic (e.g. the Labrador Sea).

The Pacific Ocean takes up more carbon in the HOS than in the CTL simulations (+4.9 PgC in SSP1-2.6 and +1.7 PgC in SSP5-8.5). To analyze what is happening in the Pacific, we considered three different regions: (1) the North Pacific (20°N-66°N), the Equatorial Pacific (20°N-10°S), and the South Pacific (10°S-35°S). In the North Pacific,

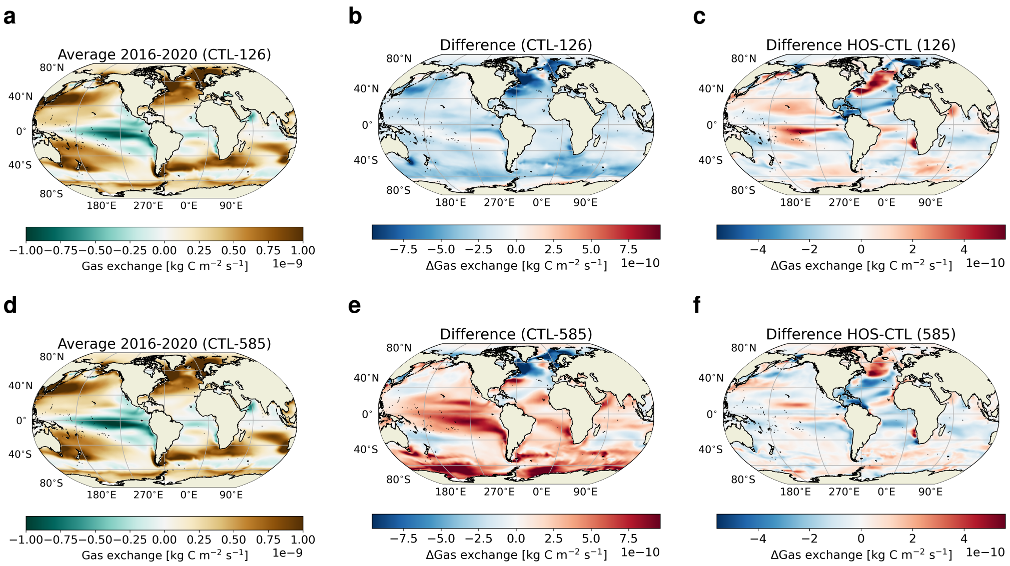

Figure 4. Results for oceanic CO_2 uptake in kg C m^{-2} s^{-1}. Panels represent the same as in Fig. 2. Positive values (brown colors) in a and d represent uptake by the ocean and negative values (blue colors) represent outgassing.

the relative cooling of the surface ocean (Fig. S7) results in an increase of solubility of CO_2 driving increased uptake (Fig. 3e, f). A similar, but opposite, response is seen in the South Pacific. Here the surface ocean becomes relatively warmer inhibiting the uptake of CO_2. The equatorial Pacific is characterized by a band with reduced uptake and one with increased uptake. This can be related to the stronger southward shift of the ITCZ in the Pacific in HOS compared to the CTL (Fig. S2). Due to this shift, the dilutive fluxes related to net precipitation shift southward, causing relative increases of salinity in the northern section due to reduced precipitation, and relative decreases due to increased precipitation in the southern section (Fig. S8). This, in turn, also affects the stratification in these regions with a weakening in the north and a strengthening in the south (Fig. S9). These changes affect the solubility of CO_2 in the equatorial regions causing decreased uptake in the northern section and increased uptake in the southern section.

We find the largest difference in carbon uptake (-2.0 PgC in SSP1-2.6 and -9.3 PgC in SSP5-8.5) in the Atlantic. The regions with sea ice show similar behavior as the Arctic Ocean with decreased uptake related to a larger sea-ice cover in the HOS simulations. In the ice-free subpolar region, an increase in uptake is observed which is associated to decreases in sea surface salinity (SSS; Fig. S8) due to the applied freshwater forcing in this region which promotes the uptake of CO_2. In the subtropical region we generally see a decrease in uptake. To explain this we consider several variables, i.e. SST (Fig. S7), SSS (Fig. S8), DIC (Fig. S12), Alk (Fig. S13) and NPP (Fig. S6), which all show a relative decrease in this region. The net effect of the changes in these variables is a reduction in pH (Fig. S16) and reduced uptake capacity of the ocean. In the Canary Upwelling System and along the North Equatorial Current we do see an increase in NPP (Fig. S6), due to increased nutrient concentrations (Fig. S11) related to increased upwelling of nutrients (Fig. S10 and S15). In the region of the North Equatorial Current this leads to increased uptake of the ocean, and only in SSP5-8.5 also in the Canary Upwelling System. Outside the North Atlantic, large responses are seen in the equatorial region and the Benguela Upwelling System which are characterized by reduced upwelling (Fig. S10),

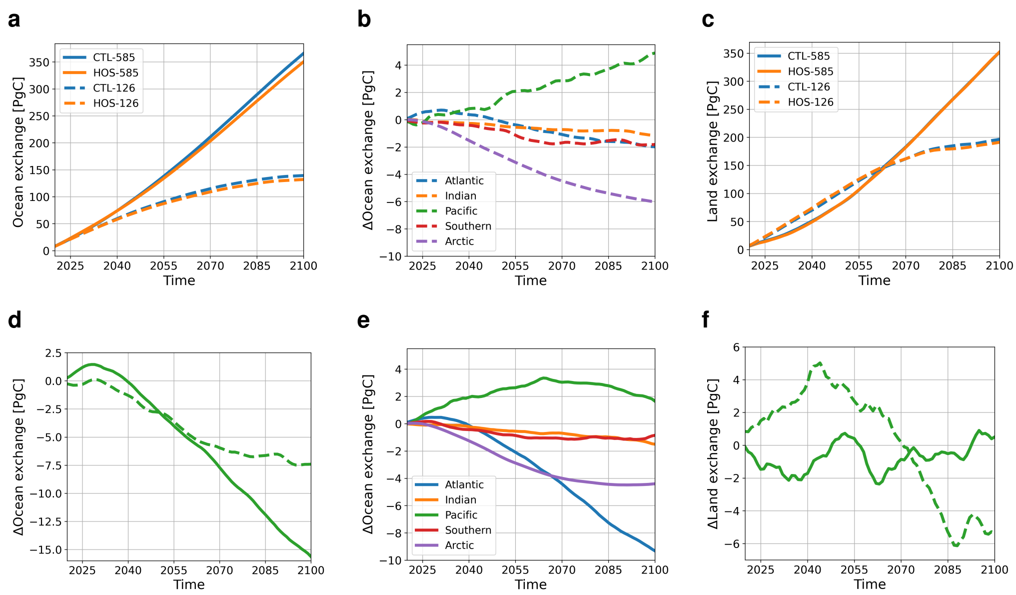

Figure 5. (a) Cumulative uptake of CO_2 in the ocean from 2016 onward in PgC. (b) Difference in the cumulative oceanic CO_2 uptake between the HOS and CTL simulations in SSP1-2.6 for different ocean basins. (c) As (a) but for the land. (d) The difference in the cumulative oceanic CO_2 uptake between the HOS and CTL simulations. (e) As in (b) but for SSP5-8.5. (f) As in (d) but for the land. In a and c blue lines represent the control simulations, and the orange lines the HOS simulations. In all subplots dashed lines represent SSP1-2.6 and solid lines SSP5-8.5. Negative values in b, d-f represent reduced uptake in the HOS simulations compared to the CTL simulations.

promoting additional uptake of CO_2 in the ocean. In the Atlantic Ocean, we find that DIC (Fig. 6) and nutrient (Fig. 7) concentrations decrease in the surface ocean due to the weakening of the AMOC and increase in the deep ocean. The reduction in DIC clearly shows the reduced uptake capacity of the ocean, and the reduction in PO_4 also explains the decrease in NPP (Fig. S6) observed in the Atlantic basin.

The Indian Ocean has a relatively weak response and is very similar for both emission scenarios with a small decrease in uptake (-1.2 PgC in SSP1-2.6 and -1.5 PgC in SSP5-8.5). This is related to the relatively warmer SSTs in the HOS simulations (Fig. S7). The Southern Ocean also has a small decrease in uptake, with a larger decrease in SSP1-2.6 (-1.8 PgC compared to -0.9 PgC in SSP5-8.5). This larger decrease can be explained by the fact that the sea-ice cover is larger in SSP1-2.6 compared to SSP5-8.5 (Fig. S5).

3.3 Terrestrial carbon cycle response

In CTL-126, the terrestrial biosphere, integrated over the entire simulation period, shows a net uptake of CO_2 in most regions (Fig. 8a). The Net Biosphere Production (NBP) maxima are located on the equator for the tropical rainforests, the boreal forests in the high latitude Northern Hemisphere, and the eastern United States and China. The few locations that show net emission of CO_2 are very local and present in the high latitude Northern Hemisphere, the Tibetan Plateau, South East Asia and South America. If we look at the development over time (Fig. 9a, b) we see that the tropical rainforests have

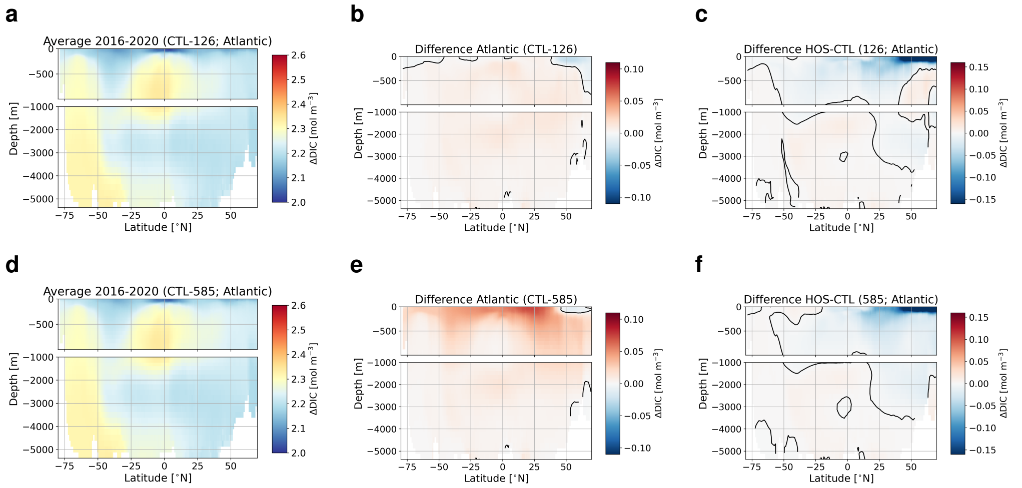

Figure 6. Results for zonally averaged DIC concentrations in the Atlantic basin in mol m^{-3}. Panels represent the same as in Fig. 2. Black contour lines in b, c, e and f represent the 0 mol m^{-3} contour. Note the different scaling of the surface ocean (top 1000 m) compared to the deep ocean.

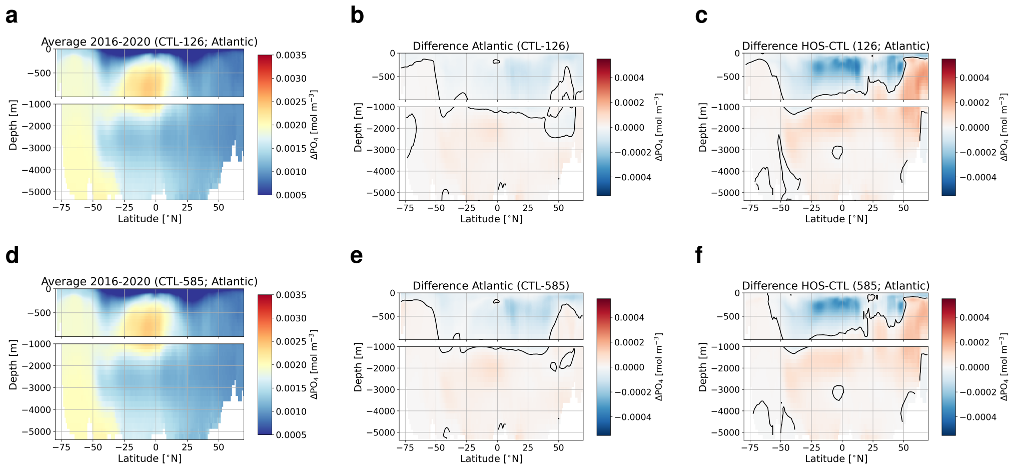

Figure 7. Results for zonally averaged PO_4 concentrations in the Atlantic basin in mol m^{-3}. Panels represent the same as in Fig. 2. Black contour lines in b, c, e and f represent the 0 mol m^{-3} contour. Note the different scaling of the surface ocean (top 1000 m) compared to the deep ocean.

a lower NBP at the end of the simulation. There are some regions that have a higher NBP in 2100, e.g. the boreal forests in Scandinavia.

The response in CTL-585 is very similar to CTL-126 with respect to the spatial pattern, except in central Africa (Fig. 8d). However, the amplitude of the response is much larger due to the CO_2 fertilization effect. Especially the tropical rainforests, but also the boreal forests, show more carbon uptake compared to CTL-126. The same is also true for regions that emit carbon, i.e., the region in the high latitude Northern Hemisphere that emits carbon is larger, and the amount of carbon emitted is also higher. The main difference with respect to CTL-126 is a region in the Congo basin which emits CO_2 in CTL-585 whereas in CTL-126 it is a region of relatively strong uptake, which is possibly related to increased wildfire activity in this region in SSP5-8.5 (Fig. S17). When we look at the development over time (Fig. 9d, e) we find a completely different pattern in CTL-585 compared with CTL-126. The tropical rainforests show an increase in NBP related to the CO_2 fertilization effect whereas northern Siberia shows a decrease related to increased respiration due to permafrost melt (Fig. S19 and S20).

Integrated globally the terrestrial biosphere takes up 5.3 PgC less in SSP1-2.6 and 0.5 PgC more in SSP5-8.5 (Fig. 5) in the HOS simulations compared to the CTL simulations. However, looking at spatial patterns of the cumulative uptake, we see a very similar response to the AMOC weakening (HOS-CTL) for both emission scenarios (Fig. 8c, f). In both emission scenarios we find that the increased southward shift in the ITCZ in the HOS simulations lead to decreased NBP in central America, and increased NBP in Southern America. A similar shift can be seen in Africa, but with a smaller latitudinal shift and amplitude. The shift and amplitude are slightly stronger in SSP1-2.6. The boreal forests become relatively lower in NBP in the HOS simulations with a larger amplitude in SSP1-2.6. This is because in SSP1-2.6, the forests have lower Gross Primary Production (GPP; Fig. S18) over the course of the century which can be related to the relative cooling in the Northern Hemisphere seen in the HOS simulations (Fig. S8). This relative cooling is stronger in SSP1-2.6, related to the increased sea-ice cover and therefore higher albedo in the Arctic. Another effect of the Northern Hemispheric cooling is an increase in NBP in the permafrost regions in Siberia and North America in the HOS simulations. The cooling reduces permafrost melt (Fig. S19) and therefore reduces soil respiration (Fig. S20), with a larger amplitude in Siberia for SSP5-8.5.

3.4 Total response

In total we see an increase of atmospheric CO_2 concentration of 2.6 and 4.2 ppm in 2100 in SSP1-2.6 and SSP5-8.5 due to the AMOC weakening (HOS-CTL). In SSP1-2.6 this response is caused partly due to reduced uptake of the ocean and partly due to reduced uptake of the land. In SSP5-8.5 it is completely driven by the ocean as the globally integrated uptake over the land is approximately the same in CTL-585 as in HOS-585. Eventually the AMOC strength in 2100 has decreased by 5.8 and 3.2 Sv in the HOS simulations compared to the CTL simulations. Under the assumption of linearity, this results in a positive feedback strength of 0.44 ppm Sv^{-1} and 1.3 ppm Sv^{-1} for SSP1-2.6 and SSP5-8.5 respectively. This can be considered a positive feedback since increased CO_2 concentrations in future climates are generally associated with a weakening of the AMOC (e.g. Weijer et al., 2020). This AMOC-pCO_2 feedback is small on the global scale, due to competing effects but locally large changes in carbon uptake can occur.

Fig. 10 gives an overview of the most important climate changes and how the marine and terrestrial respond to these changes. In Fig. 10c, d the difference between SSP1-2.6 and 5-8.5 is highlighted. In the terrestrial biosphere the prime effect of the AMOC weakening is the southward shift of the GPP maxima in the tropical rainforests (Fig. S18). Though this could potentially have beneficial effects for the southern regions, it could have detrimental effects for the northern regions (e.g. the Sahel region) and could for example increase the latitudinal extent of the Sahara desert. This shift, caused by a shift in precipitation (Fig. S2), also has effects for the probability of wildfires (Fig. S17), which can increase in regions with reduced precipitation. We cannot conclude whether the AMOC

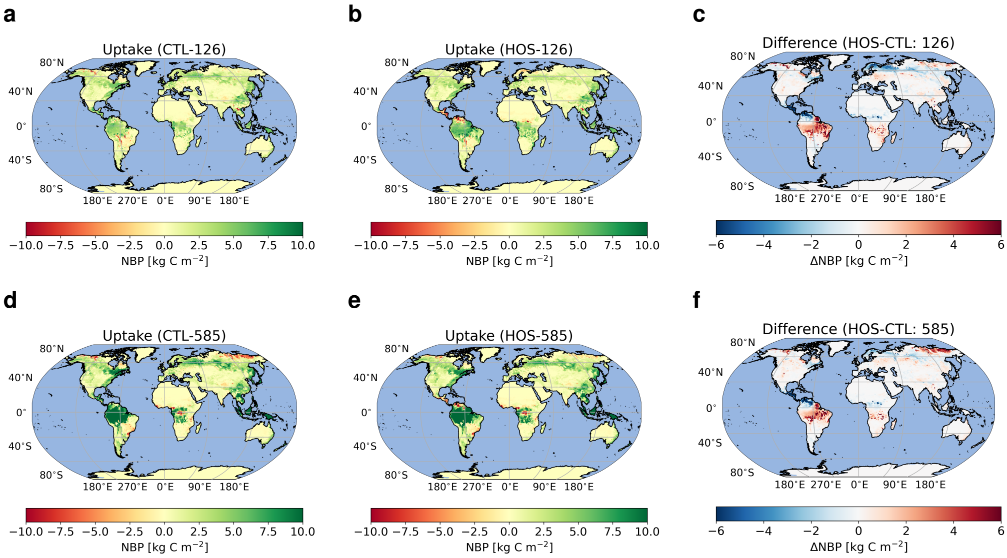

Figure 8. Results for the CO_2 exchange with the land integrated over the entire simulation period in kg C m^{-2}. The top row (a-c) represents SSP1-2.6 and the bottom row (d-f) represents SSP5-8.5. The left column (a, d) represents the uptake in the control simulations, the middle column (b, e) the uptake in the HOS simulations, and the right column (c, f) the difference between the HOS and CTL simulations. In a, b, d, and e green colors represent net CO_2 uptake by the land, and red colors represent net emissions into the atmosphere.

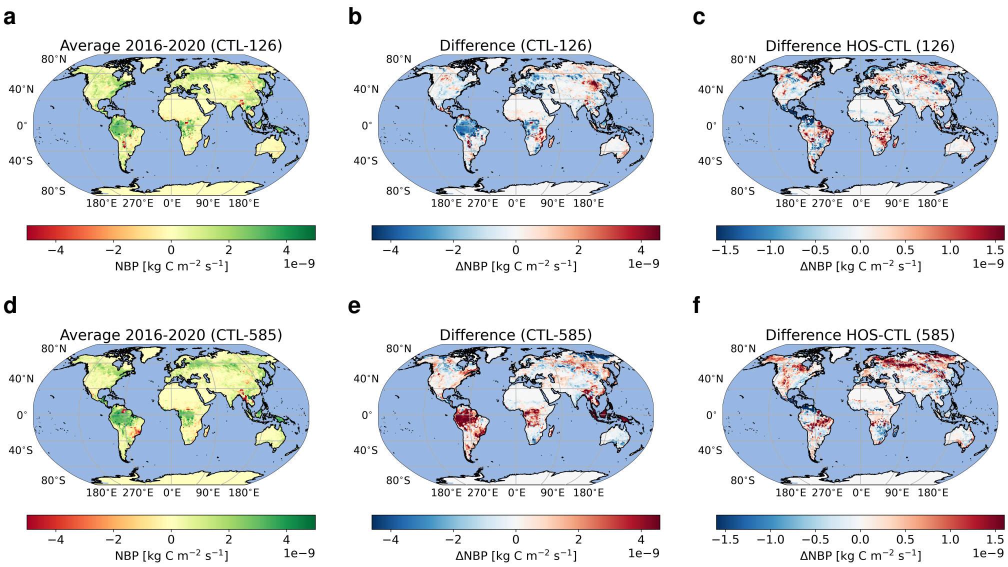

Figure 9. Results for Net Biosphere Production (NBP) in kg C m^{-2} s^{-1}. Panels represent the same as in Fig. 2. Green colors represent uptake of CO_2 into the land and red colors represent emission of CO_2 to the atmosphere.

weakening would result into a collapse of the Amazonian rainforests or an increase in the Sahara desert since the model is used without a dynamic vegetation model. In the ocean, a decrease in NPP (Fig. S6) and surface nutrient concentrations (Fig. S11) occurs. The changes in NPP can have effects on the entire food web and thereby have a negative impact on ecosystems and ecosystem functions. If the trend of the surface ocean becoming more depleted of nutrients (Fig. 7) continues, this might drive a large decline in NPP for the coming centuries. Another important effect of the AMOC weakening is increased ocean acidification (i.e. a decrease in pH; Fig. S16). Lower pH values increase the stress on calcifying organisms and reduces the uptake capacity of the ocean, which might increase the AMOC-pCO_2 feedback strength on longer timescales.

In many climate and carbon cycle variables we see a similar response in spatial pattern, but sometimes with a slightly different amplitude (Fig. 10c, d). In the terrestrial biosphere, the main differences are seen in the boreal forests in Scandinavia and Russia (box 1 in Fig. 10), and in the Siberian permafrost regions (box 2). The difference in the boreal forests can be explained by looking at the temperature differences between the HOS and CTL simulations. In SSP1-2.6, the northern hemisphere cools more, which causes increased GPP reduction in the boreal forests. For the permafrost region we find a stronger response in SSP5-8.5, because in SSP1-2.6 there is not much permafrost melt in the CTL simulation; therefore the additional cooling in the HOS simulation does not have a large effect on the permafrost melt. In the ocean, we find the largest changes in the subpolar North Atlantic and the Arctic sea-ice regions (boxes 7 and 8 in Fig. 10). In the subpolar region there is a relatively stronger decrease in SSS and SST (Fig. S7 and S8) in SSP1-2.6 compared to 5-8.5 leading to a larger increase in solubility of CO_2 and therefore more uptake. Because of the increased cooling, and lower background temperatures in SSP1-2.6, sea-ice cover does not diminish over the simulation whereas in SSP5-8.5 we see in both simulations a strong reduction in sea-ice cover (Fig. S4). This is the reason why we see a stronger reduction in the Arctic in SSP1-2.6.

4 Summary and discussion

In this study, we have investigated the carbon cycle response to a weakening of the Atlantic Meridional Overturning Circulation (AMOC) under climate change scenarios. We did this by forcing a state-of-the-art Earth System Model, the Community Earth System Model v2 (CESM2), on a nominal 1° resolution with emissions from two different SSP scenarios (SSP1-2.6 and SSP5-8.5) and an additional freshwater flux in the North Atlantic to artificially decrease the AMOC. To our knowledge, this is the first study that utilizes a model of this high complexity with a horizontal resolution of 1° to study the effects of an AMOC weakening on the carbon cycle. We find a positive feedback in both emission scenarios of 0.44 ppm Sv^{-1} and 1.3 ppm Sv^{-1} for SSP1-2.6 and SSP5-8.5, respectively. The response in SSP1-2.6 is driven by both the land and ocean carbon reservoirs, whereas in SSP5-8.5 it is driven solely by the ocean. The response is small, being the effect of many compensating effects over both the land and the ocean. Looking at regional response patterns, both emission scenarios show similar behavior in many climate and carbon cycle variables. In absolute numbers, the response is stronger in SSP5-8.5, but when the high CO_2 concentrations are taken into account, the relative response is actually weaker in SSP5-8.5 compared to SSP1-2.6.

Our simulations show the climate response to an AMOC weakening, such as a southward shift of the ITCZ and the bipolar seesaw, similar to many previous studies (Obata, 2007; Zickfeld et al., 2008; Orihuela-Pinto et al., 2022). The AMOC weakening in our simulations follows a very similar trajectory as in Orihuela-Pinto et al. (2022), which used an older version of CESM (i.e. v1.2) under pre-industrial boundary conditions. In our study, the AMOC weakening results in a small increase in atmospheric CO_2 concentrations. This small effect, especially on the multi-decadal to centennial timescales assessed here, was also found in more idealized models (e.g. Zickfeld et al., 2008; Nielsen et al., 2019; Gottschalk et al., 2019), but as described in Gottschalk et al. (2019) the relative response of the ocean and land reservoirs are dependent on climatic boundary conditions and the used model. Here, we have used a member of the newest generation of Earth System Models with a relatively high spatial resolution (i.e. nominal 1°× 1° ocean grid). When considering studies with induced AMOC weakening we find, integrated over the entire ocean, a similar response as in Zickfeld et al. (2008), and spatially as in Obata (2007), though local differences remain which can be attributed to the use of a higher resolution, and a more complex model in our study. It is also possible to collapse the AMOC without an additional freshwater forcing. In Nielsen et al. (2019) they used such an alternative method under Pleistocene conditions, which resulted in a much slower response in the ocean compared to our simulations. The response of the terrestrial biosphere, especially the changes related to the southward shift of the ITCZ, is also similar to that of previous studies using static vegetation (e.g. Obata, 2007; Nielsen et al., 2019). In Köhler et al. (2005) a dynamic vegetation model is used, and they show that an AMOC collapse affects vegetation type. This leads to reduced carbon storage in the high latitudes and increased carbon storage in the Northern Hemisphere midlatitudes. This dynamic behavior is not captured in our simulations and unfortunately, it is not possible to assess what the effect of dynamic vegetation would be based on Köhler et al. (2005) since they consider Pleistocene conditions.

The result that the pattern of the carbon cycle response to an AMOC weakening is independent of the cumulative CO_2 emissions on multi-decadal to centennial timescales has been shown before. In Zickfeld et al. (2008), for example, the marine carbon cycle remains independent on the used emission scenario for the first 200 years of their simulation, and for the terrestrial carbon cycle this is 150 years. After this period the different emissions start to diverge, though the qualitative behavior remains similar. In our simulations, globally integrated variables show little change as a response to the AMOC weakening. However, on regional scales the effects of an AMOC weakening can be large, e.g. SATs can decrease or increase by more than 3 °C locally (Fig. 2) and some regions become much drier and other see a large increase in precipitation (Fig. S2). These changing climate conditions, on top of already greenhouse gas driven climate change, require climate adaptation which might be difficult to achieve in such a short time frame (i.e. decades). The climate changes associated to an AMOC weakening also cause changes in the carbon cycle. Such changes can increase, for example, desertification and reduce (but also increase) crop yields. This may lead locally to increased food stress, potentially leading to more frequent and more severe famines. The changes in the ocean can lead to more frequent marine heatwaves in the Southern Hemisphere due to the warming, and reduced (global) NPP due to changing nutrient distributions, which might impact food web dynamics and ecosystem function. However, due to the cooling effect of the bipolar seesaw we would can also expect a (relative) reduction in marine heatwaves in the Northern Hemisphere. These effects show that an AMOC collapse can have local effects that have a beneficiary impact or a detrimental impact on the terrestrial and marine biospheres.

Interestingly, the relative effects on multi-decadal timescales are independent to the (cumulative) greenhouse gas emissions. This means that the uncertainty around the effects of a possible AMOC collapse or weakening is not related to past emissions. However, in a future climate without AMOC weakening, emissions do have an influence on when the AMOC might collapse. Furthermore, the small positive feedback found in this study might make the AMOC more likely to tip earlier. Even though on these timescales the relative effects are not dependent on the greenhouse gas emissions, this might be different on intermediate (multi-centennial to millennial) timescales. Because the ocean circulation is associated with timescales on the intermediate timescales, we can expect the most important effects to occur in this time frame. We find, for example, that the surface ocean is becoming more depleted of nutrients (Fig. 7), which might depress NPP for centuries.

Other long term effects that might be relevant are tipping cascades (e.g. Dekker et al., 2018), meaning that a collapse of the AMOC could set off an other tipping element in the Earth System. In our simulations, we find decreasing temperatures in the Northern Hemisphere due to the AMOC weakening, which reduces the probability of tipping for example melting of the Greenland Ice Sheet, Arctic sea ice, and Northern Hemispheric permafrost. However, due to the bipolar seesaw, the Southern Hemisphere becomes warmer, which might increase the probability of tipping the Antarctic Ice Sheets. Another tipping point connected to the AMOC is the die off of the Amazonian rainforest. Because we do not use a dynamic vegetation model in this study, we cannot investigate whether the AMOC weakening in our simulations would lead to such a die off.

By using a low and a high emission scenario we have tried to cover uncertainties regarding future emissions. However, we have only used one Earth System Model, which means that the results presented here could be model dependent. Especially ocean productivity shows large spread in the CMIP6 ensemble, which can influence the uptake capacity of the ocean. Another bias in Earth System Models is a too stable AMOC, meaning we need a large freshwater flux in the North Atlantic Ocean to weaken the AMOC. This flux is generally too high to represent for example Greenland Ice Sheet melt, but necessary to achieve a weakened AMOC. This large freshwater flux also leads to freshening of the surface ocean in the subpolar gyre which influences the carbonate chemistry and carbon uptake capacity unrealistically. We have not taken this effect into account explicitly, but it could potentially result in reduced uptake capacity of the ocean, and therefore more CO_2 in the atmosphere, increasing the feedback strength.

Finally, we have shown in a relatively high resolution, state-of-the-art Earth System Model, that the spatial pattern of the carbon cycle response to an AMOC weakening is not dependent on cumulative CO_2 emissions. As a follow up study it would be interesting to see what happens on multi-centennial and longer timescales, and what the pCO_2 response would be under an AMOC recovery. Though not analyzed thoroughly, NPP in the ocean shows large decreases due to the AMOC weakening. This could effect food web dynamics in the ocean with possible (detrimental) changes in fishery yields, food securities and income. These ecosystem and socio-economic effects are worth investigating, to see how a change in the climate system cascades through ecosystems to socio-economic systems.

Appendix A Open Science

Yearly output for the most important variables, data necessary to replicate the figures, and the scripts used for creating the figures can be downloaded from `https://doi.org/10.5281/zenodo.8376701` (Boot et al., 2023b).

Acknowledgments

This study has been supported by the Netherlands Earth System Science Centre (NESSC), which is financially supported by the Ministry of Education, Culture and Science (OCW; grant no. 024.002.001). The authors want to thank Michael Kliphuis (IMAU, Utrecht University) for performing the CESM2 simulations, which were performed at at SURFsara in Amsterdam on the Dutch Supercomputer Snellius within NWO-SURF project 17239.

References

Behrenfeld, M. J., O'Malley, R. T., Siegel, D. A., McClain, C. R., Sarmiento, J. L., Feldman, G. C., … Boss, E. S. (2006). Climate-driven trends in contemporary ocean productivity. *Nature*, *444*(7120), 752–755. Retrieved from `https://doi.org/10.1038/nature05317` doi: 10.1038/nature05317

Boot, A., von der Heydt, A. S., & Dijkstra, H. A. (2022). Effect of the Atlantic Meridional Overturning Circulation on atmospheric pCO$_{2}$ variations. *Earth System Dynamics*, *13*(3), 1041–1058. Retrieved from https://esd.copernicus.org/articles/13/1041/2022/ doi: 10.5194/esd-13-1041-2022

Boot, A., von der Heydt, A. S., & Dijkstra, H. A. (2023a). Effect of Plankton Composition Shifts in the North Atlantic on Atmospheric pCO2. *Geophysical Research Letters*, *50*(2), e2022GL100230. Retrieved from https://agupubs.onlinelibrary.wiley.com/doi/abs/10.1029/2022GL100230 doi: https://doi.org/10.1029/2022GL100230

Boot, A., von der Heydt, A. S., & Dijkstra, H. A. (2023b, September). *GBC_2023: v1.1_25_09_23 (v1.1).* [dataset]. Zenodo. doi: 10.5281/zenodo.8376701

Buckley, M. W., & Marshall, J. (2016, mar). Observations, inferences, and mechanisms of the Atlantic Meridional Overturning Circulation: A review. *Reviews of Geophysics*, *54*(1), 5–63. Retrieved from https://doi.org/10.1002/2015RG000493 doi: https://doi.org/10.1002/2015RG000493

Burke, E. J., Zhang, Y., & Krinner, G. (2020). Evaluating permafrost physics in the Coupled Model Intercomparison Project 6 (CMIP6) models and their sensitivity to climate change. *The Cryosphere*, *14*(9), 3155–3174. Retrieved from https://tc.copernicus.org/articles/14/3155/2020/ doi: 10.5194/tc-14-3155-2020

Caesar, L., Rahmstorf, S., Robinson, A., Feulner, G., & Saba, V. (2018). Observed fingerprint of a weakening Atlantic Ocean overturning circulation. *Nature*, *556*(7700), 191–196. Retrieved from https://doi.org/10.1038/s41586-018-0006-5 doi: 10.1038/s41586-018-0006-5

Cheng, W., Weijer, W., Kim, W. M., Danabasoglu, G., Yeager, S. G., Gent, P. R., … Zhang, J. (2018). Can the Salt-Advection Feedback Be Detected in Internal Variability of the Atlantic Meridional Overturning Circulation? *Journal of Climate*, *31*(16), 6649–6667. Retrieved from https://journals.ametsoc.org/view/journals/clim/31/16/jcli-d-17-0825.1.xml doi: https://doi.org/10.1175/JCLI-D-17-0825.1

Cuffey, K. M., & Clow, G. D. (1997, nov). Temperature, accumulation, and ice sheet elevation in central Greenland through the last deglacial transition. *Journal of Geophysical Research: Oceans*, *102*(C12), 26383–26396. Retrieved from https://doi.org/10.1029/96JC03981 doi: https://doi.org/10.1029/96JC03981

Danabasoglu, G. (2019). *NCAR CESM2 model output prepared for CMIP6 CMIP esm-hist.* Earth System Grid Federation. Retrieved from https://doi.org/10.22033/ESGF/CMIP6.7575 doi: 10.22033/ESGF/CMIP6.7575

Danabasoglu, G., Lamarque, J.-F., Bacmeister, J., Bailey, D. A., DuVivier, A. K., Edwards, J., … Strand, W. G. (2020). The Community Earth System Model Version 2 (CESM2). *Journal of Advances in Modeling Earth Systems*, *12*(2), e2019MS001916. Retrieved from https://doi.org/10.1029/2019MS001916 doi: https://doi.org/10.1029/2019MS001916

Dekker, M. M., von der Heydt, A. S., & Dijkstra, H. A. (2018). Cascading transitions in the climate system. *Earth System Dynamics*, *9*(4), 1243–1260. Retrieved from https://esd.copernicus.org/articles/9/1243/2018/ doi: 10.5194/esd-9-1243-2018

Ditlevsen, P., & Ditlevsen, S. (2023). Warning of a forthcoming collapse of the Atlantic meridional overturning circulation. *Nature Communications*, *14*(1), 4254.

Eyring, V., Bony, S., Meehl, G. A., Senior, C. A., Stevens, B., Stouffer, R. J., & Taylor, K. E. (2016, may). Overview of the Coupled Model Intercomparison Project Phase 6 (CMIP6) experimental design and organization. *Geosci. Model Dev.*, *9*(5), 1937–1958. Retrieved from https://gmd.copernicus.org/

articles/9/1937/2016/https://gmd.copernicus.org/articles/9/1937/2016/gmd-9-1937-2016.pdf doi: 10.5194/gmd-9-1937-2016

Gottschalk, J., Battaglia, G., Fischer, H., Frölicher, T. L., Jaccard, S. L., Jeltsch-Thömmes, A., ... Stocker, T. F. (2019). Mechanisms of millennial-scale atmospheric CO2 change in numerical model simulations. *Quaternary Science Reviews*, *220*, 30–74. Retrieved from http://www.sciencedirect.com/science/article/pii/S0277379118310473 doi: https://doi.org/10.1016/j.quascirev.2019.05.013

Henson, S. A., Laufkötter, C., Leung, S., Giering, S. L. C., Palevsky, H. I., & Cavan, E. L. (2022). Uncertain response of ocean biological carbon export in a changing world. *Nature Geoscience*, *15*(4), 248–254. Retrieved from https://doi.org/10.1038/s41561-022-00927-0 doi: 10.1038/s41561-022-00927-0

Jackson, L. C., Kahana, R., Graham, T., Ringer, M. A., Woollings, T., Mecking, J. V., & Wood, R. A. (2015). Global and European climate impacts of a slowdown of the AMOC in a high resolution GCM. *Climate Dynamics*, *45*(11), 3299–3316. Retrieved from https://doi.org/10.1007/s00382-015-2540-2 doi: 10.1007/s00382-015-2540-2

Katavouta, A., & Williams, R. G. (2021). Ocean carbon cycle feedbacks in CMIP6 models: contributions from different basins. *Biogeosciences*, *18*(10), 3189–3218. Retrieved from https://bg.copernicus.org/articles/18/3189/2021/ doi: 10.5194/bg-18-3189-2021

Köhler, P., Joos, F., Gerber, S., & Knutti, R. (2005). Simulated changes in vegetation distribution, land carbon storage, and atmospheric CO2 in response to a collapse of the North Atlantic thermohaline circulation. *Climate Dynamics*, *25*(7), 689. Retrieved from https://doi.org/10.1007/s00382-005-0058-8 doi: 10.1007/s00382-005-0058-8

Kwiatkowski, L., Torres, O., Bopp, L., Aumont, O., Chamberlain, M., Christian, J. R., ... Ziehn, T. (2020). Twenty-first century ocean warming, acidification, deoxygenation, and upper-ocean nutrient and primary production decline from CMIP6 model projections. *Biogeosciences*, *17*(13), 3439–3470. Retrieved from https://bg.copernicus.org/articles/17/3439/2020/ doi: 10.5194/bg-17-3439-2020

Lawrence, D. M., Fisher, R. A., Koven, C. D., Oleson, K. W., Swenson, S. C., Bonan, G., ... Zeng, X. (2019, dec). The Community Land Model Version 5: Description of New Features, Benchmarking, and Impact of Forcing Uncertainty. *Journal of Advances in Modeling Earth Systems*, *11*(12), 4245–4287. Retrieved from https://doi.org/10.1029/2018MS001583 doi: https://doi.org/10.1029/2018MS001583

Lenton, T. M., Held, H., Kriegler, E., Hall, J. W., Lucht, W., Rahmstorf, S., & Schellnhuber, H. J. (2008). Tipping elements in the Earth's climate system. *Proceedings of the National Academy of Sciences*, *105*(6), 1786–1793. Retrieved from https://www.pnas.org/doi/abs/10.1073/pnas.0705414105 doi: 10.1073/pnas.0705414105

Liu, Y., Moore, J. K., Primeau, F., & Wang, W. L. (2023). Reduced CO2 uptake and growing nutrient sequestration from slowing overturning circulation. *Nature Climate Change*, *13*(1), 83–90. Retrieved from https://doi.org/10.1038/s41558-022-01555-7 doi: 10.1038/s41558-022-01555-7

Long, M. C., Moore, J. K., Lindsay, K., Levy, M., Doney, S. C., Luo, J. Y., ... Sylvester, Z. T. (2021). Simulations With the Marine Biogeochemistry Library (MARBL). *Journal of Advances in Modeling Earth Systems*, *13*(12), e2021MS002647. Retrieved from https://doi.org/10.1029/2021MS002647 doi: https://doi.org/10.1029/2021MS002647

Lynch-Stieglitz, J. (2017). The Atlantic Meridional Overturning Circulation and Abrupt Climate Change. *Annual Review of Marine Science*, *9*(1), 83–104. Retrieved from https://doi.org/10.1146/annurev-marine-010816-060415

doi: 10.1146/annurev-marine-010816-060415
Marchal, O., Stocker, T. F., & Joos, F. (1998, jun). Impact of oceanic reorganizations on the ocean carbon cycle and atmospheric carbon dioxide content. *Paleoceanography*, *13*(3), 225–244. Retrieved from https://doi.org/10.1029/98PA00726 doi: https://doi.org/10.1029/98PA00726
McKay, D. I. A., Staal, A., Abrams, J. F., Winkelmann, R., Sakschewski, B., Loriani, S., ... Lenton, T. M. (2022). Exceeding 1.5°C global warming could trigger multiple climate tipping points. *Science*, *377*(6611), eabn7950. Retrieved from https://www.science.org/doi/abs/10.1126/science.abn7950 doi: 10.1126/science.abn7950
Nielsen, S. B., Jochum, M., Pedro, J. B., Eden, C., & Nuterman, R. (2019, apr). Two-Timescale Carbon Cycle Response to an AMOC Collapse. *Paleoceanography and Paleoclimatology*, *34*(4), 511–523. Retrieved from https://doi.org/10.1029/2018PA003481 doi: https://doi.org/10.1029/2018PA003481
Nohara, D., Yoshida, Y., Misumi, K., & Ohba, M. (2013, mar). Dependency of climate change and carbon cycle on CO2 emission pathways. *Environmental Research Letters*, *8*(1), 14047. Retrieved from https://dx.doi.org/10.1088/1748-9326/8/1/014047 doi: 10.1088/1748-9326/8/1/014047
Obata, A. (2007, dec). Climate Carbon Cycle Model Response to Freshwater Discharge into the North Atlantic. *Journal of Climate - J CLIMATE*, *20*, 5962–5976. doi: 10.1175/2007JCLI1808.1
O'Neill, B. C., Carter, T. R., Ebi, K., Harrison, P. A., Kemp-Benedict, E., Kok, K., ... Pichs-Madruga, R. (2020). Achievements and needs for the climate change scenario framework. *Nature Climate Change*, *10*(12), 1074–1084. Retrieved from https://doi.org/10.1038/s41558-020-00952-0 doi: 10.1038/s41558-020-00952-0
Orihuela-Pinto, B., England, M. H., & Taschetto, A. S. (2022). Interbasin and interhemispheric impacts of a collapsed Atlantic Overturning Circulation. *Nature Climate Change*, *12*(6), 558–565. Retrieved from https://doi.org/10.1038/s41558-022-01380-y doi: 10.1038/s41558-022-01380-y
Rahmstorf, S. (2002). Ocean circulation and climate during the past 120,000 years. *Nature*, *419*(6903), 207–214. Retrieved from https://doi.org/10.1038/nature01090 doi: 10.1038/nature01090
Sarmiento, J. L., Hughes, T. M. C., Stouffer, R. J., & Manabe, S. (1998). Simulated response of the ocean carbon cycle to anthropogenic climate warming. *Nature*, *393*(6682), 245–249. Retrieved from https://doi.org/10.1038/30455 doi: 10.1038/30455
Schmittner, A. (2005). Decline of the marine ecosystem caused by a reduction in the Atlantic overturning circulation. *Nature*, *434*(7033), 628–633. Retrieved from https://doi.org/10.1038/nature03476 doi: 10.1038/nature03476
Schmittner, A., & Galbraith, E. D. (2008). Glacial greenhouse-gas fluctuations controlled by ocean circulation changes. *Nature*, *456*(7220), 373–376. Retrieved from https://doi.org/10.1038/nature07531 doi: 10.1038/nature07531
Smith, R., Jones, P. W., Briegleb, P. A., Bryan, O., Danabasoglu, G., Dennis, M. L., ... Yeager, S. G. (2010). The Parallel Ocean Program (POP) reference manual: Ocean component of the Community Climate System Model (CCSM)..
Swingedouw, D., Bopp, L., Matras, A., & Braconnot, P. (2007, dec). Effect of land-ice melting and associated changes in the AMOC result in little overall impact on oceanic CO2 uptake. *Geophysical Research Letters*, *34*(23). Retrieved from https://doi.org/10.1029/2007GL031990 doi: https://doi.org/10.1029/2007GL031990
Tagliabue, A., Kwiatkowski, L., Bopp, L., Butenschön, M., Cheung, W., Lengaigne, M., & Vialard, J. (2021). Persistent Uncertainties in Ocean Net Primary Production Climate Change Projections at Regional Scales Raise Chal-

lenges for Assessing Impacts on Ecosystem Services. *Frontiers in Climate*, *3*. Retrieved from https://www.frontiersin.org/articles/10.3389/fclim.2021.738224 doi: 10.3389/fclim.2021.738224

Vellinga, M., & Wood, R. A. (2002). Global Climatic Impacts of a Collapse of the Atlantic Thermohaline Circulation. *Climatic Change*, *54*(3), 251–267. Retrieved from https://doi.org/10.1023/A:1016168827653 doi: 10.1023/A:1016168827653

Weijer, W., Cheng, W., Drijfhout, S. S., Fedorov, A. V., Hu, A., Jackson, L. C., ... Zhang, J. (2019, aug). Stability of the Atlantic Meridional Overturning Circulation: A Review and Synthesis. *Journal of Geophysical Research: Oceans*, *124*(8), 5336–5375. Retrieved from https://doi.org/10.1029/2019JC015083 doi: https://doi.org/10.1029/2019JC015083

Weijer, W., Cheng, W., Garuba, O. A., Hu, A., & Nadiga, B. T. (2020, jun). CMIP6 Models Predict Significant 21st Century Decline of the Atlantic Meridional Overturning Circulation. *Geophysical Research Letters*, *47*(12), e2019GL086075. Retrieved from https://doi.org/10.1029/2019GL086075 doi: https://doi.org/10.1029/2019GL086075

Whitt, D. B., & Jansen, M. F. (2020, jul). Slower nutrient stream suppresses Subarctic Atlantic Ocean biological productivity in global warming. *Proceedings of the National Academy of Sciences*, *117*(27), 15504–15510. Retrieved from https://doi.org/10.1073/pnas.2000851117 doi: 10.1073/pnas.2000851117

Wilson, J. D., Andrews, O., Katavouta, A., de Melo Viríssimo, F., Death, R. M., Adloff, M., ... Ying, R. (2022). The biological carbon pump in CMIP6 models: 21st century trends and uncertainties. *Proceedings of the National Academy of Sciences*, *119*(29), e2204369119. Retrieved from https://www.pnas.org/doi/abs/10.1073/pnas.2204369119 doi: 10.1073/pnas.2204369119

Yamamoto, A., Abe-Ouchi, A., & Yamanaka, Y. (2018). Long-term response of oceanic carbon uptake to global warming via physical and biological pumps. *Biogeosciences*, *15*(13), 4163–4180. Retrieved from https://bg.copernicus.org/articles/15/4163/2018/ doi: 10.5194/bg-15-4163-2018

Zhang, R., & Delworth, T. L. (2005). Simulated Tropical Response to a Substantial Weakening of the Atlantic Thermohaline Circulation. *Journal of Climate*, *18*(12), 1853–1860. Retrieved from https://journals.ametsoc.org/view/journals/clim/18/12/jcli3460.1.xml doi: https://doi.org/10.1175/JCLI3460.1

Zhu, J., Zeng, X., Gao, X., & Zhang, H. (2022). Response of Terrestrial Net Primary Production to Quadrupled CO2 Forcing: A Comparison between the CAS-ESM2 and CMIP6 Models. *Biology*, *11*(12). Retrieved from https://doi.org/10.3390/biology11121693 doi: https://doi.org/10.3390/biology11121693

Zickfeld, K., Eby, M., & Weaver, A. J. (2008, sep). Carbon-cycle feedbacks of changes in the Atlantic meridional overturning circulation under future atmospheric CO2. *Global Biogeochemical Cycles*, *22*(3). Retrieved from https://doi.org/10.1029/2007GB003118 doi: https://doi.org/10.1029/2007GB003118

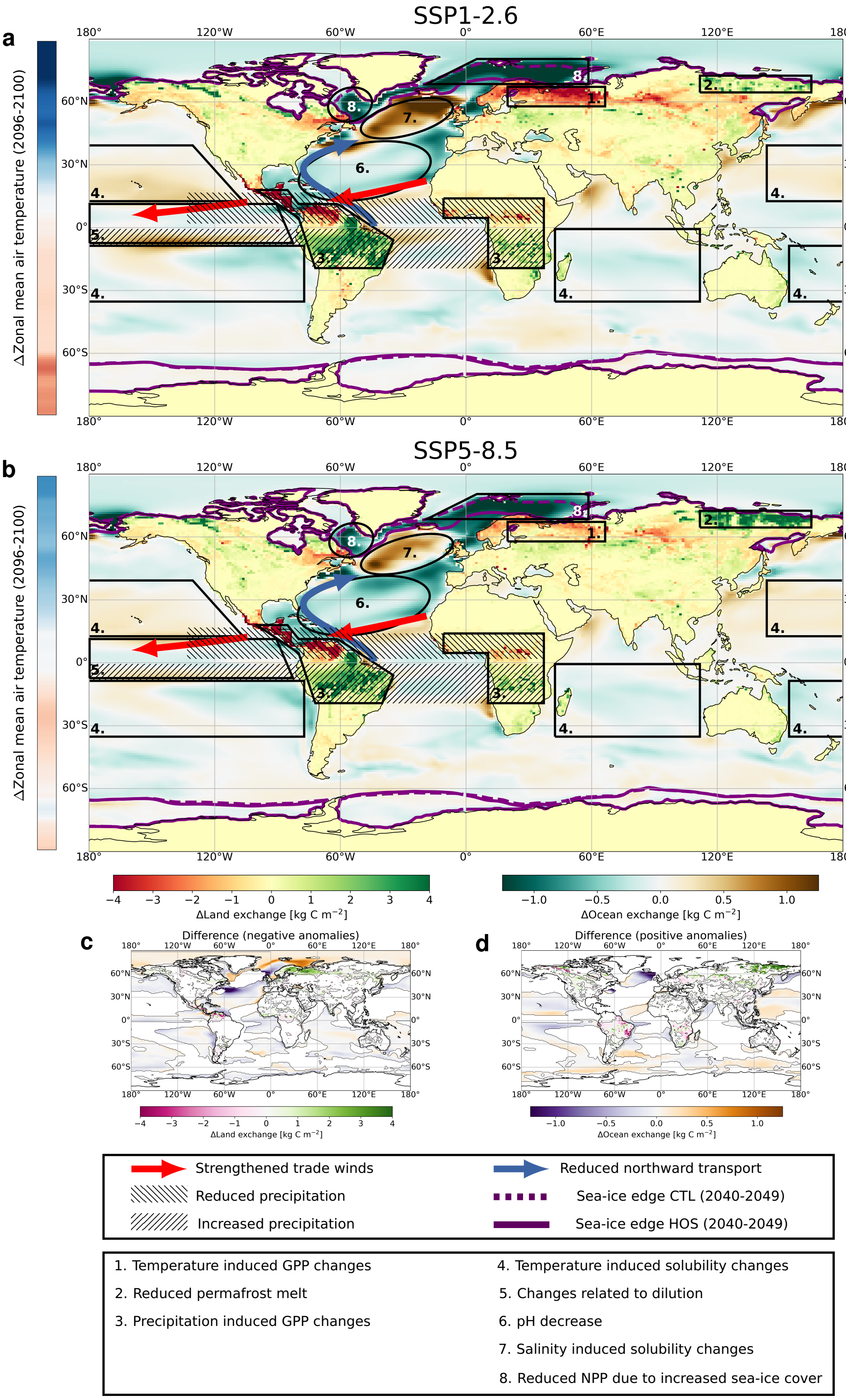

Figure 10. Summarizing figure with dominant mechanisms included for SSP1-2.6 (a) and SSP5-8.5 (b). (a) and (b) represent results from HOS minus the CTL simulations. The sea-ice edge is taken as where the ice fraction is 0.25 and denoted by the purple lines, where dashed lines represent the CTL simulations and solid lines the HOS simulations. The bar at the left shows the difference in zonal mean surface air temperature averaged over 2096-2100 between HOS and CTL. The scaling of this bar is between -2.5°C (dark blue) and 2.5°C (dark red). (c) The difference between SSP5-8.5 (b) and SSP1-2.6 (a) in the regions where (b) is negative. Negative values represent a higher negative anomaly in SSP5-8.5 compared to SSP1-2.6. (d) as in (c) but for positive anomalies. Positive values represent a higher positive anomaly in SSP5-8.5 compared to SSP1-2.6. The color bars in (c) and (d) apply to both subfigures.

Supporting Information for "Response of atmospheric pCO_2 to a strong AMOC weakening under climate change"

A. A. Boot[1], A. S. Von der Heydt[1,2], and H. A. Dijkstra[1,2]

[1]Institute for Marine and Atmospheric research Utrecht, Department of Physics,Utrecht University, Utrecht, the Netherlands

[2]Center for Complex Systems Studies, Utrecht University, Utrecht, the Netherlands

Contents of this file

Introduction This supplementary material includes additional figures of the results.

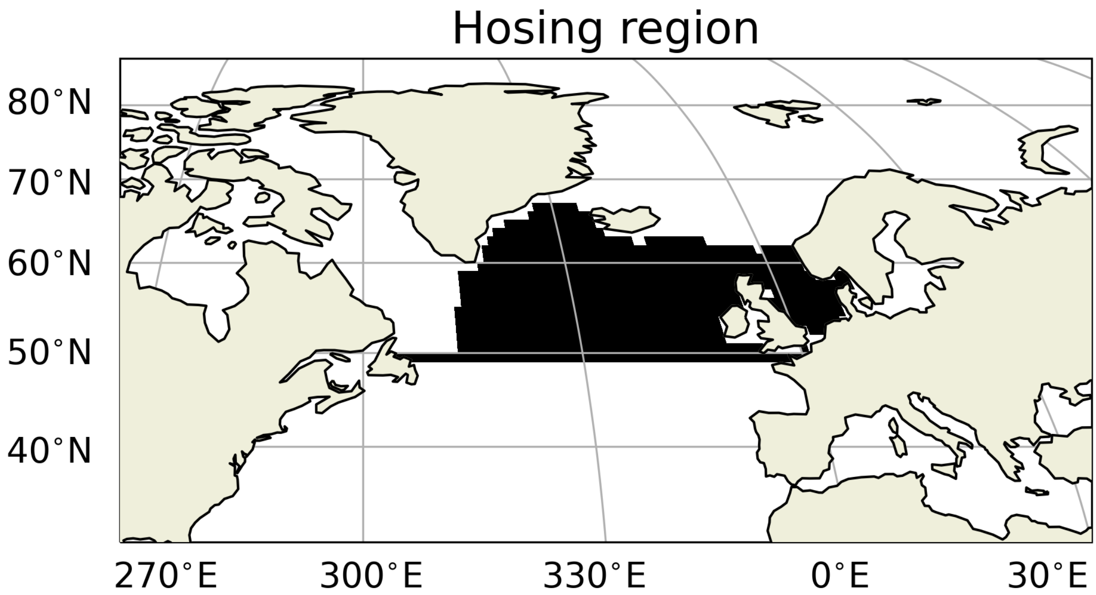

Figure S1. Region in black corresponds to the region where the freshwater forcing is applied. The freshwater forcing integrated over this region is 0.5 Sv throughout the entire simulation period.

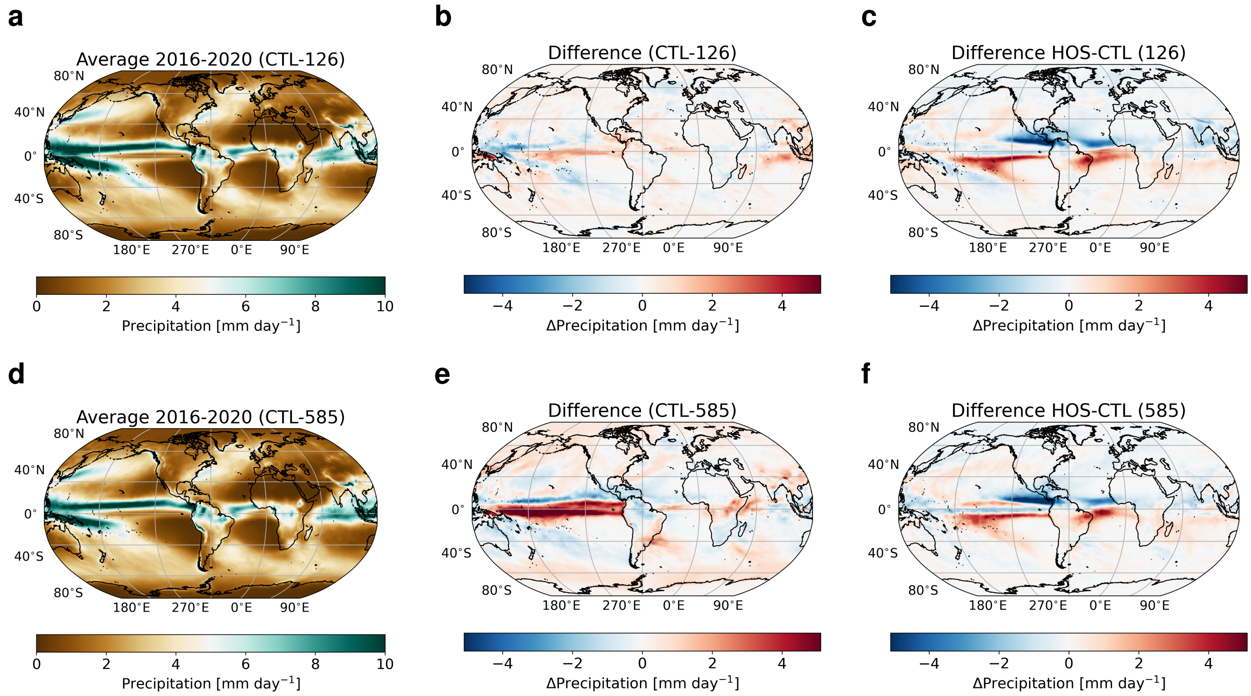

Figure S2. Results for precipitation in mm day^{-1}. he top row (a-c) is for SSP1-2.6, and the bottom row (d-f) for SSP5-8.5. The left column (a, d) represents the average over 2016-2020 in the control simulations. The middle row (b, e) represents the difference between the average of 2096-2100 and 2016-2020 for the control simulations. The right row (c, f) represents the difference between the hosing and control simulations averaged over 2096-2100. Note the different scaling between b and e.

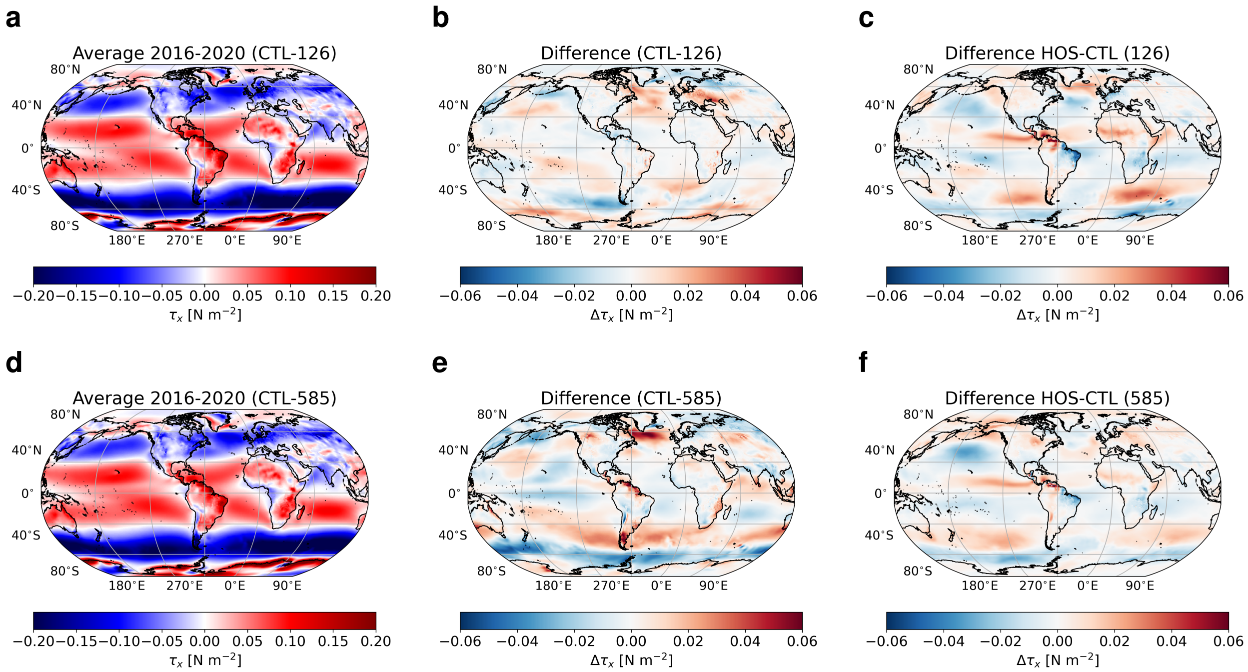

Figure S3. Results for the zonal wind stress in N m^{-2}. Panels represent the same as in Fig. S2.

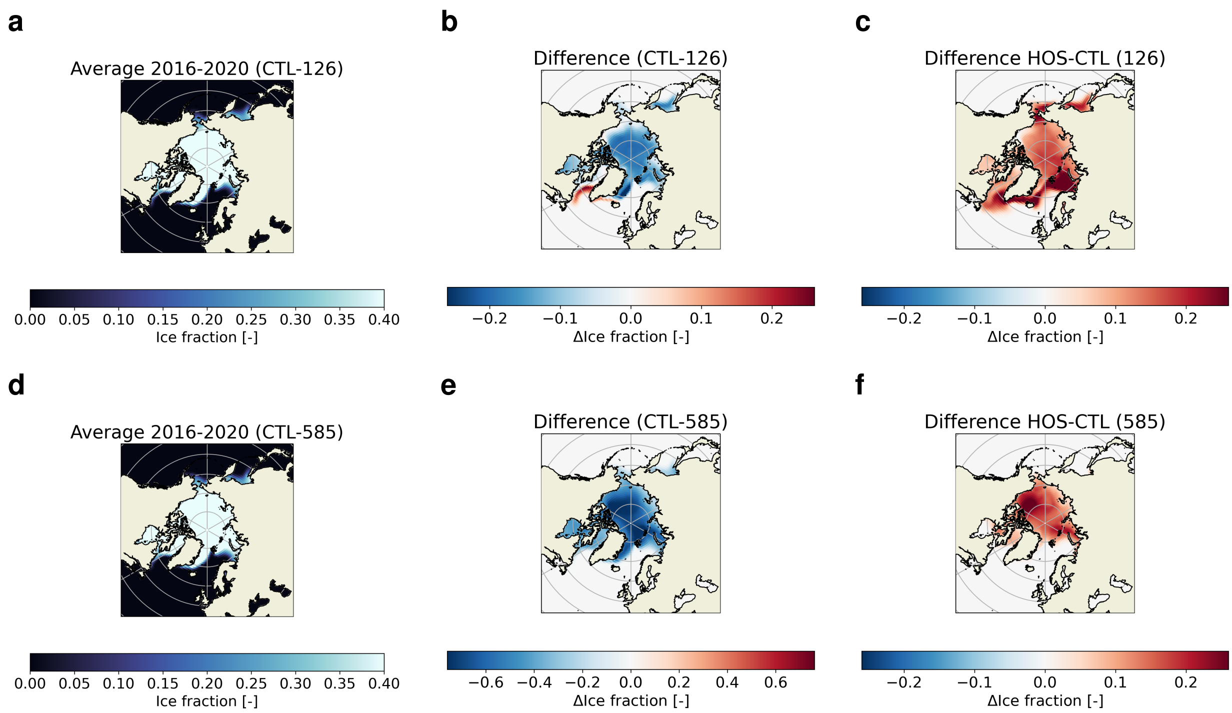

Figure S4. Results for the ice fraction in the Arctic. Panels represent the same as in Fig. S2. Note the different scaling for e.

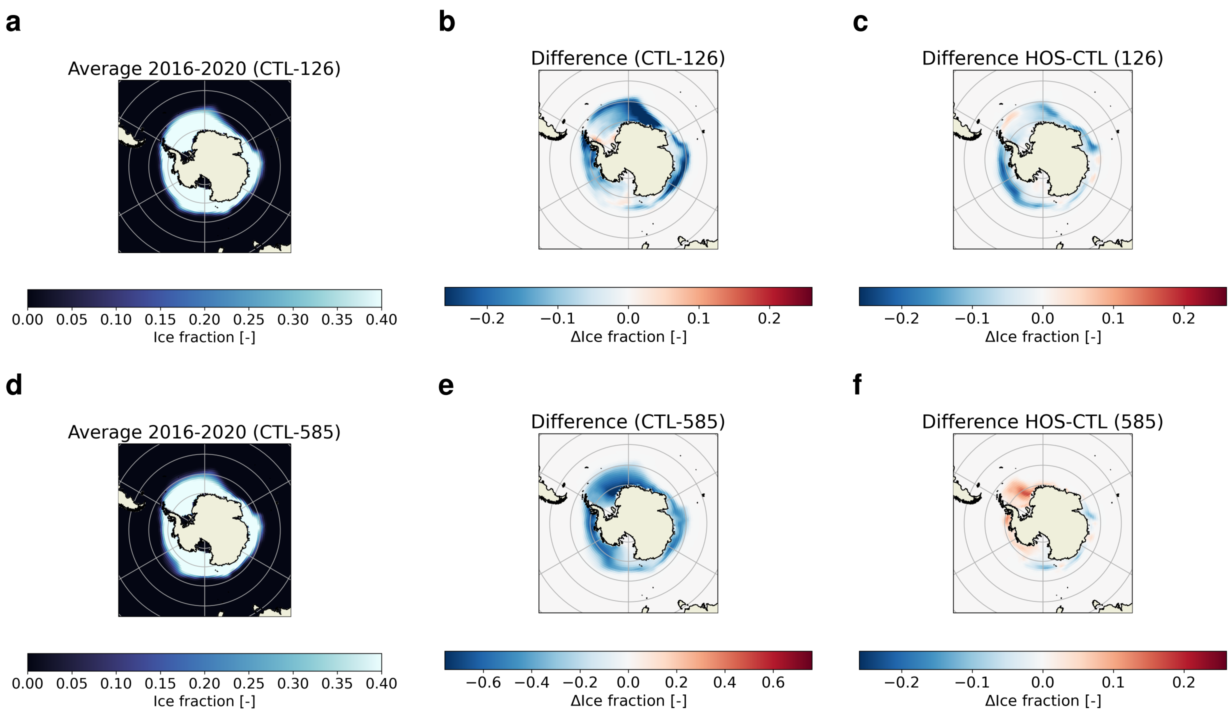

Figure S5. Results for the ice fraction in the Antarctic. Panels represent the same as in Fig. S2. Note the different scaling for e.

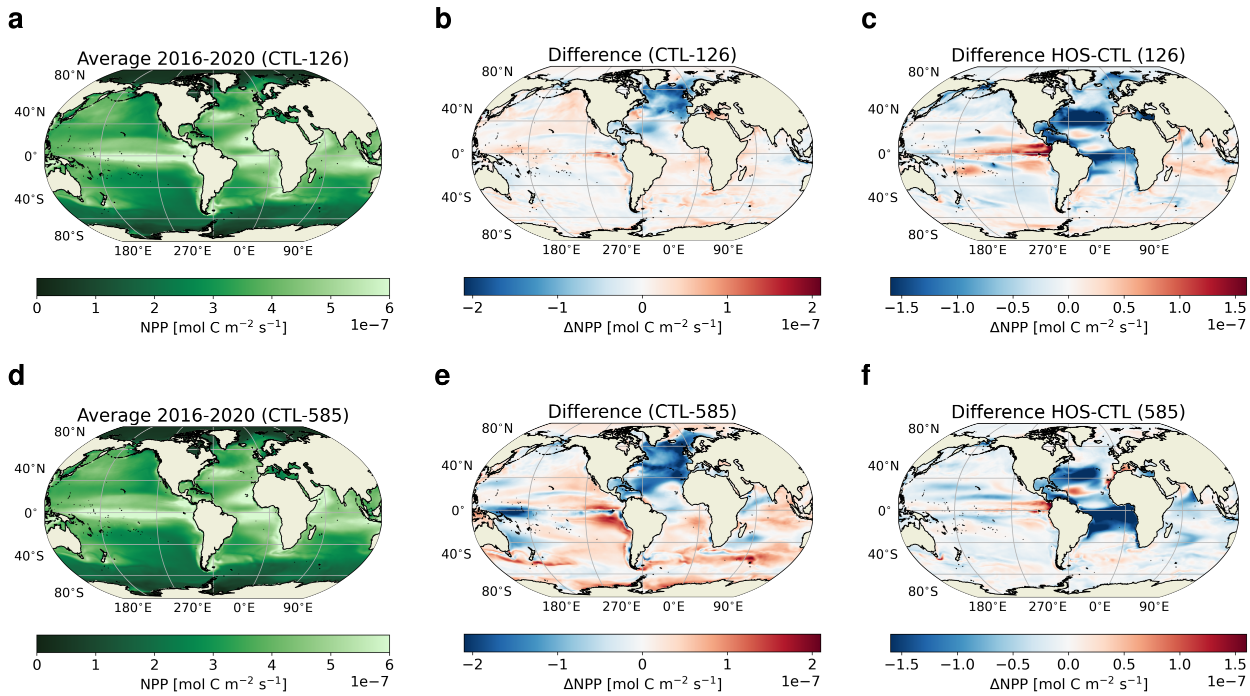

Figure S6. Results for Net Primary Production (NPP) integrated over the surface layer (0-150 m) in mol m^{-2} s^{-1}. Panels represent the same as in Fig. S2

.

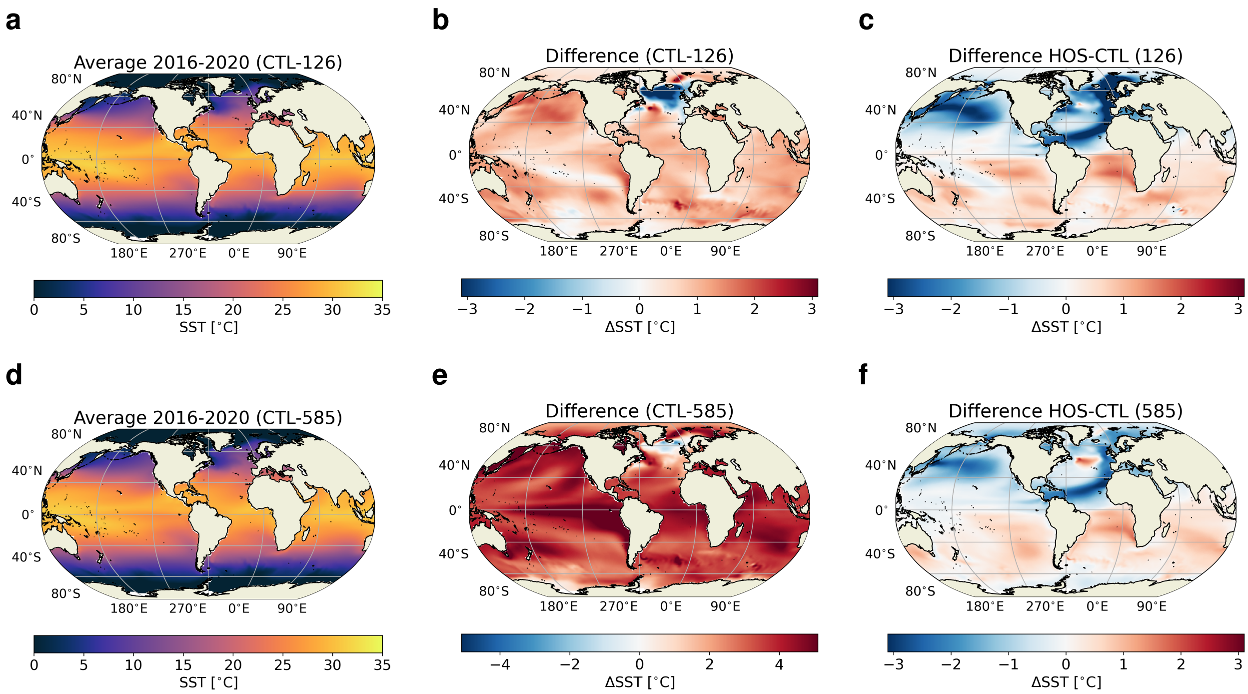

Figure S7. Results for Sea Surface Temperature (SST) in $^{\circ}C$. Panels represent the same as in Fig. S2. Note the different scaling in e.

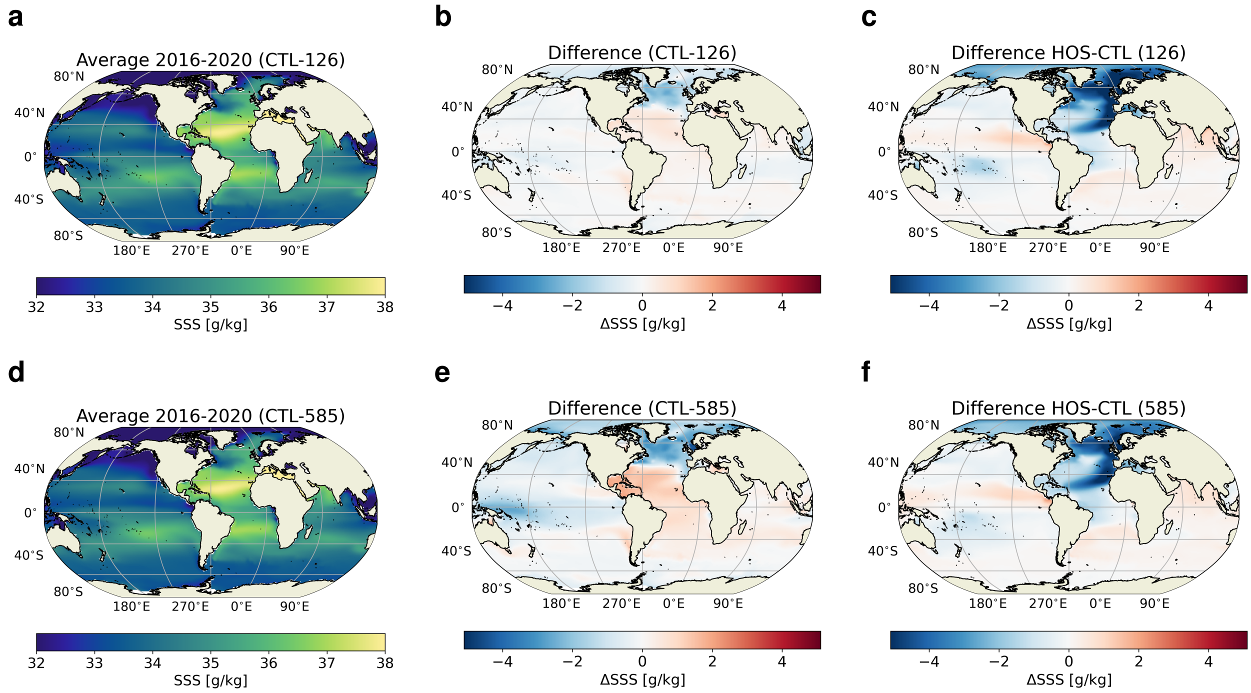

Figure S8. Results for Sea Surface Salinity (SSS) in g/kg. Panels represent the same as in Fig. S2.

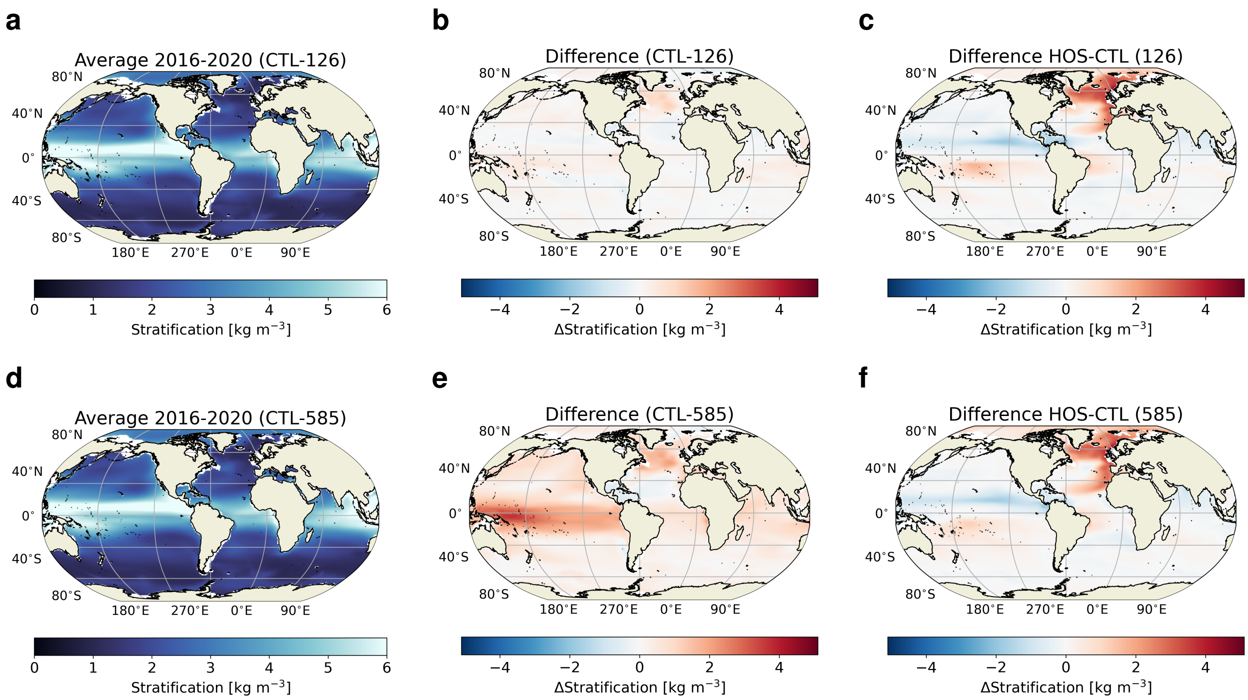

Figure S9. Results for stratification in kg m^{-3}, where stratification is defined as the densitiy difference between 200 m depth and the surface (ref). Panels represent the same as in Fig. S2.

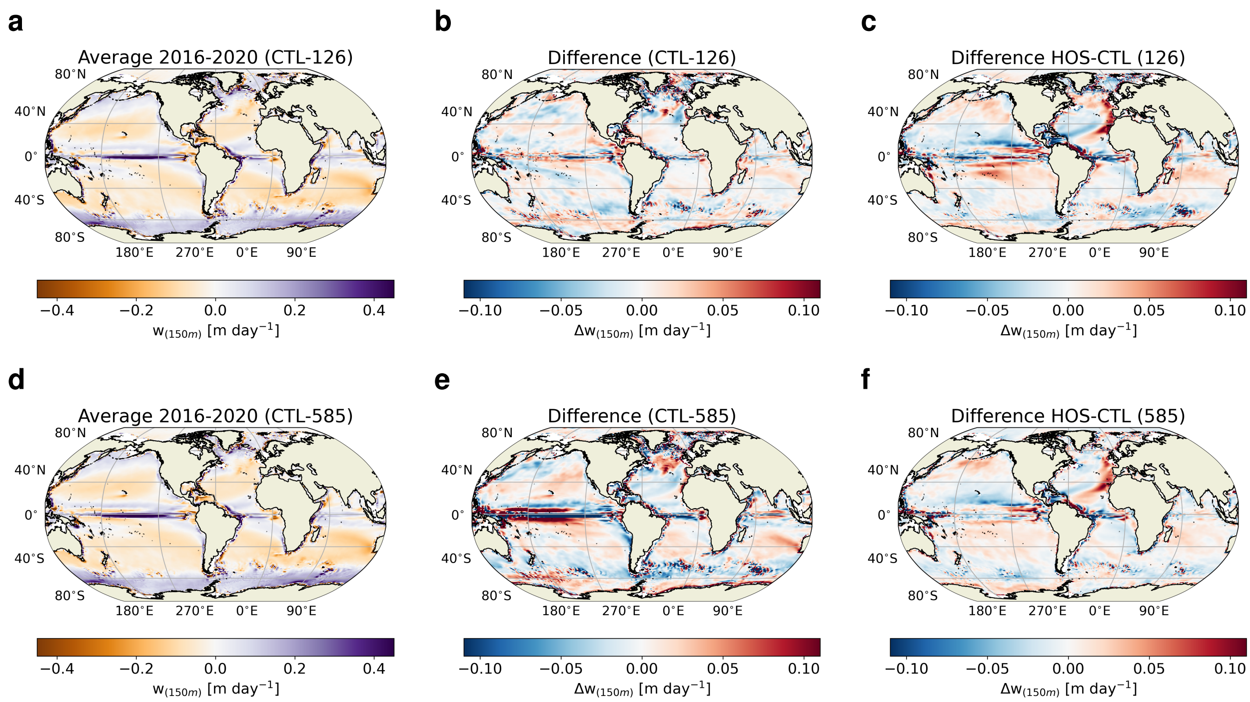

Figure S10. Results for vertical velocities at 150 m depth in m day^{-1}. Panels represent the same as in Fig. S2. Positive values (purple colors) in a and e represent upwelling and negative values (orange colors) downwelling.

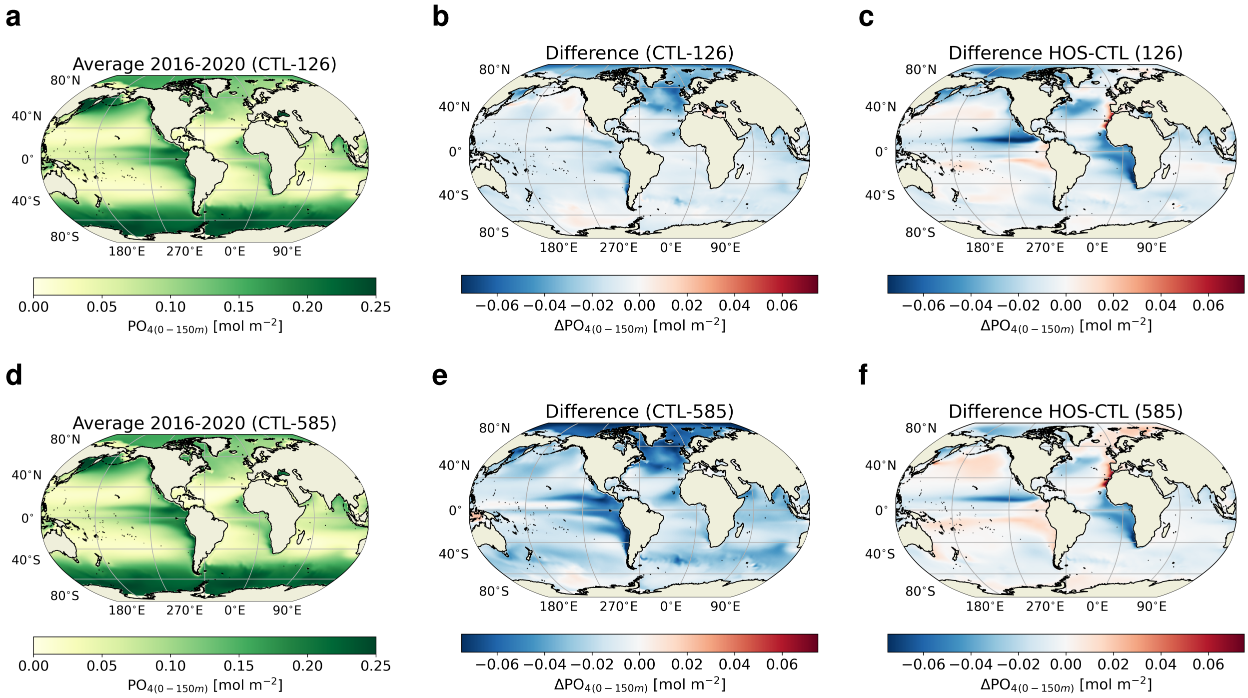

Figure S11. Results for PO_4 concentrations integrated over the surface layer (0-150 m) in mol m^{-2}. Panels represent the same as in Fig. S2.

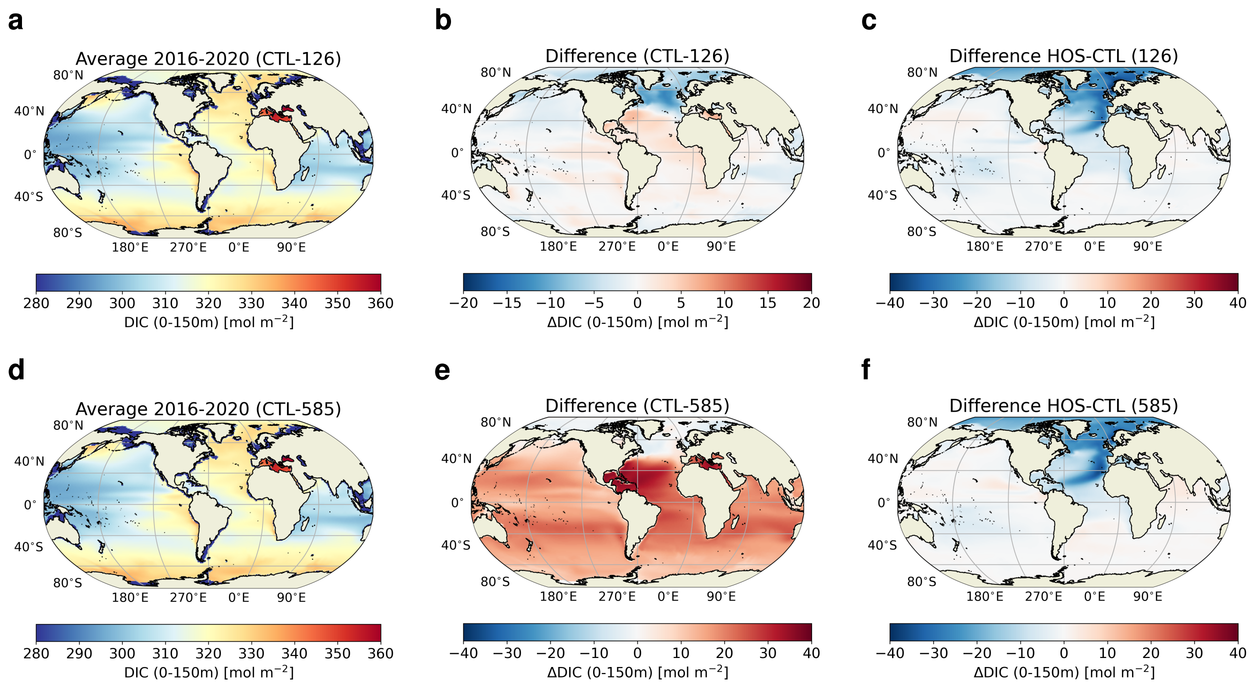

Figure S12. Results for DIC concentrations integrated over the surface layer (0-150 m) in mol m^{-2}. Panels represent the same as in Fig. S2. Note the different scaling in e.

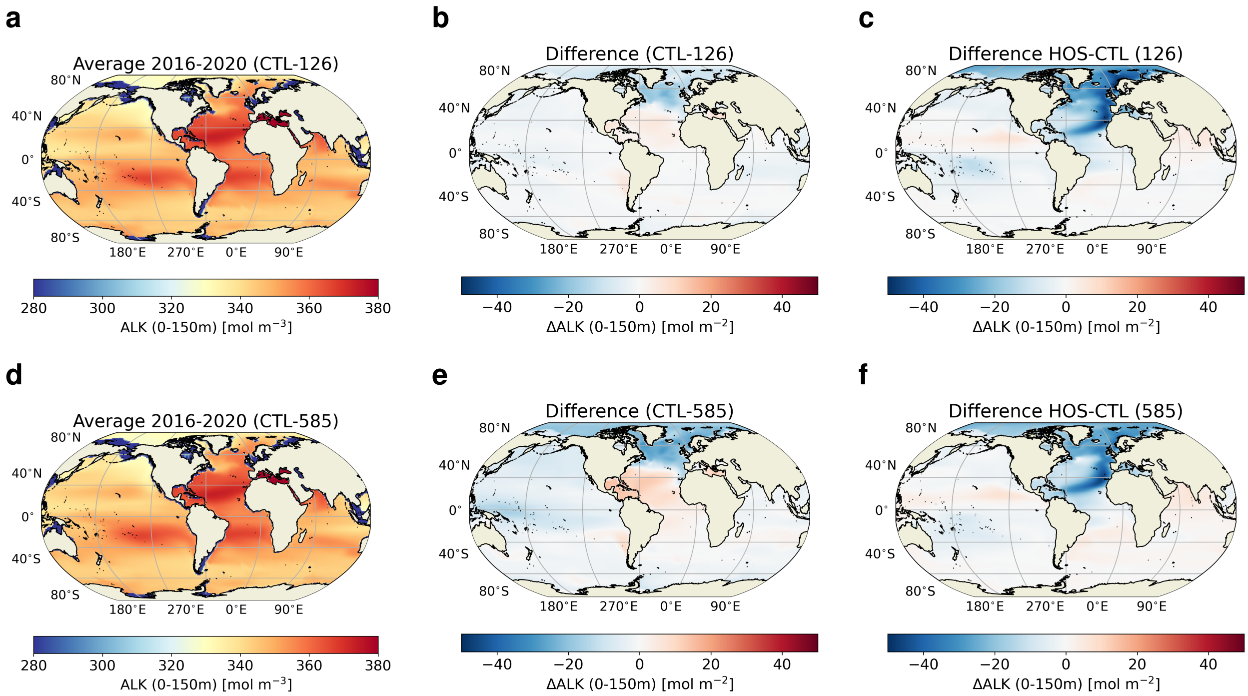

Figure S13. Results for alkalinity concentrations integrated over the surface layer (0-150 m) in mol m^{-2}. Panels represent the same as in Fig. S2. Note the different scaling in e.

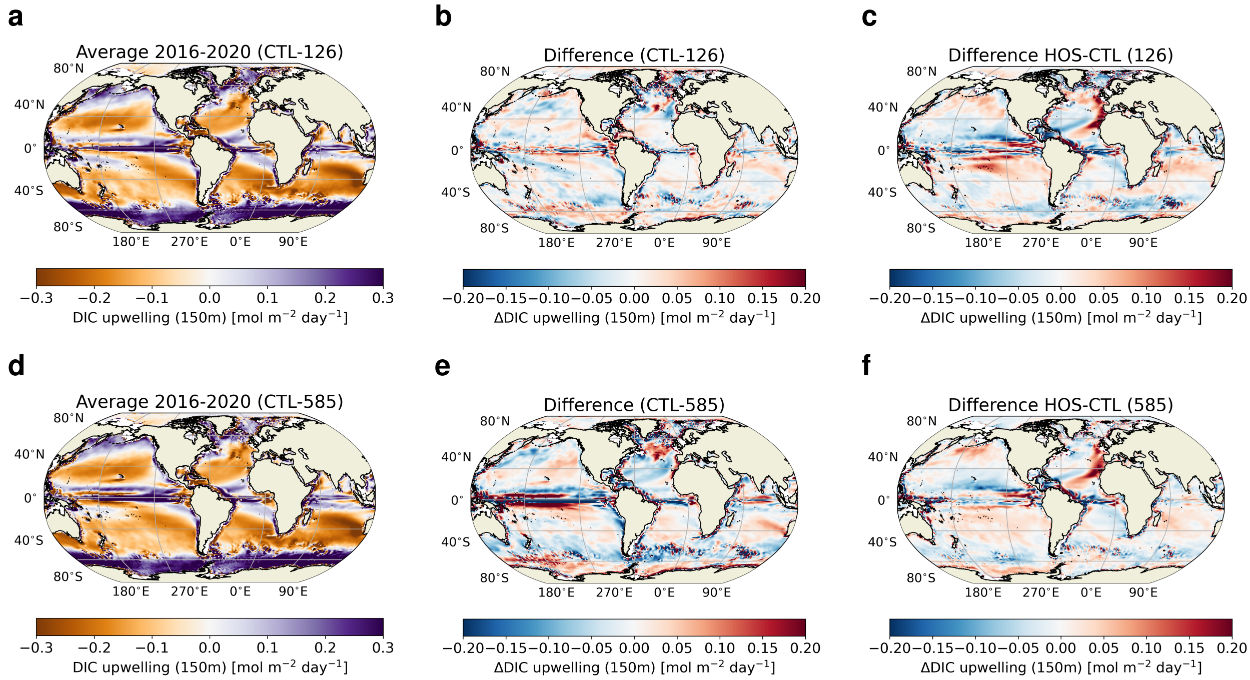

Figure S14. Results for upwelling of DIC at 150 m depth in mol m^{-2} day^{-1}. Panels represent the same as in Fig. S2. Positive values (purple colors) in a and d represent a flux going into the surface layer (top 150 m).

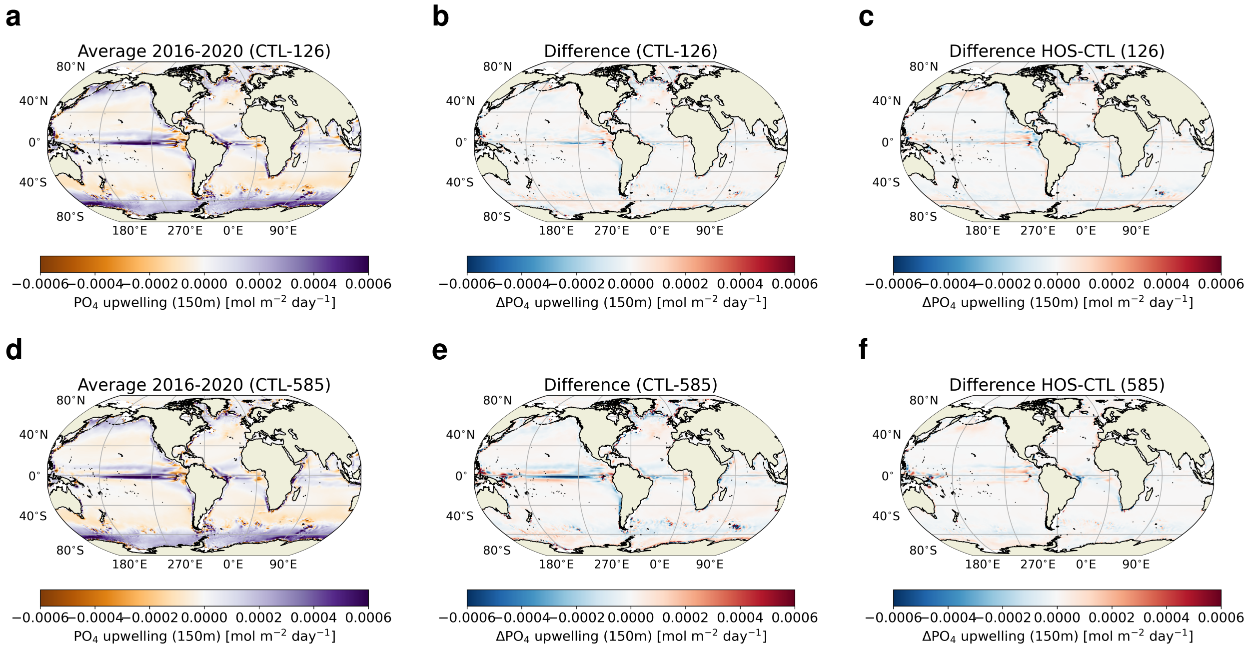

Figure S15. Results for upwelling of PO_4 at 150 m depth in mol m^{-2} day^{-1}. Panels represent the same as in Fig. S2.

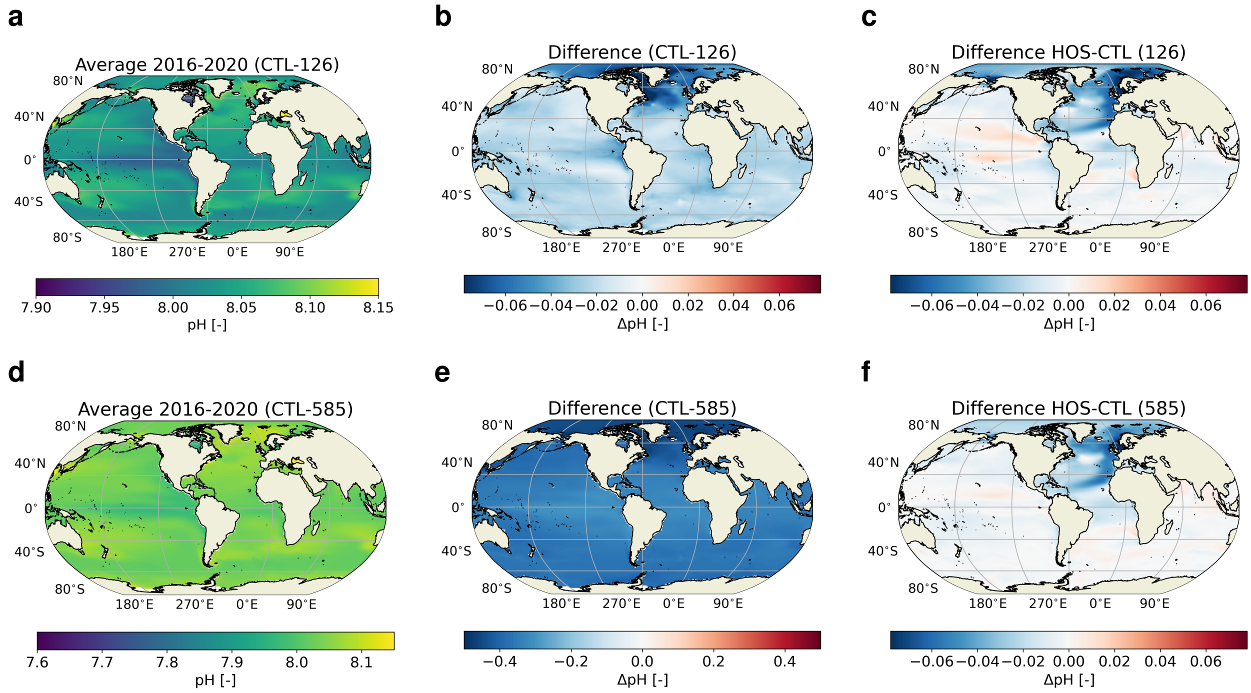

Figure S16. Results for surface pH. Panels represent the same as in Fig. S2. Note that the scaling of the colorbar is different for the subplots.

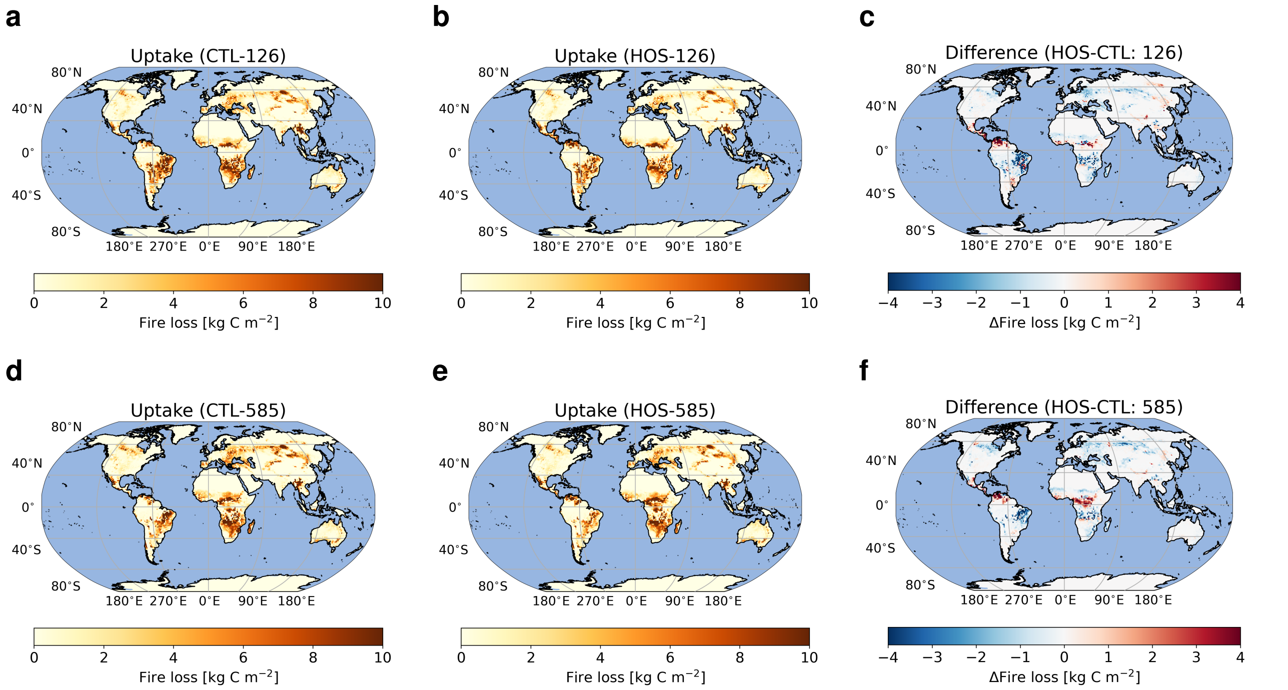

Figure S17. Results for biomass loss due to fire integrated over the entire simulation period in kg C m^{-2}. The top row (a-c) represents SSP1-2.6 and the bottom row (d-f) represents SSP5-8.5. The left column (a, d) represents the uptake in the control simulations, the middle column (b, e) the uptake in the hosing simulations, and the right column (c, f) the difference between the hosing and control simulations.

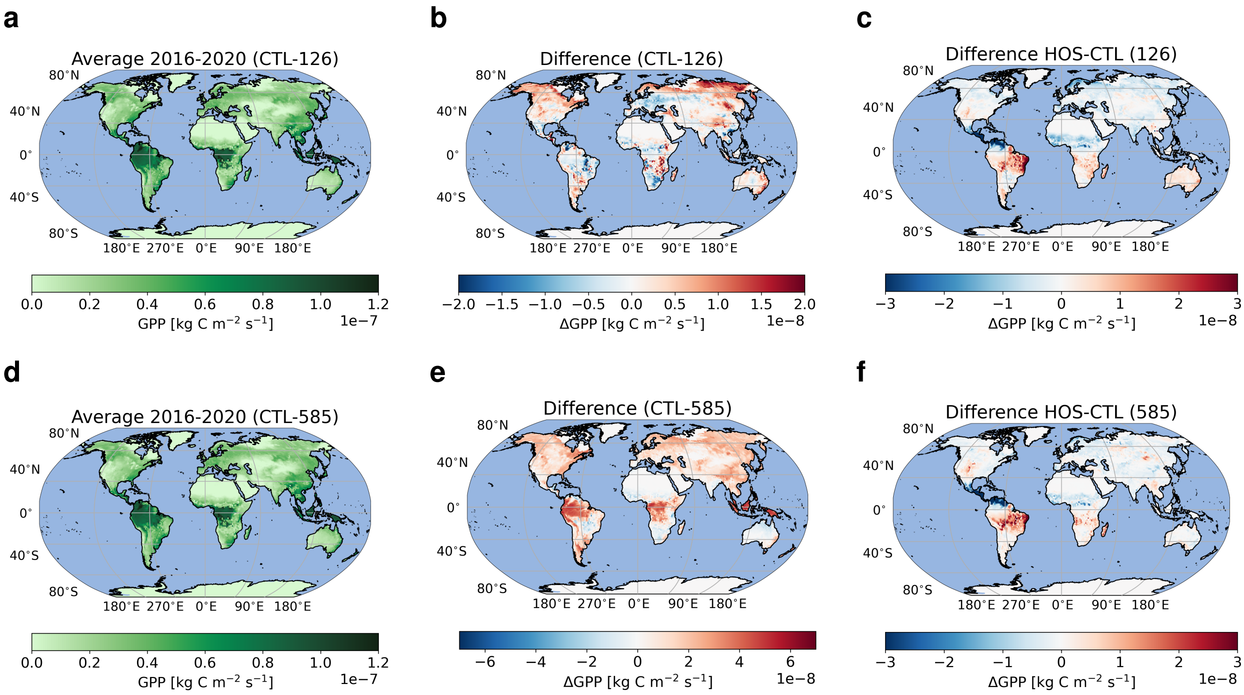

Figure S18. Results for Gross Primary Production (GPP) in kg C m^{-2} s^{-1}. Panels represent the same as in Fig. S2. Note the different scaling in e.

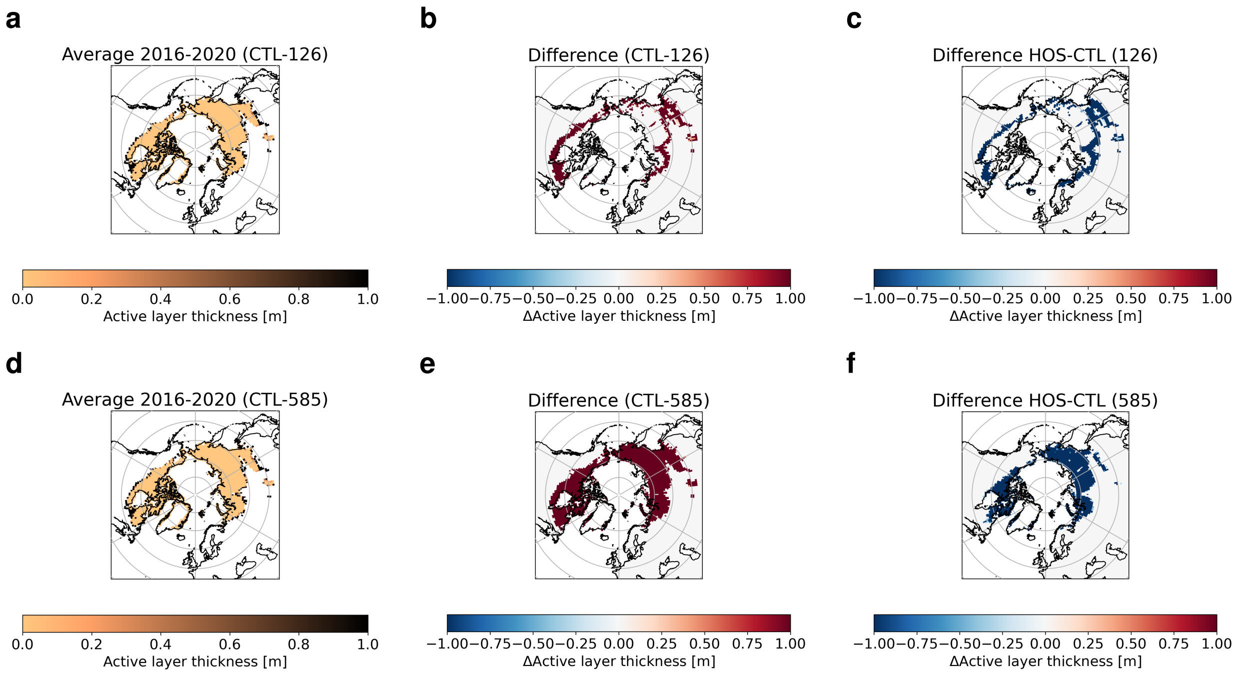

Figure S19. Results for Active Layer Thickness (ALT) in m, which serves as a proxy for annually minima of (horizontal) permafrost extent. Panels represent the same as in Fig. S2.

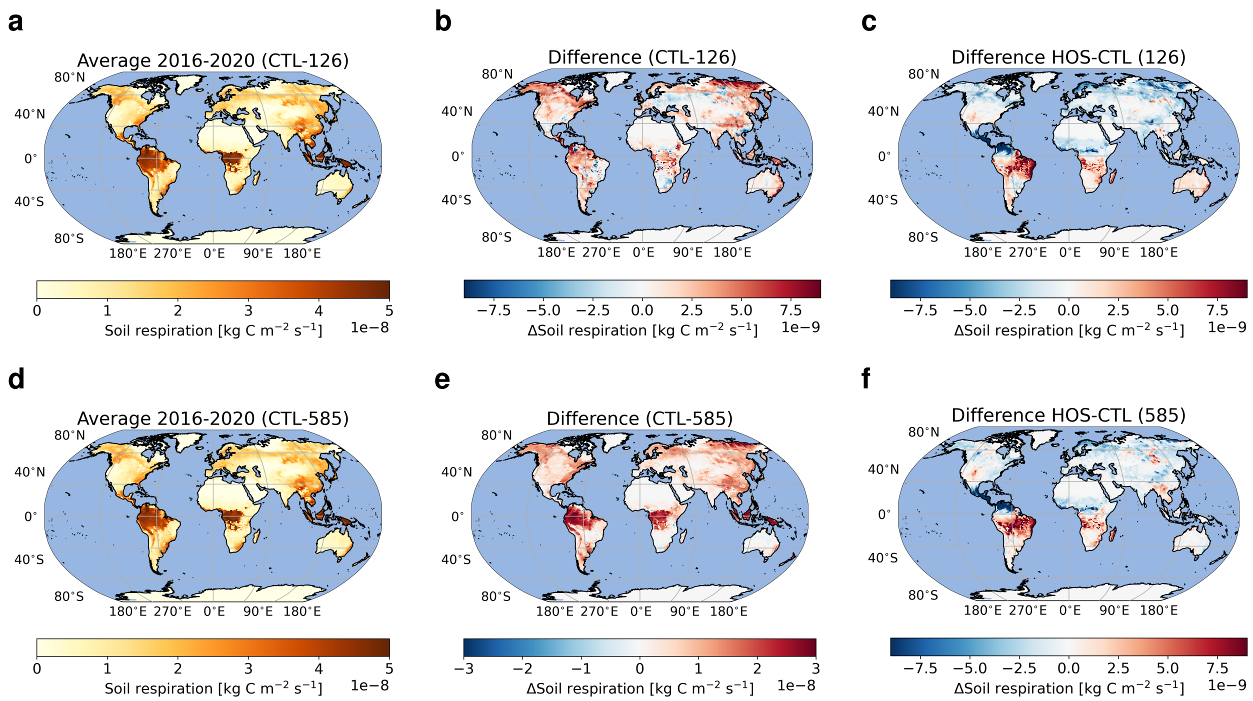

Figure S20. Results for soil respiration in kg C m^{-2} s^{-1}. Panels represent the same as in Fig. S2. Note the different scaling in e.

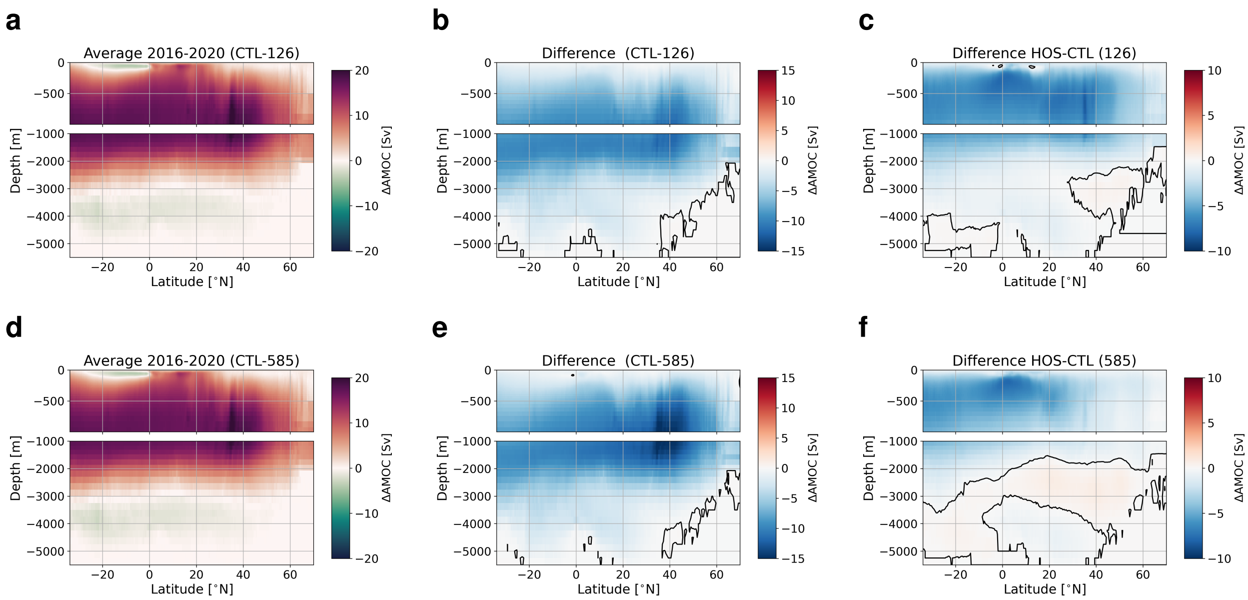

Figure S21. Results for the Atlantic Meridional Overturning Circulation in Sv. Panels represent the same as in Fig. S2. Black contour lines in b, c, e and f represent the 0 Sv contour. Note the different scaling of the surface ocean (top 1000 m) compared to the deep ocean.